Loughborough University

This item was submitted to Loughborough's Research Repository by the author.
Items in Figshare are protected by copyright, with all rights reserved, unless otherwise indicated.

Minimum environmental impact discharging

PLEASE CITE THE PUBLISHED VERSION

PUBLISHER

© P. Mebine

LICENCE

CC BY-NC-ND 4.0

REPOSITORY RECORD

Mebine, P.. 2019. “Minimum Environmental Impact Discharging”. figshare. https://hdl.handle.net/2134/12945.

Loughborough University

This item was submitted to Loughborough University as a PhD thesis by the author and is made available in the Institutional Repository (https://dspace.lboro.ac.uk/) under the following Creative Commons Licence conditions.

creative commons

COMMONS DEED

Attribution-NonCommercial-NoDerivs 2.5

You are free:

- to copy, distribute, display, and perform the work

Under the following conditions:

Attribution. You must attribute the work in the manner specified by the author or licensor.

Noncommercial. You may not use this work for commercial purposes.

No Derivative Works. You may not alter, transform, or build upon this work.

- For any reuse or distribution, you must make clear to others the license terms of this work.
- Any of these conditions can be waived if you get permission from the copyright holder.

Your fair use and other rights are in no way affected by the above.

This is a human-readable summary of the Legal Code (the full license).

Disclaimer

For the full text of this licence, please go to:
http://creativecommons.org/licenses/by-nc-nd/2.5/

Loughborough University

University Library

Author/Filing Title ..... MEBINE, P. .....

.....

Class Mark ..... T .....

Please note that fines are charged on ALL overdue items.

FOR REFERENCE ONLY

040327124X

Minimum Environmental Impact Discharging

By

Promise MEBINE

(M.Sc., B.Sc.)

A Doctoral Thesis

Submitted in partial fulfilment of the requirements

for the award of

Doctor of Philosophy of Loughborough University

2003-2006

© by P. Mebine (2006)

Loughborough University
Pilkington Library
Date SEPT 2006
Class T
Acc No. 040327124X

Abstract

Many contaminants exhibit decay. Decay mechanisms include consumption by bacteria or radioactive decay (temporal decay uniform across the flow), heat loss or evaporation through the surface (decay decreasing with depth), and break up by turbulence (decay proportional to the product of velocity and depth). This thesis investigates how the decay of pollutants in a river effects the dilution process and the selection of discharge siting to achieve minimum environmental impact.

For a non-symmetric river with non-reversing flow, exact solutions are presented that illustrate the effect on the optimal position for a steady discharge of cross-channel variation in the decay (uniform, decreasing or increasing with depth). The optimal position is shifted to deeper or to shallower water accordingly as the temporal decay divided by flow speed decreases or increases with water depth.

When advection dominates diffusion, there are special directions (rays) along which information is carried. For steady, unstratified, plane parallel flow, the effects of decay are allowed for in specifying these special directions. Two special cases are considered. Firstly, for a smoothly varying depth, a general result has been derived for the curvature of the rays as effected by spatial non-uniformity in decay, mixing, flow speed and flow direction. Secondly, for discontinuous variations in depth, diffusivity, velocity and decay, approximate concentration formulae are derived. Ray bending indicates that the downstream propagation of pollutant is principally in the low-decay region.

Computational results are used to give pictorial illustration of the concentration distributions and of the difference between discharging at non-optimal and optimal sites.

Dedication

To God Almighty

MEID

Mebine, 2006

Acknowledgement

I wish to acknowledge my sincere gratitude to my Supervisor Prof. Ron(W) Smith. His keen enthusiasm for work and constant good humoured spirits have been a source of encouragement to me. His comments and criticisms have been appreciated as much as his learned guidance and advice throughout the course of this study. I really appreciate his patience, expertise and unlimited trust. I learned from him how to conduct research but most importantly he taught me other great values and tools that I can use in my life. Prof. Ron(W) Smith, I admired your buoyancy and persistent good humor, and it was a great honour to work with you!

I would also like to thank Dr. A. Kay for accepting to be the interim supervisor when my supervisor was away for sabbatical in 2003. His comments and suggestions were helpful. Members of the department of Mathematical Sciences at Loughborough University who helped me in different ways (either directly or indirectly) should not be forgotten. I sincerely appreciate them all.

Special thanks goes to my sponsor Bayelsa State Government of Nigeria for providing me with the financial support through the award of a PhD research fellowship.

Last, but by no means least I am deeply indebted to my family. I express my sincere gratitude for their valuable advice, goodwill and continued encouragements, and I would particularly like to thank Chief P. Y. Fawei-Prake, Chief N. K. Ebitimi-Dabbey, Engr. I. Ezetu, Rev. Goodlive Mebine, Mr. & Mrs. Ngozi T. Ezikwa, Messrs. Saturday Mebine, Ayibakuro Mebine, Ambrose S. Mebine, Henry-Sam B. Mebine, Alex Faboh, Fyneman Bipeledei and Tobin Seibokuro. I gratefully acknowledge my late father Mr. Ekemeghe-suodei Thomas B. Mebine, who did not live to see my PhD achievement. Special thanks are due to my wife, Mrs. Charity Bose Mebine, for her moral and spiritual support, and my children, the Woyins (Woyinpreye, Woyinwomoemi and Woyindouye), for their great tolerance and understanding.

MEID Mebine, 2006

Contents

Thesis Access Form i

Thesis Title ii

Certificate Of Originality iii

Abstract iv

Dedication v

Acknowledgement vi

List of Figures xi

List of Tables xiv

Nomeclature xv

1 General Introduction 1

1.1 Introduction 2

1.2 Concept and definition of the Research 3

1.3 The Objective of the Research 4

1.4 An Overview of the Sources and Effects of Pollutants 5

1.5 An Overview of Mixing and its Importance 7

1.6 Structure of Mathematical Models 10
1.7 Organisation of the Thesis 13
1.8 Concluding remarks 14
1.9 References 14

2 Mathematical Formulations **23**
2.1 Introduction 24
2.2 Law of conservation 24
2.3 Advection-diffusion-reaction equation 24
2.4 Depth-Averaging 28
2.5 Concluding remarks 34
2.6 References 35

3 The diffusion centre of a river **36**
3.1 Introduction 37
3.2 Governing equations 39
3.3 Pollutant modes 40
3.4 Flow parameters in straight channels 43
3.5 Linearly increasing depth 44
3.5.1 Constant decay 45
3.5.2 Decay that decreases with depth 47
3.5.3 Decay that increases with depth more than the velocity 49
3.6 Ratio λ/u as an indicator for changes in y_1 50
3.7 Concluding remarks 51
3.8 References 52

4 Ray approximation for steady discharges in rivers **55**
4.1 Introduction 56
4.2 Advection-diffusion equation 57

4.3 The ray ansatz 58
4.3.1 Eikonal and Transport equations 58
4.3.2 Exponential Decay 60
4.3.3 Amplitude Factor 62
4.4 Ray tracing algorithm 63
4.5 Model problems to determine the curvature 64
4.5.1 Conserved contaminants 65
4.5.2 Constant decay-diffusivity ratio 66
4.5.3 Decay-diffusivity ratio that decreases with depth 68
4.5.4 Decay-diffusivity ratio that increases with depth 72
4.6 Sensitivity of curvature to decay-difffusivity ratio 77
4.7 Caustic problems and other observed phenomena 80
4.7.1 Caustics 80
4.7.2 Reflection-refraction processes 81
4.8 Concluding remarks 81
4.9 References 82

5 Decay and depth discontinuity effects upon steady discharges in rivers 86

5.1 Introduction 87
5.2 Advection-diffusion equation and flux matching 88
5.3 Exponential solutions 89
5.4 Incident rays 91
5.5 Reflected rays 93
5.6 Transmitted rays and decay-jump parameter M 94
5.7 Reduction to two scaled ray patterns 96
5.8 Decay-adjusted phases and position factor P 98
5.9 Transmitted amplitude 101
5.10 Reflection coefficient 102

5.11 Concentrations 104
5.12 Concluding remarks 107
5.13 References 108

6 Computational scheme for steady discharges in rivers **110**
6.1 Introduction 111
6.2 Background and model equation 111
6.3 Flow profiles 113
6.4 Finite-difference scheme 115
6.5 Regular grid spacing with constant coefficients 117
6.6 Regular grid spacing with non-constant coefficients 121
6.6.1 Kay benchmark problem 124
6.7 Optimal and non-optimal discharge 127
6.7.1 Constant decay 128
6.7.2 Decay that decreases with depth 132
6.7.3 Decay that increases with depth more than the velocity 135
6.8 Evolution of Fourier modes and Stability Analysis 135
6.9 Concluding remarks 138
6.10 References 138

7 Conclusions and Further Work **142**
7.1 Conclusions 143
7.2 Further Work 144

List of Figures

1.1 Plan and Profile schematics of the spreading of a discharge into a river. . . 9

2.1 Schematic of a control volume with crossflow. 25

2.2 Sketch of Configuration of a uniform straight channel. 33

3.1 Magnitude of shoreline pollution if a discharge is not at the diffusion centre. 37

3.2 Normalized modes for linearly increasing depth. 41

3.3 First mode $\phi_1(y)$ for constant decay Λ and linearly increasing depth. 47

3.4 First mode $\phi_1(y)$ for decay that decreases with depth. 48

3.5 First mode $\phi_1(y)$ for decay that increases with depth. 50

4.1 Ray paths for conserved contaminant spreading. 66

4.2 Ray paths for constant decay-diffusivity ratio: (a) $\beta = 2$; (b) $\beta = 4$; (c) $\beta = 8$. 67

4.3 Ray paths for decay-diffusivity that decreases with depth, $m = -2$: (a) $\beta = 2$; (b) $\beta = 4$; (c) $\beta = 8$. 69

4.4 Ray paths for decay-diffusivity ratio that decreases with depth, $m = -3/2$: (a) $\beta = 2$; (b) $\beta = 4$; (c) $\beta = 8$. 71

4.5 Ray paths for decay-diffusivity ratio that decreases with depth, $m = -5/2$: (a) $\beta = 2$; (b) $\beta = 4$; (c) $\beta = 8$. 73

4.6 Ray paths for decay-diffusivity ratio that increases with depth, $m = 1/2$: (a) $\beta = 2$; (b) $\beta = 4$; (c) $\beta = 8$. 74

4.7 Ray paths for decay-diffusivity ratio that increases with depth, $m = 3/2$: (a) $\beta = 2$; (b) $\beta = 4$; (c) $\beta = 8$. 76

4.8 Curvature as a function of ray angle for different powers of m: (a) $\beta = 0$; (b) $\beta = 2$; (c) $\beta = 4$; (d) $\beta = 8$. 78

4.9 Curvature-strength derivative as a function of ray angle for different powers of m: (a) $\beta = 0$; (b) $\beta = 2$; (c) $\beta = 4$; (d) $\beta = 8$. 79

5.1 Steady source in flow along a depth discontinuity with a jump in decay. . . 87

5.2 The variety of rays (continuous and dashed) either side of a discontinuity. . 91

5.3 There are only two possible scaled ray patterns: a) $M < 0$ and b) $M > 0$. . 97

5.4 The two decay-adjusted phase patterns: a) $M < 0$ and b) $M > 0$. 100

5.5 The two transmitted amplitude patterns: a) $M < 0$ and b) $M > 0$. 101

5.6 Reflection coefficient as function of reflection point for three depth ratios. . 103

5.7 Ray approximations to concentration for half-depth far side. 105

5.8 Ray approximation to concentration for double-depth far side. 106

6.1 (a) Variable depth, velocity and diffusivity profiles; (b) Decay profiles for (i) constant decay $m = 0$, (ii) decay that decreases with depth $m = -1/2$, (iii) decay that increases with depth more than the velocity $m = 3/2$. 114

6.2 Crank-Nicolson finite difference solutions at the first and second longitudinal steps. 120

6.3 Error plots of Crank-Nicolson finite difference solutions at the first and second longitudinal steps. 121

6.4 Crandall finite difference solutions at the first and second longitudinal steps. 122

6.5 Error plots of Crandall finite difference solutions at the first and second longitudinal steps. 123

6.6 Concentration contours of midpoint discharge for the Kay exact solution (6.17) versus the numerical computation with (a) no-flux boundary conditions, (b) Zero concentration far boundary condition. 126

6.7 Concentration contours for optimal discharge with (a) no-flux boundary conditions, (b) zero concentration far boundary condition. 129

6.8 Concentration contours of discharge (a) halfway above the midpoint discharge with no-flux boundary conditions, (b) halfway above the midpoint discharge with zero concentration far boundary condition. 130

6.9 Concentration contours of discharge (a) halfway below the midpoint discharge with no-flux boundary conditions, (b) halfway below the midpoint discharge with zero concentration far boundary condition. 131

6.10 Concentration contours for constant decay with decay strength $\Lambda B^2/K = 2$ (a) midpoint discharge, (b) optimal discharge 133

6.11 Concentration contours for decay that decreases with depth and with decay strength $\Lambda B^2/K = 2$ (a) midpoint discharge, (b) optimal discharge. 134

6.12 Concentration contours for decay that increases with depth and with decay strength $\Lambda B^2/K = 2$ (a) midpoint discharge, (b) optimal discharge. 136

List of Tables

3.1 Optimal discharge positions for linearly increasing depth and constant decay. 46

3.2 Discharge positions for decay that decreases with depth. 49

3.3 Discharge positions for decay that increases with depth. 50

Notations and Dimensions

Herein all the mathematical symbols and abbreviations that are used throughout in the thesis are explained in their order of appearance according to the chapters. **Boldface** type means a vector quantity.

Chapter 2

Symbol	Meaning	Dimension
M	change of mass of a dissolved tracer in a given system	ML^{-3}
t	time	T
Δ	a unit change operator	
S	source or sink reaction term	T^{-1}
CV	control volume	L^3
$x\,,y\,,z$	longitudinal, transverse and vertical distances	L
$\chi(x\,,y\,,z)$	concentration or accumulation of contaminant	ML^{-3}
$r(y)$	rate constant	T^{-1}
$\phi_x, \phi_y, \phi_z,$	diffusive fluxes along x, y and z direction	$ML^{-2}T^{-1}$
$\sum \phi_{in}, \sum \phi_{out}$	total fluxes in and out of CV system	$ML^{-2}T^{-1}$
e_x, e_y, e_z	diffusion coefficients along x, y and z direction	L^2T^{-1}
$e_x\frac{\partial \chi}{\partial x}, e_y\frac{\partial \chi}{\partial y}, e_z\frac{\partial \chi}{\partial z}$	turbulent diffusive fluxes along x, y and z directions	$ML^{-2}T^{-1}$
$\mathbf{e}$	diagonal matrix of the diffusion coefficients (e_x, e_y, e_z)	L^2T^{-1}
∇	gradient operator	
$u_x\,,u_y\,,u_z$	velocity components along $x\,,y$ and z directions	LT^{-1}
$\mathbf{u}$	velocity vector of the component velocities (u_x, u_y, u_z)	LT^{-1}
ρ_0	fluid bulk density	ML^{-3}
$a(x,y)\,,b(x,y)$	river bed and surface	L
$h(y)$	local water depth	L
$\lambda(y)$	first-order decay parameter	T^{-1}
$\overline{u\,\chi}$	depth-average	
Ψ	depth-averaged contaminant concentration	M
χ'	contaminant concentration of vertical-deviation	M
u'_x, u'_y	velocities of vertical-deviation along x and y directions	LT^{-1}
r'	vertical deviation of rate constant	T^{-1}
$u(y)$	steady non-reversing velocity	LT^{-1}
κ_x, κ_y	longitudinal and transverse dispersion coeffficients	L^2T^{-1}
B	characteristic width	
H	characteristic average or maximum depth	
L	characteristic longitudinal length	
U	reference flow velocity	
κ	average transverse mixing	L^2T^{-1}

Chapter 3

Symbol	Meaning	Dimension
x, y	longitudinal and transverse distances	L
$c(x, y)$	concentration of contaminant	ML^{-3}
a, b	river bed and surface	L
$h(y)$	local water depth	L
$u(y)$	steady non-reversing velocity	LT^{-1}
$\kappa(y)$	transverse diffusivity	L^2T^{-1}
$\lambda(y)$	first-order decay parameter	T^{-1}
n	integer	
C_n	weights	
$\phi_n(y)$	pollutant modes	ML^{-3}
μ_n	spatial decay rates	
$f(y)$	cross-stream discharge profile	ML^{-3}
Q	volume flux	MT^{-1}
q	contaminant discharge rate	MT^{-1}
B	reference width	
H	reference depth	
U	reference flow velocity	
K	reference transverse mixing	
Λ	decay strength	
m	degree of contaminant decay	

Chapter 4

Symbol	Meaning	Dimension
x, y	longitudinal and transverse distances	L
$c(x, y)$	concentration of contaminant	ML^{-3}
a, b	river bed and surface	L
$h(y)$	local water depth	L
$\mathbf{u}(\mathbf{x}, \mathbf{y})$	vertically-averaged steady velocity vector	LT^{-1}
$D(x, y)$	vertically-averaged effective transverse diffusivity across the flow	L^2T^{-1}
$\lambda(y)$	first-order decay parameter	T^{-1}
∇	horizontal gradient operator	
$A(x, y)$	amplitude	
$\Phi(x, y)$	exponential decay or phase function	
i	an imaginary unit	
s	arc length	L
$\mathbf{t}$	a unit tangent vector	
$f(x, y)$	function	
$\mathbf{k}$	a unit vertical vector	
$\mathbf{n}$	ray normal unit vector	
$K(s)$	curvature	
$\mathbf{K}$	advection-diffusion vector	
$\|\mathbf{M}\|$	advection-diffusion vector and decay-diffusivity ratio parameter	
p	parameter that labels rays	
$J(p, s)$	ray separation	
$\Psi(p)$	constant along rays	
N	number of rays	
n	number count of rays	
R_n	rays	
(x_0, y_0)	source point	
H	reference depth	
Λ	decay strength	
m	degree of contaminant decay-diffusivity ratio	
β	strength of decay-diffusivity ratio	
B	reference width	

Chapter 5

Symbol	Meaning	Dimension
r	depth ratio	
M	non-dimensional parameter for jump in the longitudinal decay	
P	a position factor	
h_i	constant depth	L
λ_i	decay rate	T^{-1}
u_i	longitudinal flow	LT^{-1}
D_i	transverse diffusivity	L^2T^{-1}
$c_i(x\,,y)$	contaminant concentration	ML^{-3}
i	an integer	
$x\,,y$	along-flow and cross-flow distances	L
y_0	lateral distance between the discharge and the discontinuity	L
$A_I\,,A_R\,,A_T$	incident, reflected and transmitted amplitudes	
R	reflection coefficient	
$\Phi_I\,,\Phi_R\,,\Phi_T$	incident, reflected and transmitted phases	
$\hat{\mathbf{x}}$, $\hat{\mathbf{y}}$	unit vectors along the x and y axis	
$\mathbf{t}_I\,,\mathbf{t}_R\,,\mathbf{t}_T$	directional vectors for the incident, reflected and transmitted rays	
$\theta_I\,,\theta_R\,,\theta_T$	incident, reflected and transmitted angles	0
$\tau_I\,\tau_R\,,\tau_T$	ray slopes for the incident, reflected and transmitted rays	
q	volume flux	MT^{-1}
Λ	uniformity in longitudinal decay	
$H(-M)$, $H(M)$	pair of Heaviside functions	
(x_V, y_V)	virtual source	
$T_I\,,T_R$	scaled incident and reflected tangents	
$(X,\,Y)$	non-dimensional scaled longitudinal and transverse distances	
Q	discharge strength	

Chapter 6

Symbol	Meaning	Dimension
x, y	longitudinal and transverse coordinates	L
$c(x, y)$	concentration of contaminant	ML^{-3}
a, b	river bed and surface	L
$h(y)$	local water depth	L
$u(y)$	vertically-averaged steady velocity	LT^{-1}
$\kappa(y)$	vertically-averaged effective transverse diffusivity across the flow	L^2T^{-1}
$\lambda(y)$	first-order decay parameter	T^{-1}
m	degree of contaminant decay	
U	reference flow velocity	
K	reference transverse mixing	
Λ	decay strength	
j	transverse spatial grid	
n	longitudinal spatial grid	
(n, j)	mesh point	
C_j^n	numerical approximation to concentration of contaminant	ML^{-3}
Δx , Δy	grid spacings along the x- and y-axis	
θ, P , Q_w , R	weights	
k	wave number	
J	number of transverse grid points	
Q	volume flux	MT^{-1}
(x_0, y_0)	source point	
$\delta(y - y_0)$	Dirac delta function	
Q'	non-dimensional volume flux	
$x_\star, y_\star$	non-dimensional longitudinal and transverse coordinates	
G	growth or amplification factor	
i	an imaginary unit	
B	reference width	
$\phi_0(y)$	zero or lowest eigenmode	

Chapter 1

General Introduction

1.1 Introduction

The dissertation concerns the investigation of the fate and transport of contaminants in rivers. Contaminant and effluent discharges into rivers are an almost inevitable feature of many agricultural, domestic and industrial practices such as thermal effluents from cooling facilities, contaminant releases from chemical processing plants, and sediment movement by local scouring. These discharges have the potential to tax the natural cleansing action of waterways to the point where serious environmental consequences may result. To this end, there has been growing international public concern and increased awareness of the concentration peaks associated with the discharges by river managers, engineers and scientists. Optimal strategies for discharging contaminants, general details and guidelines of effective models used for monitoring flow, water quality, contaminants transport and concentration predictions are available in literature. Particular emphasis is focused on the influence of physical master variables in the hydro-environmental modelling of rivers to minimize the concentration peaks of the discharged contaminants. For a minimum concentration it implies that the effects of pollution are minimized when the maximum concentration is minimized (Giles, 1995).

Research studies reported in literature (Munro, 1975; Gould and Munro, 1981) indicated that one measure of the fate of a contaminant is the knowledge of the decay rate. These studies have shown that decay rates of total and fecal coliform indicator bacteria vary spatially and temporally in coastal waters between T_{90} values of less than 1 hour to more than 100 hours. Further applications of the use of fecal coliform as indicator bacteria to quantify the degree of contamination of natural waters has been widely used for the monitoring and formulation of discharge outfalls and waste stabilization pond designs (Sarikaya and Saatci, 1987; Saqqar and Pescod, 1992; Mayo, 1995; Falconer and Lin, 2003). Examples from these studies suggested the significance and sensitivity of bacterial pollution at the shore to the bacterial decay rate.

The survival of the contaminants in the aquatic environment depends upon the ability to

tolerate a set of alien biological, physical and chemical conditions. The most important factors among others considered to be controlling the decay rate are dispersion, temperature, solar intensity, and PH of the environment (Mayo, 1989). Investigations using pilot plant experiments on bactericidal action of solar radiation in waste stabilization pond revealed that the decay or die-off rate of fecal coliform vary significantly with the pond depth (Sarikaya *et al.*, 1987; Sarikaya and Saatci, 1988; Mayo, 1989). The e-folding times for fecal coliform incubated at the pond surface, a depth of $1m$ and $1.5m$ respectively were found to be 14.46, 64.86 and 75 hours (Mayo, 1989). For a heat diffusion problem into a sea with a sloping bed with the typical depths $1m$ and $1.5m$ resulted respectively the e-folding times 58.33 and 87.5 hours (Macqueen and Preston, 1983; Mebine and Smith, 2006). Therefore, the testament from these examples imply that there is a qualitative and quantitative evidence that decay processes and rates vary significantly from one pollutant to another and involve site hydrography features and many other functions which are yet to be modelled. Mathematical modelling and understanding of the optimal mixing processes involving variability of contaminant decay would enhance insights into applicable criteria, critical conditions and allowable dilution for water quality standards in the natural environment.

1.2 Concept and definition of the Research

The subject 'Minimum Environmental Impact Discharging' herein referred to as **MEID** is defined as optimal mitigation processes in ameliorating water quality impairments and the ecological effects of emitting contaminants into the environment of rivers. The investigation utilises mathematical models and numerical algorithms of depth-averaged variable coefficients advection-diffusion-reaction equations for describing the variations of the pollutant concentrations. By their nature, the hydraulic geometry (width, depth, and velocity) of rivers are not constant; these variables typically increase downstream. In consequence, the mathematical models describing the flow of contaminants through rivers are quite involved. Thus, it is not surprising that many simplifying assumptions are made in the mathematical

models, and that there are important areas of the subject which are controversial and not yet modeled satisfactorily.

1.3 The Objective of the Research

Given that oil, chemical and biological waste will continue to be discharged into rivers, it is clearly apparent that rivers serve as media of waste discharges in spite of their economic importance to man and the livelihood of aquatic life. The questions posed by this work are that does it matter (a) where, and (b) what is discharged? For small discharges that do not change the flow in a non-branching straight section of a river, this work is intended to answer these questions, and proffer measures for optimal transport of contaminants in rivers. It is appropriate to note here that solutions to mitigate potential environmental impacts can incorporate optimal measures to avoid, reduce or remedy the impact in the design and formulation of rational policies towards the management of rivers. Therefore, the identification and clarification of the physical mechanisms that will lead to

- the attenuation of contaminants,
- the determination of the mixing or diffusion centre of a channel for optimal discharges, and
- optimal measures in order to enhance contaminant transport

are much needed research endeavours for environmentally aware waste discharges in rivers. Thus, the main objective of this work is concerned with the development of mathematical ideas and computer programmes to make direct computations of best discharging for rivers principally considering the effects of variability of loss mechanisms of contaminants.

Knowledge of the sources, interactions, and effects of water pollutants is essential for controlling pollutants in an environmentally safe and economically acceptable manner. In the following, a brief overview of related literature of sources and effects of pollutants is given.

1.4 An Overview of the Sources and Effects of Pollutants

There are a variety of sources of contaminants which ultimately impair our rivers, and most of these are organic solvents and petroleum hydrocarbons originating from leaking underground storage tanks, ruptured pipelines, surface spills, hazardous waste landfills and disposal sites, and as such many authors and researchers have investigated their origin and effects (Jorgenson and Johnson, 1989; Pereira *et al.*, 1996; Larkin and Hall, 1998; Mason and Sullivan, 1998; Fisher *et al.*, 1999; Fyrillas, 2000; Gromaire-Mertz, 2000; Manahan, 2000; Nebel and Wright, 2000; Ahyerre, 2001; Ahyerre *et al.*, 2001; Lee and Bang, 2000; EPA, 2003). However, early investigations of streams, rivers or estuaries by limnologists and hydrobiologists were directed largely at classification and description, with primary attention given to local phenomena such as water temperature, flow regime, water chemistry and substrate as factors affecting resident flora and fauna (Rhodes, 1950; Stommel and Farmer, 1952). As knowledge grew and the works of hydrologists, soil scientists and researchers in related disciplines were integrated into the understanding of flowing waters, it became evident that, when considered as ecological units, streams and or rivers could not be separated from their watersheds (Hynes, 1975; Fisher, 1986). Studies have shown that with the exception of a small percentage of material decomposed and oxidized in the terrestrial environment, most materials ultimately received and transported by streams and or rivers are deposited from their catchments (Mullholand and Watts, 1982). Therefore, any conceivable noxious or otherwise deleterious material, action, process or organism, whether input at the outer watershed limits or directly into a flowing channel, may have profound effects on the ecosystem of rivers (Minckley and Kubly, 2003). Consequently, site investigations and selection of discharge sites of pollutants become vital in order to control, reduce, or avoid the risk of pollution. To this end, hydrographic, engineering and theoretical aspects of studies have been carried out by various researchers (Oakley, 1981; Willis, 1981; and Smith, 1981, 1982) in an attempt to determine where appropriate to put a discharge.

In assessing the effects or impact of a pollutant it is necessary to have a clear objective,

that is, to know the target it is desired to protect and the volume of the environmental concentration of the pollutant that could be tolerated by that target. To some extent this could be done for most recognized pollutants, albeit with varying degrees of precision. It is pertinent to emphasize here that the pollutants are directly or indirectly introduced by man into the marine environment (including streams, rivers and estuaries) resulting in such deleterious effects as harm to living resources, hazards to human health, hindrance to marine activities such as fishing, impairing of quality for use of water. Investigations have shown that the most common pollutant in terms of quantity is domestic sewage. Sewage disposal have been reported to constitute environmental and health risks (Akinluyi and Odeyemi, 1984). In the marine environment the aforementioned poses two potential pollution problems: microbiological contamination and a high Biological Oxygen Demand (BOD). The former leads to health hazards of enterococcus density in marine bathing waters and swimming-associated rate of gastroenteritis (Cabelli, 1981). On the other hand, the high BOD leads to serious ecological damage. We note here that sewage is primarily organic in nature and therefore subject to bacterial decay. As a result of this bacterial activity, the oxygen concentration in the water is reduced, thereby starving aquatic life of the oxygen it needs. Another inevitable consequence is the breakdown of proteins and other nitrogenous compounds, releasing hydrogen sulphide and ammonia, both of which are potentially toxic to marine organisms in low concentrations (MCS, 2003). Baker *et al.* (2003), using recent advances in fluorescence spectrophotometer enabled the detection and analysis of river dissolved organic matter, and indicated that sewage pollution is by far the greatest volume of waste discharged to the marine environment.

Another cause of ecological damage is the dumping of sewage sludge at the sea. Dependent on the hydrography, sludge can smother the benthos, increase biomass, decrease species biodiversity and increase heavy metal concentrations (MCS, 2003). Discharges that affect both water quality and habitat quality can have complex effects on flowing communities. Nedeau *et al.* (2003) studied the effect of an industrial effluent on an urban stream

benthic community: water quality versus habitat quality, and illustrated the need for careful consideration of habitat quality and water quality in restoration programmes.

To predict pollution levels for establishing an optimum management strategy for water quality control, it is important that specific criteria of acceptability for any given situation be formulated. For instance, effluent discharges in natural water systems such as river channels, one of the basic policies is keeping concentration peaks at certain locations minimum. And the criterion behind such a strategy is a measure of the degree of mixing. In the following, we consider an overview of mixing and its importance.

1.5 An Overview of Mixing and its Importance

Mixing is simply the tendency towards a uniform distribution. In other words, mixing tends to reduce concentration differences between fluid particles or substances. The concept of mixing appears in both industry and nature and its development and importance has cut across various fields of research. Mixing processes are found in geophysical and astrophysical flows, which influence a wide range of dynamical systems (Rees, 2001). Mixing is intimately connected with turbulence, earth and natural sciences, and various branches of engineering. Various examples of mixing are found in literature. The knowledge of mixing processes is of fundamental importance in weather prediction and in chemical engineering. The importance of mixing is as well considered in the analysis of effluent streams conveying a variety of chemicals (Neely, 1982).

The study of mixing processes in natural streams is important in regulating pollution sources as well as evaluating the risks involved in accidental contaminant releases. Research on mixing processes includes theoretical and numerical modelling, as well as experimental and observational studies. At the largest scale of tens to hundreds of kilometres, studies of mixing longitudinal processes and characteristics have dated several decades back (Arons and Stommel, 1951; Francis *et al.*, 1953; Preddy, 1954; Kent and Pritchard, 1959; Pritchard, 1960; Bowden, 1963; Hansen, 1965; Yotsukura *et al.*, 1970; Beltaos, 1978; Beltaos and

Anderson, 1979). At the intermediate scale of hundreds of metres to tens of kilometres transverse mixing has a shorter history (Fischer, 1967; Okoye, 1970; Holley, 1971; Holley *et al.*, 1972; Yotsukura and Cobb, 1972; Sayre and Yeh, 1973; Engmann and Kellerhals, 1974; Sium, 1975; Yotsukura and Sayre, 1976; Lau and Krishnappan, 1977; Meyer, 1977; Beltaos, 1978, 1980; Lau and Krishnappan, 1981).

The mixing of an effluent discharged into a river can be divided into several stages. Initially, mixing with the river water is caused by the momentum and buoyancy of the plume itself and is relatively unaffected by the flow in the river. This is called the **initial mixing zone.** However, within a few metres, the plume is bent over the river current and turbulent motions in the river enhance mixing. Because rivers are generally much shallower than they are wide, the plume mixes over the depth of the river before it mixes across the width of the river. The river is divided into three fields: the **near field** which extends from the point of discharge to the point at which mixing is complete throughout the depth; the **intermediate field** within which transverse mixing across the river occurs; and the **far field** downstream of the point at which transverse mixing is complete (see Figure 1.1; Marks, 1996).

A comprehensive and relatively detailed account of flow models of river mixing reported by Rutherford (1994) showed that transverse mixing is arguably more important in water quality management than either vertical or longitudinal mixing, especially when dealing with the discharge of water from point sources or the mixing of tributary inflows.

Quantitative predictions of the rates of mixing of tracers (principally neutrally-buoyant tracers) in rivers are needed in a variety of situations including the preliminary design of outfalls, the impact assessment of discharges, water resource planning, and research on biological processes in rivers. Such predictions are mostly carried out using mathematical models and optimization techniques.

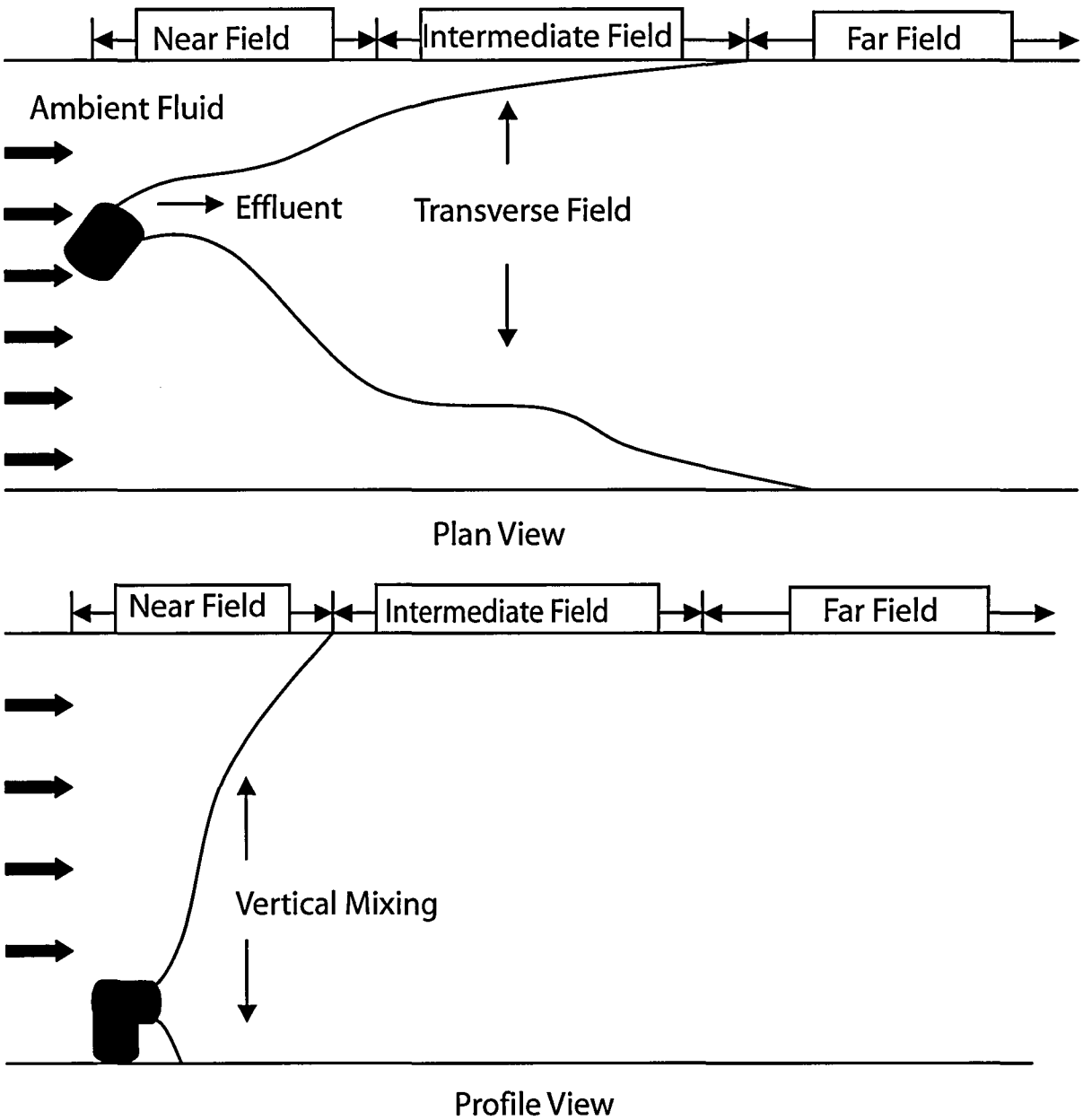


Figure 1.1: Plan and Profile schematics of the spreading of a discharge into a river.

1.6 Structure of Mathematical Models

When a tracer is injected into a stream, its concentration will generally vary with respect to both space and time. Certain specialized problems still remain within the realm of physical modelling. However, the use of mathematical models has become commonplace. The basic tool available for predicting the concentration is the principle of conservation of tracer mass, in differential form. In its most general form, the resulting partial differential equation involves formidable difficulties; even a numerical solution would be so laborious as to be impractical, at best. The increased efficiency of digital computers has triggered a strong research effort in the refinement of mathematical models. While offering almost unlimited flexibility in the simulation of various alternatives, these models have the additional appeal of smaller developments and operating costs.

Mathematical models of river flow exist at various levels of sophistication. The detailed description of flow phenomena is best accomplished in a three-dimensional spatial framework; however, the complexity of a formulation in three dimensions often requires tremendous amounts of computational effort. Where valid, the simplification to a two-dimensional representation can offer a considerable reduction in complexity and expense. This involves an integration of the three-dimensional equations of fluid dynamics over flow depth. Hansen (1962) is credited for being the first to outline the depth-averaged two-dimensional formulation. Since after the pioneering work of Hansen, depth-averaged formulation to flow problems has been employed by several other researchers to diverse areas such as erosion and accretion processes, heat diffusion, contaminant dispersion and mixing problems. Leendertse (1967, 1970) followed Hansen in applying two-dimensional modelling concepts to the study of estuarine and coastal hydrodynamics. McGuirk and Rodi (1978) developed a depth-averaged velocity and contaminant distribution model of open channel flow, which described the recirculation region immediately downstream of a side discharge into a flowing river. Holley and Nerat (1983) used depth-averaged dispersion of an inert, neutrally buoyant contaminant in steady river flow to describe field calibration of stream-

tube dispersion model. Holley and Nerat's work, which was based on engineering study, used depth-averaged stream-tube dispersion model of Holley (1975). Yotsukura and Sayre (1976) extended the work of Yotsukura and Cobb (1972), which considered the transverse diffusion of solutes in natural streams using depth-averaged advection-diffusion equation to the study of transverse mixing in natural channels taken into account orthogonal curvilinear (natural) coordinate system. The transformed mixing equation obtained by Yotsukura and Sayre unified and generalized essential concepts of several existing models which were successfully used for simulating steady state transverse mixing in irregular natural channels.

Wastes are commonly discharged steadily from point sources and it is important to choose the correct location for the outfall. The littoral zone in rivers contains more abundant plant and animal communities than the main channel and a commonly encountered problem is to choose the optimum source location, which minimizes bankside concentrations. There have been several theoretical studies of contaminant discharges in river flows with a view to finding the optimal site of discharge. The optimal choice is the best position of discharge, which minimizes the transverse mixing distance of the contaminant plume. This is an important measure in controlling water pollution problems by large-scale processes and sewage works, which are designed to avoid intermittent high-level discharges, and instead are aimed at steady low-level discharges (Smith, 1982). For a continuous point release in a river Smith (1982) finds that the optimal site is somewhere near the middle of such a channel; this keeps the contaminant plume formed away from the banks as long as possible. This is the same thing as saying that the best discharge site is the location where complete mixing is achieved as quickly as possible. For the optimal placement of underwater outfalls Martínez *et al.* (2000) considered a control problem arising in the process of waste water purification. Alvarez-Vázquez *et al.* (2002) made an extension of Martínez *et al.* model and formulated a mathematical analysis of the optimal location of wastewater outfalls. Using optimal control techniques, where the control is the position of the outfalls, Alvarez-Vázquez *et al.* demonstrated the evolution of the optimal locations somewhere in the deeper water

for a coastal beach. In the case of sudden or instantaneous contaminant release, the optimal discharge locations are quite different. For steady flows in rivers Smith (1981, 1984) and Daish (1985) have shown that the cross-stream location of an instantaneous contaminant release can have a persistent and marked effect upon the concentrations experienced far downstream.

The dispersion of pollutants in rivers is greatly affected by the depth topography. Kay (1987) discussed the importance of depth topography and modelled the effect of cross-stream depth variations upon dispersion of contaminants, and suggested that outfall of an effluent discharge should be kept away from the shoreline for the avoidance of it being affected by the contaminants. In the study of dispersion of methanol in natural rivers, Jamali *et al.* (2005) reported that the hydraulic geometry (width, depth, and velocity) are not constant and showed their effects. They used their solution to assess the potential environmental impacts of methanol releases into a hypothetical river. The resulting downstream concentrations of methanol were considerably lower than those calculated assuming constant hydraulic geometry. This points to the importance of varying coefficients in the study of the fate and transport of contaminants in rivers.

One critical element in designing management strategies for rivers is the understanding of the dynamics of perturbations introduced into the water. After the initial discharge of contaminants into the rivers, physical processes such as advective transport, dispersion and contaminant decay mechanisms play important roles in determining the movement and change in concentration of contaminants. Thus, they influence decision on methods used for detection and remediation. At present, many uncertainties exist in mathematical modelling of depth-averaged variable coefficients advection-diffusion with variable decay mechanisms in river flows. Several mathematical models, which exhibit decay of pollutants, are present in literature (Nassehi and Bikangaga, 1993; Bikangaga and Nassehi, 1995; Smith, 2000; Yoo *et al.*, 2003; Araújo *et al.*, 2005). However, no comprehensive analysis of the effects of the variability of decay with depth in the advection-diffusion of pollutants has been attempted

in conjunction with numerical models. Hence, it is no gainsaying that in order to present managerial policies for water quality control, it is vital to have knowledge of the effects of the variability of decay of pollutants in the context of **MEID**. This is the distinctive centre point of the present research.

1.7 Organisation of the Thesis

This thesis covers the theoretical, numerical and applications of **MEID** using mathematical models. Having emphasized the challenging nature of the subject, let us also stress that it is possible to make good progress provided we accept and acknowledge the limitations of our mathematical models. In this introductory chapter, we have briefly examined the preliminary concepts of the subject and review of related literature. It must be emphasized here that no attempt at completeness has been made in terms of the references.

The second chapter is concerned with the relevant physical- mathematical formulations and various functional relationships underlying the fate and transport of contaminants.

The third chapter considers the explanation and mathematical definition of the diffusion centre of a river. The method of eigenmodes is employed which eventually introduces diffusion longitudinal and pollutant modes. Several test cases are considered given benchmark analytical results for the determination of the diffusion centre.

The fourth chapter provides ray approximation for steady discharges. The derivations give formulae for the phase function, the curvature and the amplitude factor. Ray tracing algorithms are constructed to compute the ray curvature numerically.

The fifth chapter considers the investigation of the effects of diffusivity-velocity augmented fractional change in contaminant decay upon contaminant dispersion for steady discharges in a vertically well-mixed current in rivers with discontinuous variations in depth. The method of steady-state response to a propagating incident wave technique was applied to derive approximate concentration formulae.

The sixth chapter gives advection-diffusion-reaction finite difference, implicit numerical

schemes. The numerical methods are applied to achieve high-order accuracy with stability over a wide range of parameters in rivers.

The seventh chapter is concerned with the conclusions and recommendations for further work.

1.8 Concluding remarks

The sciences do not try to explain, they hardly even try to interpret, they mainly make models. By a model is meant a mathematical construct which, with the addition of certain verbal interpretations, describes observed phenomena. The justification of such a mathematical construct is solely and precisely that it is expected to work. – **John Von Neumann** (1903 - 1957)

The motivation for the development of the concepts within this work is to provide realistic models of solute transport in rivers with special considerations to the behaviour of reactive flows which can be described by Partial Differential Equations of advection-diffusion-reaction models. The chapter that follows gives the mathematical formulations of the equations governing the fate and transport of contaminants.

1.9 References

1. Akinyluyi, T. O. and Odeyemi, O.: 1984, Human waste disposal and faecal pollution of the River Niger Delta Waters. *Water International*, **9**, 1, 37 - 41.

2. Ahyerre, M.: 2001, Deposits in sewer networks, a significant source of storm water pollution. *Houille Blanche*, **6-7**, 21 - 27.

3. Ahyerre, M., Oms, C. and Chebbo, G.: 2001, The erosion of organic solids in combined sewers. *Water Science and Technology*, **43**, 3, 95 -102.

4. Alvarez-Vázquez, L. J., Martínez, A., Rodríguez, C. and Vázquez-Méndez, M. E.:

2002, Mathematical analysis of the optimal location of wastewater outfalls. *IMA J Appl Math*, **67**, 1, 23 - 39.

5. Araújo, A., Ferreira, J. A. and de Oliveira, P.: 2005, The role of abstract numerical properties in the change of character of reactive flows. *J. Math. Fluid Mech.*, **7**, S141 - S163.

6. Arons, A. B. and Stommel, H.: 1951, A mixing-length theory of tidal flushing. *Trans. Am. Geophys. Union*, **32**, 419 - 421.

7. Baker, A., Inverarity, R., Charlton, M., and Richmond, S.: 2003, Detecting river pollution using fluorescence spectrophotometry: case studies from the Ouseburn, NE England. *Environmental Pollution*, **124**, 57 - 70.

8. Beltaos, S.: 1978, Transverse Mixing in Natural Streams. *Alberta Research Council Internal Report SWE-78/0*, Albert Research Council, Alberta, Canada.

9. Beltaos, S.: 1978, Mixing Processes in Natural Streams. *Proceedings of the Transport Processes and River Modelling Workshop*, National Water Research Institute, Burlington, Ontario, Canada.

10. Beltaos, S.: 1980, Transverse Mixing Tests in Natural Streams. Journal of the Hydraulics Division, ASCE, **106**, HY10.

11. Beltaos, S. and Anderson, M.D.: 1979, Mixing Characteristics of the North Saskatchewan River Below Edmonton-Part I. *Alberta Research Council Internal Report SWE-79/01*, Alberta, Canada.

12. Bikangaga, J. H. and Nassehi, V.: 1995, Application of Computer Modelling Techniques to the Determination of Optimum Effluent Discharge Policies in Tidal Water Systems. *Wat. Res.*, **29**, 10, 2367 - 2375.

13. Bowden, K. F.: 1963, The mixing processes in a tidal estuary. *Int. J. Air Water Pollut.*, **7**, 343 - 356.

14. Cabelli, V. J.: 1981, A health effects data base for the derivation of microbial guidelines for municipal sewage effluents. Coastal Discharges-engineering aspects and experience. *Proceedings of the Conference organized by the Institution of Civil Engineers and held in London on 7-9 October 1980.*

15. Daish, N. C.: 1985, Optimal discharge profiles for sudden contaminant releases in steady, uniform open-channel flow. *J. Fluid Mech.*, **159**, 303 - 321.

16. Falconer, R. A. and Lin, B. : 2003, Hydro-environmental modelling of riverine basins using dynamic rate and partitioning coefficients. *Int. J. River Basin Management*, **1**, 81- 89.

17. Fischer, H. B.: 1967, Transverse mixing in a sand-bed channel. *U.S. Geol. Surv. Prof. Pap.* 575-D, D267 - 72.

18. Fisher, S. G.: 1986, Structures and dynamics of desert streams. Pages 119139 in W. G. Whit-ford (ed.), Pattern and Process in Desert Ecosystems. UNM Press, Albuquerque.

19. Fisher, T. S., Hayward, D. G., Stephens, R.D., and Stenstorm, M.K.: 1999, Dioxins and furans in runoff. *J. Envir. Engrg.*, **125**, 185 - 191.

20. Francis, J. R. D., Stommel, H., Farmer, H. G., and Parson, D. Jr.: 1953, Observations of mixing processes in a tidal estuary. *Woods Hole Oceanogr. Inst., Ref. No.* 22 - 53.

21. Fyrillas, M. M.: 2000, Advection-dispersion mass transport associated with a non-aqueous-phase liquid pool. *J. Fluid Mech.*, **413**, 49 - 63.

22. Giles, R. T.: 1995, Optimal strategies for discharging pollutants into narrow estuaries. *Water Research*, **29**, 2, 563- 569.

23. Gould, D. J. and Munro, D.: 1981, Relevance of Microbial Mortality to outfall Design. Coastal Discharges-engineering aspects and experience. *Proceedings of the Conference organized by the Institution of Civil Engineers and held in London on 7-9 October 1980.*

24. Gromaire-Mertz, M.C.: 2000, Urban wet weather pollution in combined sewer networks-characteristics and origin. *Houille Blanche*, **2**, 66 - 70.

25. Hansen, W.: 1962, Hydrodynamic Methods Applied to Oceanographic Problems. *Proceedings of the Symposium on Mathematical-Hydrodynamical Methods of Physical Oceanography*, Institute fur Meereskunde der Universitat Hamburg, West Germany, 25 - 34.

26. Holley, E. R.: 1971, Transverse mixing in rivers. *Rep. S132*, Delft Hydraul. Lab., Delft, Netherlands.

27. Holley, E. R., Siemons, J. and Abraham, G.: 1972, Some Aspects of Analyzing Transverse Diffusion in Rivers. *Journal of Hydraulic Research*, International Association for Hydraulic Research, Delft, the Netherlands, **10**, 1, 27 - 57.

28. Holley, F. M., Jr. and Nerat, G.: 1983, Field Calibration of Stream-Tube Dispersion Model. *Journal of Hydraulic Engineering*, ASCE, **109**, 11, 1455 - 1470.

29. Holley, F. M., Jr.: 1975, Two Dimensional Mass Dispersion in Rivers. *Hydrology Paper No. 78*, Colorado State University, Fort Collins.

30. Hynes, H. B. N.: 1975, The streams and its valley. *Verh. Internat. Verein. Limnol.*, **19**, 115.

31. Jamali, M., Lawrence, G. A. and Maloney, K.: 2005, Dispersion in varying-geometry rivers with application to methanol releases. *Journal of Hydraulic Engineering*, **131**, 5, 390 - 396.

32. Jorgenson, S.E. and Johnson, I.: 1989, Principles of Environmental Science and Technology. Second revised Edition, Elsevier Science Publishers B.V..

33. Kay, A.: 1987, The Effect of Cross-Stream Depth Variations upon Contaminant Dispersion in a Vertically Well-mixed Current. *Estuarine, Coastal and Shelf Science*, **24**, 2, 177 - 204.

34. Kent, R. E. and Pritchard, D. W.: 1959, A test of mixing length theories of in a coastal plain estuary. *J. Mar. Res.*, **18**, 62 - 72.

35. Larkin, G. A. and Hall, K. J.: 1998, Hydrocarbon pollution in the Brunette River watershed. *Water Quality Research Journal of Canada*, **33**, 73 - 94.

36. Lau, Y. L. and Krishnappan, B. G.: 1977, Transverse Dispersion in Rectangular Channels. *Journal of the Hydraulics Division*, ASCE, **103**, HY10, Proc. Paper 12294, 1173 - 1189.

37. Lau, Y. L. and Krishnappan, B. G.: 1981, Modeling Transverse Mixing in Natural Streams. *Journal of the Hydraulics Division*, ASCE, **107**, HY2.

38. Lee, J. H. and Bang, K.W.: 2000, Characterization of urban storm water runoff. *Water Research*, **34**, 1773-1780.

39. Leendertse, J. J.: 1967, Aspects of a Computational Model for Long-Period Water Wave Propagation. RM-5294-PR, The Rand Corporation, Santa Monica, Calif.

40. Leendertse, J. .J.: 1970, A water-Quality Simulation Model for Well-Mixed Estuaries and Coastal Seas, Vol. I, Principles of Computation. RM-6230-RC, The Rand Corp., Santa Monica, Calif.

41. Macqueen, J. F. and Preston, R. W.: 1983, Cooling water discharges into a sea with sloping bed. *Water Research*, **17**, 4, 389 - 395.

42. Manahan, S. E.: 2000, Environmental Chemistry. Seventh Edition, CRC Press LLC.

43. Marks, B. J.: 1996, Initial Dilution of a Horizontal Jet in a Strong Current. *M. Sc. thesis*, University of British Columbia, Vancouver, B.C.

44. Martínez, A., Rodríguez, C., Vázquez-Méndez, M.E.: 2000, A control problem arising in the process of waste water purification. *Journal of Computational and Applied Mathematcs*, **114**, 1, 67 - 79.

45. Mason, R. P. and Sullivan, K. A.: 1998, Mercury and methylmercury transport through an urban watershed. *Water Research*, **32**, 321 - 330.

46. Mayo, A. W.: 1989, Effect of pond depth on bacterial mortality rate. *J. Envir. Engrg.*, **115**, 5, 964 - 977.

47. Mayo, A. W.: 1995, Modeling coliform mortality in waste stabilization ponds. *J. Envir. Engrg.*, **121**, 2, 140 - 152.

48. McGuirk, J. J. and Rodi, W.: 1978, A Depth-Averaged Mathematical Model for the Near Field of Side Discharges into Open Channel Flow. *J. Fluid Mech.*, **86**, 4, 761 - 781.

49. Mebine, P. and Smith, R.: 2006, Effects of contaminant decay on the diffusion centre of a river. *Environmental Fluid Mechanics*, **6**, 101 - 114.

50. Minckley, W. L. and Kubly, D. M.: 2003, Impacts of Environmental Stressors on Streams and Rivers. *http://www.google.com/search.*

51. Mullholand, P. J. and Watts, J. A.: 1982, Transport of organic carbon to the oceans by rivers of North America: A synthesis of existing data. *Tellus*, **34**, 176186.

52. Munro, D.: 1975; Observed and predicted coliform distribution near a sea outfall. *Discharge of Sewage from Sea Outfalls* (ed. A. L. H. Gameson). Pergamon Press, 353 - 362.

53. Nebel, B. J. and Wright, R. T.: 2000, Environmental Science: the way the world works. Seventh Edition, Upper Saddle River, NJ 07458.

54. Nedeau, E. J., Merritt, R. W. and Kaufman, M. G.: 2003, The effect of an industrial effluent on an urban stream benthic community: water vs. habitat quality. *Environmental Pollution*, **123**, 1 - 13.

55. Neely, W. B.: 1982, The definition and use of mixing zones. *Envir. Sci. and Technol.*, **16**, 518A.

56. Oakley, H. R.: 1981, Site investigation and selection hydrographic aspects. Coastal Discharges-engineering aspects and experience. *Proceedings of the Conference organized by the Institution of Civil Engineers and held in London on 7-9 October 1980.*

57. Okoye, J. K.: 1970, Characteristics of transverse mixing in open-channel flows. Rep. KH-R-23, Keck Lab., Calif. Inst. of Technol.

58. Overstreet, R. and Galt, J. A.: 1995, Physical Processes Affecting the Movement and Spreading of Oils in Inland Waters. NOAA/Hazardous Materials Response and Assessment Division Seattle, Washington; HAZMAT Report 95-7.

59. Pereira, W. E., Domagalski, J. L., Hostettler, F. D., Brown, L. R. and Rapp, J. B.: 1996, Occurrence and accumulation of pesticides and organic contaminants in river sediment, water and clam tissues from the San Joaquin River and tributaries, California. *Environmental Toxicology and Chemistry*, **15**, 172 - 180.

60. Preddy, W. S.: 1954, The mixing and movement of water in estuary of the Thames. *J. Mar. Biol. Assoc. UK*, **33**, 645 - 662.

61. Pritchard, D. W.: 1960, The movement and mixing of contaminants in tidal estuaries. *Proc. Int. Conf. Waste Disposal Mar. Environ.*, 1st edition E. A. Pearson, 512 - 525. London: Pergamon.

62. Rees, J. M.: 2001, Mixing Processes in Geophysical and Astrophysical Flows. *Environmental Fluid Mechanics*, **1**, 333 - 343.

63. Rhodes, R. F.: 1950, Effect of Salinity on Current Velocities, From: Evaluation of Present State of Knowledge of Factors Affecting Tidal Hydraulics and Related Phenomena. *U. S. Army Corps. Eng., Comm. Tidal Hydraulic., Rep. No. 1.*

64. Rutherford, J. C.: 1994, River Mixing. John Wiley and Sons Ltd., England.

65. Saqqar, M. M. and Pescod, M. B.: 1992, Modelling coliform reduction in wastewater stabilization ponds. *Water Sc. Tecnol.*, **26**, 7 - 8, 1667 - 1677.

66. Sarikaya, H. Z., Saatci, A. M. and Abdulfattah, A. F.: 1987, Effect of pond depth on bacteria die-off. *J. Envir. Engrg.*, **113**, 6, 1350 - 1362.

67. Sarikaya, H. Z. and Saatci, A. M.: 1987, Bacterial die-off in waste stabilization ponds. *J. Envir. Engrg.*, **113**, 2, 366 - 382.

68. Sarikaya, H. Z. and Saatci, A. M.: 1988, Optimum pond depths for bacterial die-off. *Water Research*, **22**, 8, 1047 - 1054.

69. Smith, R.: 1981, The importance of discharge siting upon contaminant dispersion in narrow rivers and estuaries. *J. Fluid Mech.*, **108**, 43 - 53.

70. Smith, R.: 1982, Where to put a steady discharge in a river. *J. Fluid Mech.*, **115**, 1 - 11.

71. Smith, R.: 2000, Optimal and near-optimal advection-diffusion finite-difference Schemes II. Unsteadiness and non-uniform grid. *Proc. R. Soc. Lond.* A, **456**, 489 - 502.

72. Stommel, H. and Farmer, H. G.: 1952, On the nature of estuarine circulation, (Chaps. 1, 2, 3, 4, 7). *Woods Hole Oceanogr.Inst. Ref. Nos.* 52 - 51, 52 - 63, 52 - 88.

73. The Marine Conservation Societys (MCS) Good Beach Guide (2003), Sewage Pollution. *http://www.goodbeachguide.co.uk/.*

74. Tennekes, H. and Lumley, J. L.: 1972, A First Course in Turbulence. Cambridge, Mass: MIT Press.

75. United States Environmental Protection Agency (EPA) (2003), Vessel Discharges. *http://www.epa.gov/owow/oceans/regulatory/vesseldisch.html.*

76. Willis, D. A.: 1981, Site investigation and selection engineering aspects. Coastal Discharges-engineering aspects and experience. Proceedings of the Conference organized by the Institution of Civil Engineers and held in London on 7 - 9 October 1980.

77. Yoo, M. K., Cho, S. W., and Jun, K. S.: 2003, Unsteady Dispersion of Nonconservative Pollutants in Natural Rivers. *www.kfki.baw.de/conferences/ICHE/2000-Seoul/pdf/251/RAP-291.PDE*

78. Yotsukura, N., Fischer, H. B., and Sayre, W. W.: 1970, Measurement of Mixing Characteristics of the Missouri River Between Sioux City, Iowa, and Plattsmouth, Nebraska. *U. S. Geological Survey Professional Paper 1899*-G, U. S. Geological Survey, Washington, D. C.

79. Yotsukura, N. and Cobb, E. D.: 1972, Transverse Diffusion of Solutes in Natural Streams. *U. S. Geological Survey Professional Paper 582*-C, U. S. Geological Survey, Washington, D. C.

Chapter 2

Mathematical Formulations

2.1 Introduction

The present chapter provides a brief and, hopefully transparent, formulation of the partial differential equations of advection-diffusion-reaction describing the fate and transport of contaminants. The presentation follows closely the work of Rutherford (1994), though modifications necessary for treating contaminant decay have been introduced. In establishing the mathematical model, we shall adopt the general law of conservation, on which all phenomenological descriptions of change in the physical world are based.

2.2 Law of conservation

Let M denotes a change in mass of a dissolved tracer in a given system. Then the Conservation of Mass requires that

$$\frac{\partial M}{\partial t} = \sum \phi_{in} - \sum \phi_{out} \pm S, \tag{2.1}$$

where S is a source or sink reaction term. The relevance of equation (2.1) in this study is seen in the inclusion of the reaction term. To derive the governing equation (2.1), consider the control volume (CV) depicted in the rectangular Cartesian coordinate system, Figure 2.1, where the x-axis is measured in the longitudinal (downstream) or the flow direction, y-axis is measured transversely (cross-stream), and z-axis is measured vertically upwards.

2.3 Advection-diffusion-reaction equation

The standard advection-diffusion-reaction model deals with time evolution of chemical or biological species in a flowing medium such as water or air. The mathematical equations describing this evolution are partial differential equations that can be derived from mass balances. If we consider a parcel of fluid that moves at a mean velocity through the system (Figure 2.1), then the average concentration or accumulation of the quantity χ considered

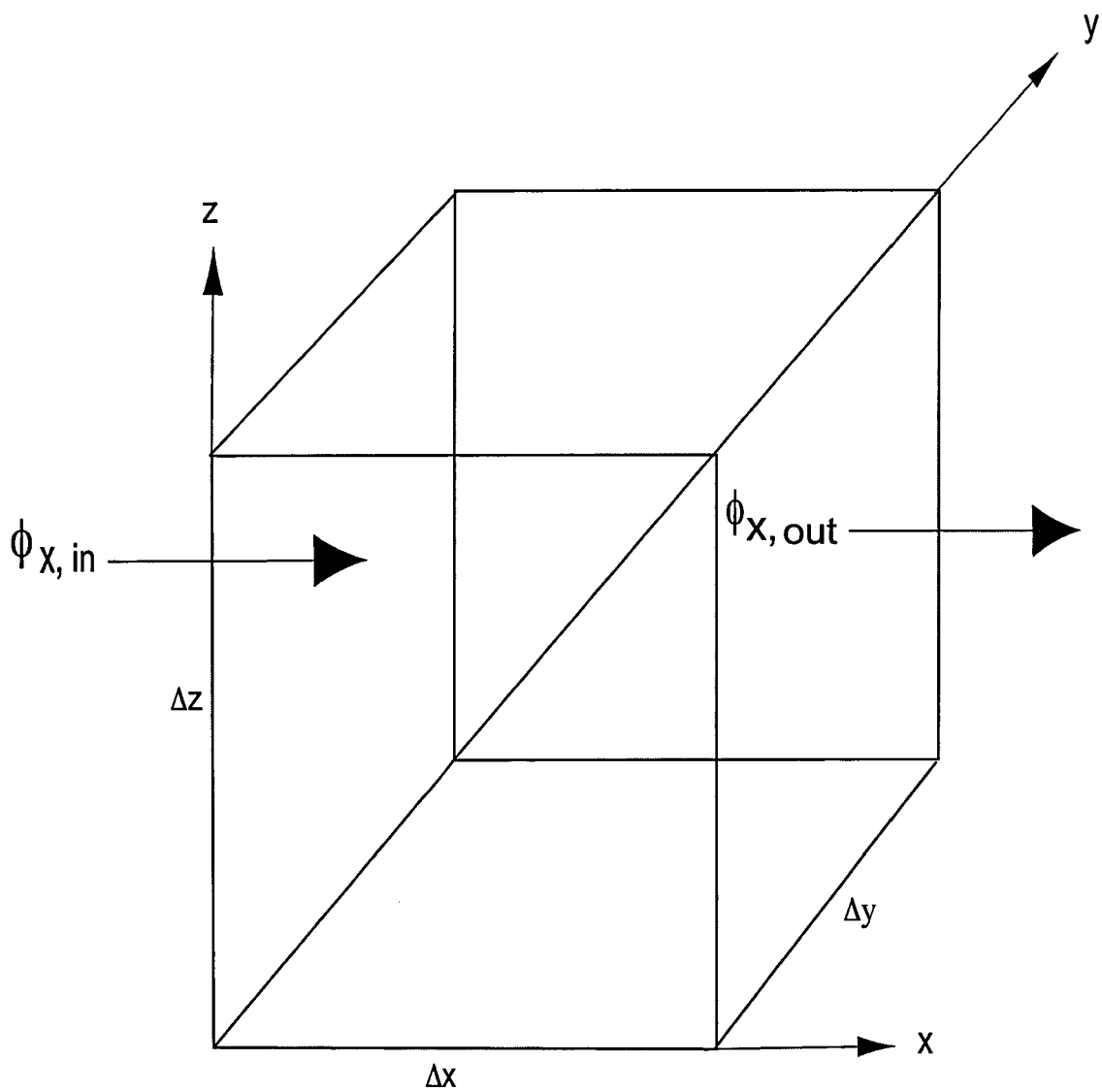


Figure 2.1: Schematic of a control volume with crossflow.

per time interval Δt in the system is given by

$$\frac{\partial M}{\partial t} = \frac{\partial \chi}{\partial t} \Delta x \, \Delta y \, \Delta z. \tag{2.2}$$

The net inflow of χ in the x, y and z- directions are

$$\phi_x \mid_x \Delta y \, \Delta z - \phi_x \mid_{x+\Delta x} \Delta y \, \Delta z = -\frac{\partial \phi_x}{\partial x} \Delta x \, \Delta y \, \Delta z \,, \tag{2.3a}$$

$$\phi_y \mid_y \Delta x \, \Delta z - \phi_y \mid_{y+\Delta y} \Delta x \, \Delta z = -\frac{\partial \phi_y}{\partial y} \Delta x \, \Delta y \, \Delta z \,, \tag{2.3b}$$

$$\phi_z \mid_z \Delta x \, \Delta y - \phi_z \mid_{z+\Delta z} \Delta x \, \Delta y = -\frac{\partial \phi_z}{\partial z} \Delta x \, \Delta y \, \Delta z \,. \tag{2.3c}$$

where ϕ_x, ϕ_y and ϕ_z are the fluxes of the quantity χ in the x, y and z-directions, respectively. Equations (2.3a- 2.3c) sum up to give

$$\sum \phi_{in} - \sum \phi_{out} = -\frac{\partial \phi_x}{\partial x} \Delta x \, \Delta y \, \Delta z - \frac{\partial \phi_y}{\partial y} \Delta x \, \Delta y \, \Delta z - \frac{\partial \phi_z}{\partial z} \Delta x \, \Delta y \, \Delta z. \tag{2.4}$$

The reaction term in the system is kinetic rate law integrated over the volume, giving

$$S = \pm r \, \chi \, \Delta x \, \Delta y \, \Delta z, \tag{2.5}$$

where r is the rate constant. The reaction term actually decribes the rate of decay/loss/evaporation of χ in the system. By combining equations (2.2), (2.4) and (2.5) we can therefore write equation (2.1) for the CV as

$$\begin{aligned} &\frac{\partial \chi}{\partial t} \Delta x \, \Delta y \, \Delta z \\ &= -\frac{\partial \phi_x}{\partial x} \Delta x \, \Delta y \, \Delta z - \frac{\partial \phi_y}{\partial y} \Delta x \, \Delta y \, \Delta z - \frac{\partial \phi_z}{\partial z} \Delta x \, \Delta y \, \Delta z - r \, \chi \, \Delta x \, \Delta y \, \Delta z. \qquad (2.6) \\ &\Rightarrow \frac{\partial \chi}{\partial t} = -\frac{\partial \phi_x}{\partial x} - \frac{\partial \phi_y}{\partial y} - \frac{\partial \phi_z}{\partial z} - r \, \chi. \qquad (2.7) \end{aligned}$$

In most general problems, typical of a river channel, advection and turbulent diffusion

occur in each of the three coordinate directions (Rutherford, 1994). Consequently, the diffusive fluxes would be different in the respective axes, and for Newtonian fluids, the component velocities are also incorporated. Following Ficks law of Molecular Diffusion, these fluxes are written as

$$\phi_x = -e_x \frac{\partial \chi}{\partial x} + u_x \chi\ , \quad \phi_y = -e_y \frac{\partial \chi}{\partial y} + u_y \chi\ , \quad \phi_z = -e_z \frac{\partial \chi}{\partial z} + u_z \chi, \tag{2.8}$$

where $e_x, e_y, e_z, \frac{\partial \chi}{\partial x}, \frac{\partial \chi}{\partial y}, \frac{\partial \chi}{\partial z}, u_x, u_y$ and u_z are the diffusion coefficients (turbulent), tracer concentration gradients and velocity components in the x-, y-, and z-directions, respectively.

Putting equations (2.8) into equation (2.7) gives

$$\begin{aligned} & r\chi + \frac{\partial \chi}{\partial t} + \frac{\partial}{\partial x}\Big(u_x \chi\Big) + \frac{\partial}{\partial y}\Big(u_y \chi\Big) + \frac{\partial}{\partial z}\Big(u_z \chi\Big) \\ & = \frac{\partial}{\partial x}\Big(e_x \frac{\partial \chi}{\partial x}\Big) + \frac{\partial}{\partial y}\Big(e_y \frac{\partial \chi}{\partial y}\Big) + \frac{\partial}{\partial z}\Big(e_z \frac{\partial \chi}{\partial z}\Big). \end{aligned} \tag{2.9}$$

Equation (2.9) is written in the so-called **Conservation form**, and possible other forms are found in literature. In the classical vectorial analysis notation, as can be found for instance in Apostol (1964), equation (2.9) becomes

$$r\chi + \frac{\partial \chi}{\partial t} + \nabla \cdot \Big(\mathbf{u}\chi\Big) = \nabla \cdot \Big(\mathbf{e} \nabla \chi\Big), \tag{2.10}$$

where $\mathbf{u} = \Big(u_x, u_y, u_z\Big)$, ∇ is the gradient operator $\nabla = \Big(\frac{\partial}{\partial x}, \frac{\partial}{\partial y}, \frac{\partial}{\partial z}\Big)^T$ and $\mathbf{e}$ is the diagonal matrix $\mathbf{e} = diag\Big(e_x, e_y, e_z\Big)$. In Einsteinian notation equation (2.9) is written as

$$r\chi + \frac{\partial \chi}{\partial t} + \frac{\partial}{\partial x_i}\Big(u_i \chi\Big) = \frac{\partial}{\partial x_i}\Big(e_{ij} \frac{\partial \chi}{\partial x_j}\Big). \tag{2.11}$$

For an incompressible fluid, equation (2.10) can be simplified using the continuity or conservation of mass equation for the ambient fluid. For incompressible fluid, the density is a constant ρ_0 everywhere, and the conservation of mass equation reduces to the continuity

equation (2.12)

$$\nabla \cdot \mathbf{u} = \mathbf{0} \tag{2.12}$$

(see, for example Batchelor (1967)). If we expand the advective term in equation (2.10), we can write

$$\nabla \cdot (\mathbf{u}\chi) = (\nabla \cdot \mathbf{u})\chi + \mathbf{u} \cdot \nabla\chi, \tag{2.13}$$

and by virtue of the continuity equation (2.12) the term $(\nabla \cdot \mathbf{u})\chi = 0$; thus, the equation (2.11) takes the form:

$$r\chi + \frac{\partial \chi}{\partial t} + u_i \frac{\partial \chi}{\partial x_i} = \frac{\partial}{\partial x_i}\left(e_{ij} \frac{\partial \chi}{\partial x_j}\right), \tag{2.14}$$

where equation (2.14) is the advection-diffusion-reaction equation of an incompressible fluid.

2.4 Depth-Averaging

The three-dimensional advection-diffusion equation (2.14) incorporating the decay (that is, reaction) term will form the basis for analysing mixing problems in real rivers in this work. One practical difficulty is that the full equation is complicated and requires a lot of information about water depths, velocities, diffusion coefficients and bathymetry; more than can conveniently be gathered during field experiments in natural channels. In addition the three-dimensional equation is difficult to solve in a complex natural channel. Thus, any hope of making progress would mean considering necessary steps to simplifying the equation (2.14) without loosing grip of the essential ingredients required for analysing mixing problems. One major procedure of simplifying the mixing equation is to average it over the depth of the channel. The resulting depth-averaged concentration equation would then be used in the midfield region in which vertical concentration gradients are small, and hence

attention is focused on transverse and longitudinal change. This is the case in most rivers where the aspect ratio (width/depth) is large.

To achieve the purpose of averaging, we integrate equation (2.9) term by term over the depth from the bed $z = a(x, y)$ to the surface $z = b(x, y)$ assuming steady flow. The application of Leibnitz's Theorem for Differentiation of an Integral (Abramowitz and Stegun, 1968):

$$\frac{\partial}{\partial x}\int_{a(x,y)}^{b(x,y)} f(x,z)dz = \int_{a(x,y)}^{b(x,y)} \frac{\partial f(x,z)}{\partial x}\,dz - f(x,a)\,\frac{\partial a}{\partial x} + f(x,b)\,\frac{\partial b}{\partial x} \tag{2.15}$$

in integrating equation (2.9) term by term leads to

$$\begin{aligned}
&\int_a^b r\,\chi\,dz + \int_a^b \frac{\partial \chi}{\partial t}\,dz + \frac{\partial}{\partial x}\int_a^b u_x\,\chi\,dz - \Big(u_x\,\chi\Big)_a\frac{\partial a}{\partial x} + \Big(u_x\,\chi\Big)_b\frac{\partial b}{\partial x}\\
&+\frac{\partial}{\partial y}\int_a^b u_y\,\chi\,dz - \Big(u_y\,\chi\Big)_a\frac{\partial a}{\partial y} + \Big(u_y\,\chi\Big)_b\frac{\partial b}{\partial y} - \Big(u_z\,\chi\Big)_a + \Big(u_z\,\chi\Big)_b\\
&= \frac{\partial}{\partial x}\int_a^b e_x\frac{\partial \chi}{\partial x}\,dz - \Big(e_x\frac{\partial \chi}{\partial x}\Big)_a\frac{\partial a}{\partial x} + \Big(e_x\frac{\partial \chi}{\partial x}\Big)_b\frac{\partial b}{\partial x}\\
&+\frac{\partial}{\partial y}\int_a^b e_y\frac{\partial \chi}{\partial y}\,dz - \Big(e_y\frac{\partial \chi}{\partial y}\Big)_a\frac{\partial a}{\partial y} + \Big(e_y\frac{\partial \chi}{\partial y}\Big)_b\frac{\partial b}{\partial y}\\
&-\Big(e_z\frac{\partial \chi}{\partial z}\Big)_a + \Big(e_z\frac{\partial \chi}{\partial z}\Big)_b.
\end{aligned} \tag{2.16}$$

Rearranging equation (2.16)

$$\begin{aligned}
&\Rightarrow \int_a^b r\,\chi\,dz + \int_a^b \frac{\partial \chi}{\partial t}\,dz + \frac{\partial}{\partial x}\int_a^b \Big(u_x\,\chi\,dz\Big) + \frac{\partial}{\partial y}\int_a^b \Big(u_y\,\chi\,dz\Big)\\
&= \frac{\partial}{\partial x}\int_a^b e_x\frac{\partial \chi}{\partial x}\,dz + \frac{\partial}{\partial y}\int_a^b e_y\frac{\partial \chi}{\partial y}\,dz\\
&+\Big[\chi\Big(u_x\frac{\partial a}{\partial x} + u_y\frac{\partial a}{\partial y} + u_z\Big)\Big]_a - \Big[\chi\Big(u_x\frac{\partial b}{\partial x} + u_y\frac{\partial b}{\partial y} + u_z\Big)\Big]_b\\
&-\Big(e_x\frac{\partial \chi}{\partial x}\frac{\partial a}{\partial x} + e_y\frac{\partial \chi}{\partial y}\frac{\partial a}{\partial y} + e_z\frac{\partial \chi}{\partial z}\Big)_a + \Big(e_x\frac{\partial \chi}{\partial x}\frac{\partial b}{\partial x} + e_y\frac{\partial \chi}{\partial y}\frac{\partial b}{\partial y} + e_z\frac{\partial \chi}{\partial z}\Big)_b.
\end{aligned} \tag{2.17}$$

Equation (2.17) can be simplified by imposing that at the water surface and the riverbed

the fluxes of water and tracer normal to the boundaries are zero. These are commonly known as **no-flux boundary conditions**, and hence the last four terms of the equation (2.17) reduces identically to zero. Therefore, equation (2.17) becomes

$$\int_a^b r\,\chi\,dz + \int_a^b \frac{\partial \chi}{\partial t}\,dz + \frac{\partial}{\partial x}\int_a^b \Big(u_x\,\chi\,dz\Big) + \frac{\partial}{\partial y}\int_a^b \Big(u_y\,\chi\,dz\Big) = \frac{\partial}{\partial x}\int_a^b e_x \frac{\partial \chi}{\partial x}\,dz + \frac{\partial}{\partial y}\int_a^b e_y \frac{\partial \chi}{\partial y}\,dz. \tag{2.18}$$

The integrals over the depth can be represented as

$$\frac{\partial}{\partial x}\int_a^b u_x\,\chi\,dz = \frac{\partial}{\partial x}\Big(h\,\overline{u\,\chi}\Big), \tag{2.19}$$

where the over bar denotes a depth-average and h is the local depth. Putting equation (2.19) into equation (2.18) yields

$$h\,\overline{r\,\chi} + h\frac{\partial \overline{\chi}}{\partial t} + \frac{\partial}{\partial x}\Big(h\,\overline{u_x\,\chi}\Big) + \frac{\partial}{\partial y}\Big(h\,\overline{u_y\,\chi}\Big) = \frac{\partial}{\partial x}\Big(h\,e_x\,\overline{\frac{\partial \chi}{\partial x}}\Big) + \frac{\partial}{\partial y}\Big(h\,e_y\,\overline{\frac{\partial \chi}{\partial y}}\Big). \tag{2.20}$$

Using Reynolds decomposition of averaging, the reaction, velocities and concentration can be expressed as the sum of a depth-average and a vertical deviation as follows:

$$r = \lambda + r'\,, \quad u_x = v_x + u_x'\,, \quad u_y = v_y + u_y'\,, \quad \chi = \Psi + \chi', \tag{2.21}$$

where

$$\lambda = \frac{1}{h}\int_a^b r\,dz\,, \quad v_x = \frac{1}{h}\int_a^b u_x\,dz\,, \quad v_y = \frac{1}{h}\int_a^b u_y\,dz\,, \quad \Psi = \frac{1}{h}\int_a^b \chi dz. \tag{2.22}$$

The depth-average of a product is defined as follows:

$$\overline{u_x\chi} = \overline{\Big(v_x + u'_x\Big)\Big(\Psi + \chi'\Big)} = v_x\Psi + \overline{u'_x\chi'}. \tag{2.23}$$

The depth-average of the deviations χ', r', u'_x and u'_y are zero. For e_x and e_y to be independent of the depth, implies

$$\overline{e_x\frac{\partial\chi}{\partial x}} = e_x\frac{\partial\Psi}{\partial x}\ , \quad \overline{e_y\frac{\partial\chi}{\partial y}} = e_y\frac{\partial\Psi}{\partial y}. \tag{2.24}$$

Making these substitutions into equation (2.20) gives

$$\begin{aligned} &h\lambda\Psi + h\frac{\partial\Psi}{\partial t} + \frac{\partial}{\partial x}\Big(hv_x\Psi\Big) + \frac{\partial}{\partial y}\Big(hv_y\Psi\Big) \\ &= \frac{\partial}{\partial x}\Big(-h\overline{u'_x\chi'} + he_x\frac{\partial\Psi}{\partial x}\Big) + \frac{\partial}{\partial y}\Big(-h\overline{u'_y\chi'} + he_y\frac{\partial\Psi}{\partial y}\Big), \end{aligned} \tag{2.25}$$

where $v_x\Psi$ and $v_y\Psi$ are known as the **advective fluxes** while $e_x\frac{\partial\Psi}{\partial x}$ and $e_y\frac{\partial\Psi}{\partial y}$ are **turbulent diffusive fluxes** in the longitudinal and transverse directions respectively. The terms $-\overline{u'_x\chi'}$ and $-\overline{u'_y\chi'}$ are the additional transport which are artifacts of depth-averaging and quantify the **longitudinal** and **transverse tracer fluxes** which result from vertical shear in the longitudinal and transverse velocities.

Taylor's analysis of turbulent shear flow suggests that at asymptotically large times the longitudinal dispersive flux is proportional to the longitudinal gradient in depth-averaged concentration:

$$-\overline{u'_x\chi'} = \kappa_x\frac{\partial\Psi}{\partial x}, \tag{2.26}$$

where κ_x is the longitudinal dispersion coefficient which accounts for the effects on the depth-averaged tracer concentration of depth variations in the longitudinal velocity. By

analogy, the transverse dispersive flux is given by

$$-\overline{u'_y\chi'} = \kappa_y \frac{\partial \Psi}{\partial y}, \tag{2.27}$$

where κ_y is the transverse dispersion coefficient which accounts for the effects on the depth-averaged tracer concentration of depth variations in the transverse velocity. The literature on turbulent-diffusion theory contains many discussions of the validity, or otherwise, of equations (2.26) and (2.27) [see, for example, Tennekes and Lumley (1972, pp.11, 40-52)]. Incorporating equations (2.26) and (2.27) into equation (2.25) gives

$$\begin{aligned} &h\lambda\Psi + h\frac{\partial \Psi}{\partial t} + \frac{\partial}{\partial x}(hv_x\Psi) + \frac{\partial}{\partial y}(hv_y\Psi) \\ &= \frac{\partial}{\partial x}\Big[h(e_x + \kappa_x)\frac{\partial \Psi}{\partial x}\Big] + \frac{\partial}{\partial y}\Big[h(e_y + \kappa_y)\frac{\partial \Psi}{\partial y}\Big]. \end{aligned} \tag{2.28}$$

In river channels, $\kappa_x \gg e_x$ and $\kappa_y \gg e_y$ (Rutherford, 1994), and the application of the continuity equation (2.12) gives the advection form

$$h\lambda\Psi + h\frac{\partial \Psi}{\partial t} + hv_x\frac{\partial \Psi}{\partial x} + hv_y\frac{\partial \Psi}{\partial y} = \frac{\partial}{\partial x}\Big(h\kappa_x\frac{\partial \Psi}{\partial x}\Big) + \frac{\partial}{\partial y}\Big(h\kappa_y\frac{\partial \Psi}{\partial y}\Big) \tag{2.29}$$

The above depth-averaged advection-diffusion equation (2.29) can be used in predicting tracer concentration where the channel is straight and uniform which is the case in man-made channels such as canals and laboratory flumes, and is also satisfactorily applied in the mid-field of natural rivers. However, the equation (2.29) can further be simplified to render it mathematically tractable. Therefore, by considering that the tracer source is steady and on the assumption of a long-narrow channel (that is, the length-to-width ratio is large) by employing the following scales:

$$L \simeq \frac{B^2U}{\kappa_x}, \quad \kappa_x \simeq HU, \tag{2.30}$$

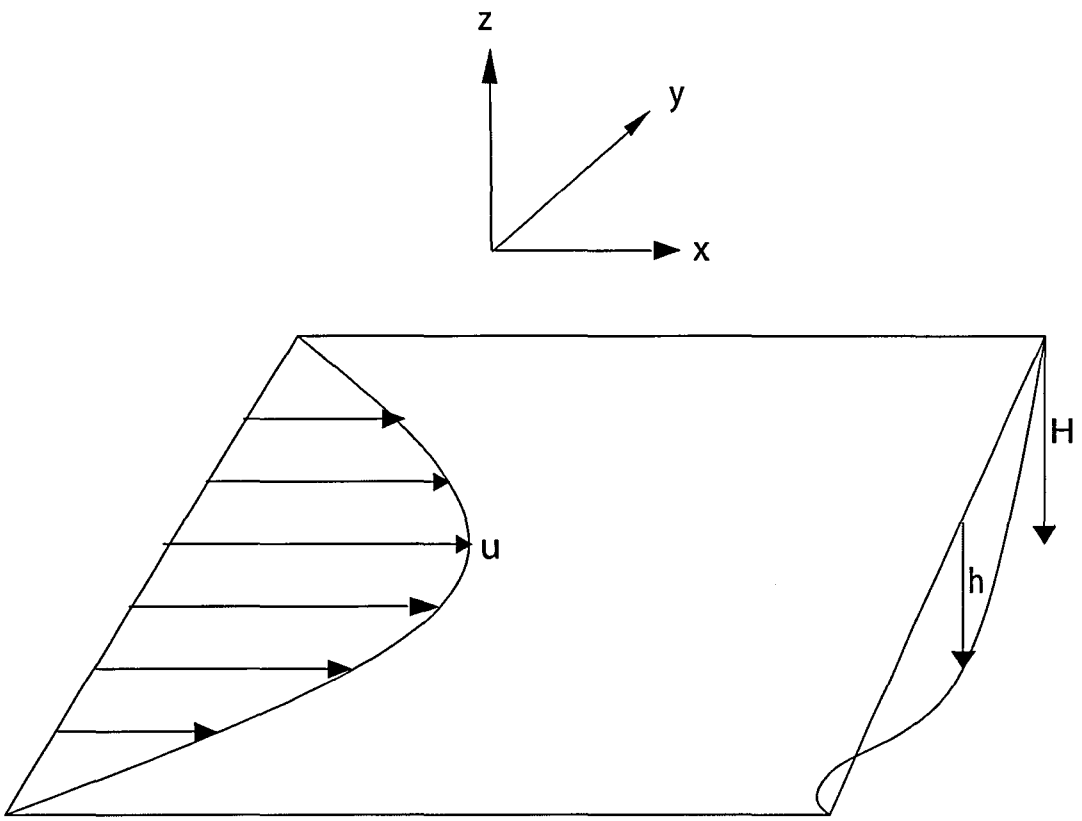


Figure 2.2: Sketch of Configuration of a uniform straight channel.

where B, H, L, U, and κ_x are characteristic width, average (or maximum) depth, longitudinal length (which is of the order of the distance which contaminant will have been advected downstream before it meets the shoreline), average or discharge velocity and longitudinal dispersion coefficient of the channel, respectively. Therefore, the reciprocal of the square of the aspect ratio (width/length) of the channel becomes

$$\left(\frac{B}{L}\right)^2 \simeq \frac{B^2\kappa_x^2}{B^4U^2} \simeq \frac{\kappa_x^2}{B^2U^2} \simeq \left(\frac{H}{B}\right)^2 \ll 1 \tag{2.31}$$

which renders the longitudinal dispersion term negligible. Also, the transverse advective term is negligible due to the large width-to-depth aspect ratio which enhances vertical equilibrium much more rapidly than transverse equilibrium. In this case $\kappa_y = \kappa$, and at the

banks the no-flux boundary conditions are applied. If now the x-distance is measured in the local downstream direction with a local uniform longitudinal velocity u that depends on the y-distance the local transverse direction (see Figure 2.2; Daish, 1985), equation (2.29) reduces to

$$h\lambda\Psi + hu\frac{\partial\Psi}{\partial x} = \frac{\partial}{\partial y}\Big(h\kappa\frac{\partial\Psi}{\partial y}\Big) \tag{2.32}$$

with

$$h\kappa\frac{\partial\Psi}{\partial y} = 0\,,\ y = a\,,\ b. \tag{2.33}$$

For a fast equalization of concentration in depth and with constant coefficients equation (2.32) reduces to

$$\lambda\Psi + u\frac{\partial\Psi}{\partial x} = \kappa\frac{\partial^2\Psi}{\partial y^2}. \tag{2.34}$$

Equations (2.32), (2.33) and (2.34) with appropriate initial conditions will form the basis of our mathematical analysis in this work.

2.5 Concluding remarks

We have briefly discussed some important basic concepts of the fate and transport of contaminants and derived the governing advection-diffusion-reaction partial differential equations. With regard to applications in environmental modelling the aim has been to present material specifically directed at solving transport -chemistry problems in river systems such that the transport part is based on advection and diffusion processes and the chemistry part on chemical reaction processes modelled by first-order decay parameter. The next four chapters that follow give outlines of the methods of solution to the specific applicable problems respectively as the following: 1) The diffusion centre of a river; 2) Ray approximation for

steady discharges in rivers; 3) Decay and depth discontinuity effects upon steady discharges in rivers; 4) Computational scheme for steady discharges in rivers.

2.6 References

1. Abramowitz, M. and Stegun, A. I.: 1968, Handbook of Mathematical Functions. Fifth edition, Dover Publications, New York.

2. Apostol, T. M.: 1964, Calculus. Blaisdell, New York.

3. Batchelor, G. K.: 1967, An Introduction to Fluid Dynamics. Cambridge University Press, New York.

4. Daish, N. C.: 1985, Optimal discharge profiles for sudden contaminant releases in steady, uniform open-channel flow. *J. Fluid Mech.*, **159**, 303 - 321.

5. Rutherford, J. C.: 1994, River Mixing. John Wiley and Sons Ltd., England.

6. Tennekes, H and Lumley, J. L.: 1972, A First Course in Turbulence. Cambridge, Mass: MIT Press.

Chapter 3

The diffusion centre of a river

This chapter has been published (P. Mebine and R. Smith, 2006: Effects of Contaminant Decay on the Diffusion Centre of a River. *Environmental Fluid Mechanics*, **6**, 101-114.)

3.1 Introduction

Modern large-scale sewage works and industrial processes are designed to avoid intermittent high-level waste-water discharges, and instead are aimed at steady low-level discharges. The environmental impact can be further reduced by careful selection of the discharge location. In rivers, the near-shore or littoral zones contain more abundant plant, fish and animal communities than the main channel. A commonly advocated managerial policy to conserve these areas of economic importance is to choose the source location of large-scale contaminant discharges to avoid excessive shoreline concentrations. The magnitude of avoidable shoreline excesses is shown in Figure 3.1 for the illustrative case of a conserved solute discharged at a steady rate from a single point into a channel with water depth that increases from zero at the left to maximum water depth at the right of Figure 3.1.

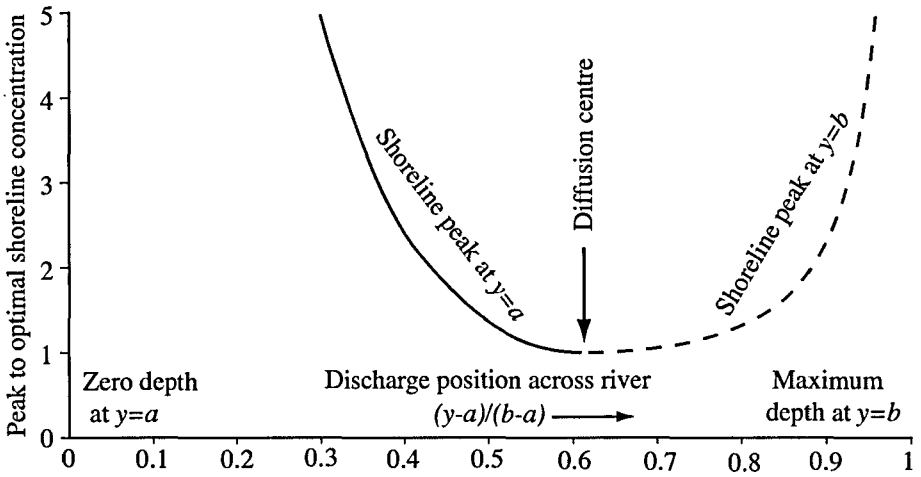


Figure 3.1: Magnitude of shoreline pollution if a discharge is not at the diffusion centre.

Yotsukura and Cobb (1972) used the degree of mixing as a measure of the effectiveness of different discharges of non-decaying solutes in a river. Their criterion for the optimal site, or diffusion centre, is that the transverse mixing distance be minimized with complete mixing achieved as quickly as possible. For a laterally symmetric river the diffusion centre coincides with the geometric centre. In general, the diffusion centre tends to be displaced

towards the deeper side of a river (as in Figure 3.1) and close to the centre with respect to volume discharge (Smith, 2004). A nice consequence of positioning a steady discharge at the diffusion centre is that at both banks the concentrations gradually increase downstream without local pollution hot-spots along either shore (Smith, 1982). In Figure 3.1, the peak shoreline pollution increases quadratically for discharge sites away from the diffusion centre, reaching 0.4 above optimal for displacements of an eighth of a channel breadth away from the diffusion centre.

Many contaminants exhibit decay. Decay mechanisms include consumption by bacteria or radioactive decay (temporal decay uniform across the flow), heat loss or evaporation through the surface (decay decreasing with depth), and break up by turbulence (decay proportional to the product of velocity and depth). For slow-moving rivers with widths of a few hundreds of metres, the time scales for transverse mixing can be of order a day and comparable with the time scales for decay. So, decay cannot be regarded as a minor perturbation that simply lowers the concentration. There are numerical models in literature which allow for the decay of contaminants (Bikangaga and Nassehi, 1995; Nassehi and Bikangaga, 1993; Yoo, Cho and Jun, 2003). However, no previous investigation of the effects of decay on the discharge sites has been attempted.

In the present work a mathematical model is used to include a profile of decay in a definition of the diffusion centre for a non-symmetric straight river with non-reversing flow. Three families of exact solutions are given with profiles of decay corresponding to consumption by bacteria, to evaporation and to break up by turbulence. It is found that the diffusion centre shifts to deeper or shallower water accordingly as the the temporal decay divided by flow speed (local downstream spatial decay rate) decreases or increases with water depth.

3.2 Governing equations

An account of flow models of river mixing by Rutherford (1994) suggested that transverse mixing is more important in water quality management than either vertical or longitudinal mixing, especially when dealing with discharge of water from point sources or the mixing of tributary inflows. In natural streams it is known that the width-to-depth aspect ratio is large and therefore vertical equilibrium (usually vertically uniform) is achieved very much more rapidly than transverse equilibrium. Thus, for lateral mixing of solute from a steady discharge in nonstratified unidirectional flow, the concentration can be regarded as being in vertical equilibrium, and hence attention is focused along and across the flow. Steady contaminant plumes also have a large length-to-width ratio, which makes the effect of transverse turbulent diffusion more important than longitudinal shear dispersion (Elder, 1959).

For a straight channel with a cross-section that is unchanging in the downstream direction, the steady-state vertical-equilibrium advection-diffusion equation, incorporating a first-order decay parameter $\lambda(y)$ that is a function of the transverse coordinate y only, is

$$\lambda h c + h u \frac{\partial c}{\partial x} - \frac{\partial}{\partial y}\left(h \kappa \frac{\partial c}{\partial y}\right) = 0. \tag{3.1}$$

The no-flux boundary conditions at the shorelines are

$$h \kappa \frac{\partial c}{\partial y} = 0 \quad \text{on} \quad y = a, b\,. \tag{3.2}$$

Here x and y are the longitudinal and transverse coordinates, $c(x, y)$ is the contaminant concentration between the shorelines $y = a, b$ in water of depth $h(y) \geq 0$, steady non-reversing velocity $u(y) \geq 0$, and transverse diffusivity $\kappa(y) \geq 0$. It is not necessary that $\lambda(y)$ be single signed, but all the examples in this work concern decaying rather than growing contaminants. If the vertical equilibrium is non-uniform (light oils, heavy oils, bed sorption,

death of bacteria in bright sunlight near the surface), then c, u and κ are appropriately weighted vertical averages (Smith, 1996).

3.3 Pollutant modes

To solve the system (3.1, 3.2), the method of modes is employed. The eigenmodes are herein described as the pollutant modes. A separation of variables solution:

$$c(x,y) = \sum_{n=0}^{\infty} C_n \exp(-\mu_n x)\, \phi_n(y) \ , \tag{3.3}$$

leads to the introduction of the pollutant modes $\phi_n(y)$ and their associated spatial decay rates (eigenvalues) μ_n:

$$\frac{\mathrm{d}}{\mathrm{d}y}\left(h\,\kappa\,\frac{\mathrm{d}\phi_n}{\mathrm{d}y}\right) + [\mu_n\, u - \lambda]\; h\,\phi_n = 0 \ , \tag{3.4}$$

with

$$h\,\kappa\,\frac{\mathrm{d}\phi_n}{\mathrm{d}y} = 0 \quad \text{on} \quad y = a, b \ . \tag{3.5}$$

Modes are only known explicitly for restricted families of exactly solvable test cases, but exist and are countable for any non-negative depth, diffusivity and velocity profiles.

It is conventional to order the modes in increasing values of the spatial decay rates

$$\mu_0 < \mu_1 < \mu_2 < \ldots . \tag{3.6}$$

This ordering corresponds to the modes becoming increasingly oscillatory with respect to y. Figure 3.2 shows the first few modes for the illustrative case of a conserved ($\lambda = 0$) solute in a channel with water depth that increases from zero at the left to maximum at the right (§3.5, equation(3.15)) with u and κ dependent on the water depth as specified in

§3.4, equation (3.11). Universal properties are: i) the zero mode $\phi_0(y)$ is single signed; ii) the n'th pollutant mode $\phi_n(y)$ has n zeros that interlace with the $n+1$ zeros of $\phi_{n+1}(y)$; iii) for $n = 1$ there is a position y_1 such that

$$\phi_1(y_1) = 0 \quad \text{with} \quad \phi_2(a)\phi_2(y_1) \leq 0 \quad \text{and} \quad \phi_2(b)\phi_2(y_1) \leq 0 \; . \tag{3.7}$$

In a river with symmetric depth, flow, mixing and decay, y_1 is at the geometric centre.

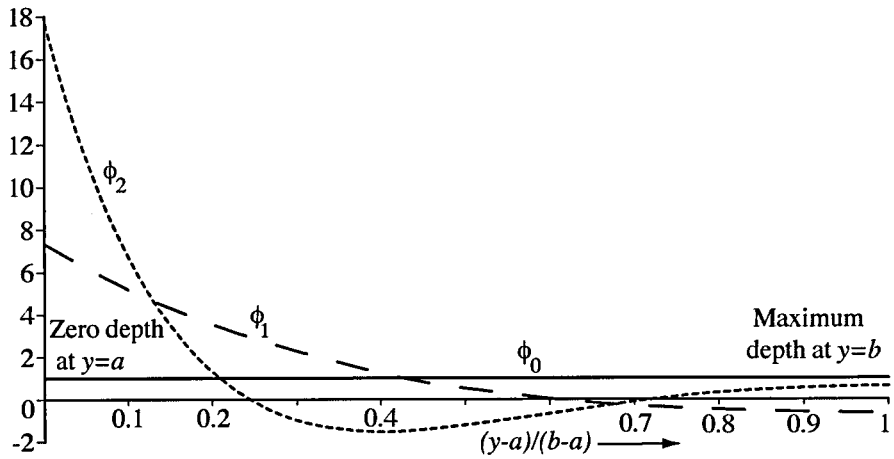


Figure 3.2: Normalized modes for linearly increasing depth.

If at $x = 0$, the cross-river concentration profile is denoted by $f(y)$, or the profile of discharge flux is denoted by $huf(y)$, then the weights C_n can be evaluated from integrals across the river

$$C_n = \int_a^b h\,u\,f(y)\phi_n(y)\,dy \Big/ \int_a^b h\,u\,\phi_n^2\,dy. \tag{3.8}$$

Normalizing the modes with respect to the volume flux Q:

$$\int_a^b h\,u\,\phi_n^2\,dy = \int_a^b h\,u\,dy = Q \; , \tag{3.9}$$

gives minor simplifications. In particular, for a pollutant flux rate q discharged at the point

y_p, the formula (3.8) takes the neat form

$$C_n = \frac{q}{Q}\,\phi_n(y_p). \tag{3.10}$$

The normalization (3.9) permits the higher modes to become large in shallow, slow-flowing water, as at the left of Figure 3.2. The shallow-water concentrations are sensitive to the weights C_n and those weights are sensitive to shallow-water positioning of the discharge. For the illustrative case, the shoreline pollution is in excess of five times optimal for the left three-tenths in Figure 3.1.

For the solution (3.3) the lowest mode $\phi_0(y)$ is the transverse equilibrium concentration profile and the lowest eigenvalue μ_0 is the spatial rate of downstream decay at large distances downstream. If C_1 is non-zero then the decay-adjusted exponential rate of approach to that transverse equilibrium is $\mu_1 - \mu_0$ with shape $C_1\,\phi_1(y)$. The sign of C_1 determines at which of the two banks there is a decay-adjusted relative pollution excess (as in Figure 3.1). Such shoreline excesses are avoided if $C_1 = 0$. It is clear from equations (3.7, 3.10) that $C_1 = 0$ can be achieved for a discharge flux confined to the single point $y_p = y_1$. In that case, the decay-adjusted relative exponential rate of approach to the transverse equilibrium is increased to $\mu_2 - \mu_0$ with shape $C_2\,\phi_2(y)$ and size $C_2 = \phi_2(y_1)q/Q$. From the inequalities (3.7), it follows that far downstream at both banks there is a negative departure relative to decay adjusted equilibrium. Shoreline pollution hot-spots (relative to decay adjusted equilibrium) have been eliminated. Consequently, y_1 is the diffusion centre.

Numerical methods for computing low modes $\phi_0(y)$, $\phi_1(y)$ of the system (3.4,3.5) and for the estimation of the root y_1, are well established (Fox, 1957). Instead, this work pursues exact solutions. One motivation is to sharpen understanding. Another motive is to add decay examples to the stock of non-trivial exact solutions for the benchmark testing of numerical computation schemes for environmental impacts in rivers (Nassehi and Passone, 2005).

3.4 Flow parameters in straight channels

Flows in natural streams tend to be turbulent. Elder (1959) showed that the local turbulent diffusivities are proportional to the product of the local water depth and longitudinal velocity. This implies (Kay, 1987; Rutherford, 1994; Smith, 1981), that the longitudinal velocity varies as square-root of the depth and the diffusivity as the three-halves power of the water depth:

$$u = U\left(\frac{h}{H}\right)^{\frac{1}{2}} \quad , \quad \kappa = K\left(\frac{h}{H}\right)^{\frac{3}{2}} \quad . \tag{3.11}$$

The capital letters H, U and K denote the depth, flow and transverse mixing at a reference position in the channel. The depth-linked formulae (3.11) ensure that in the deepest parts of the channel the velocity is greatest and transverse mixing is most vigorous (Daish, 1985). It is implicit that the pollutant is sufficiently dilute that it does not significantly modify the turbulence (for example, applicable to oil in droplets but not to a continuous oil slick).

The illustrative examples in this work use power-law models for the decay:

$$\lambda = \Lambda\left(\frac{h}{H}\right)^{m+\frac{1}{2}} \quad . \tag{3.12}$$

For positive (or negative) m the ratio $\lambda(y)/u(y)$ increases (or decreases) with depth.

With the representations (3.11, 3.12) the eigenvalue problem (3.4, 3.5) becomes

$$K\frac{d}{dy}\left(\left(\frac{h}{H}\right)^{\frac{5}{2}}\frac{d\phi_n}{dy}\right) + \left(\frac{h}{H}\right)^{\frac{3}{2}}\left[\mu_n U - \Lambda\left(\frac{h}{H}\right)^{m}\right]\phi_n = 0 \, , \tag{3.13}$$

with

$$\left(\frac{h}{H}\right)^{\frac{5}{2}}\frac{d\phi_n}{dy} = 0 \quad \text{on} \quad y = a, \, b \, . \tag{3.14}$$

For zero decay, the concept of the diffusion centre and the method of modes that is

used to identify it, are not restricted to straight non-varying channels (Smith, 1982). The mathematics looks more daunting because of the need to use of flow-following coordinates (Yotsukura and Sayre, 1976). Also, the modes split into downstream evolving $\phi_n(x,y)$ and upstream evolving $\hat{\phi}_n(x,y)$ adjoints. The diffusion centre is where $\hat{\phi}_1(x, y_1(x)) = 0$. It is evolving upstream in response to downstream changes to the cross-sectional profile on the length scale $1/\mu_2$ of cross-sectional mixing (Smith, 1982), that is, it is downstream of the discharge where shoreline pollution excesses might otherwise have occured. With decay, the principal changes would be that the transverse equilibrium $\phi_0(x,y)$ ceases to be constant across the channel and has decay $\mu_0(x)$ along the flow.

3.5 Linearly increasing depth

For illustrative purposes, the chosen depth profile across the flow is linear increase from zero depth at one side $y = 0$ to maximum depth H at the other side $y = B$:

$$h(y) = H\left(\frac{y}{B}\right) \quad \text{for} \quad 0 < y < B. \tag{3.15}$$

Decay proportional to the flow speed $\lambda = \Lambda(h/H)^{\frac{1}{2}}$ (that is, $m = 0$) has no effect on the modes. The modes are unchanged from those for a conserved solute. The lowest mode is constant across the channel $\phi_0 = 1$. Higher modes (normalized) can be represented (Smith, 1982):

$$\phi_n = \frac{\left(a_n(y/B)^{\frac{1}{2}}\right)^{-1} \sin\left(a_n(y/B)^{\frac{1}{2}}\right) - \cos\left(a_n(y/B)^{\frac{1}{2}}\right)}{(y/B)\,(\frac{5}{2})^{\frac{1}{2}} \left\{1 + \frac{\cos(a_n)\sin(a_n)}{a_n} - 2\frac{\sin(a_n)^2}{a_n^2}\right\}^{\frac{1}{2}}}. \tag{3.16}$$

The square-root terms in the denominator that normalize the modes for arbitrary a_n.

The no-flux boundary condition (3.14) at $y = B$ restricts the a_n to being non-negative

roots of the equation:

$$\sin(a_n) = -\frac{3\,a_n\,\cos(a_n)}{a_n^2 - 3}\,,\quad a_1 = 5.763\,,\ a_2 = 9.095\,,\ a_n \approx n\pi - \frac{3}{n\,\pi}\,. \tag{3.17}$$

The construction of Figure 3.1 from the modal solution (3.3) used up to 40 modes to achieve high accuracy. Figure 3.2 shows the $n = 0, 1, 2$ normalized modes. The diffusion centre is at

$$y_1/B = 0.608\,. \tag{3.18}$$

Decay proportional to the flow speed, augments the eigenvalues μ_n by Λ/U:

$$\mu_n = \frac{K\,a_n^2}{4\,U\,B^2} + \frac{\Lambda}{U}\,. \tag{3.19}$$

For $n = 2$, transverse mixing and decay give equal contributions to μ_n for $\Lambda B^2/K \approx 20$. For larger rates of decay shoreline pollution becomes insignificant unless the discharge is irresponsibly close to shore. The subsequent computations are restricted to $\Lambda B^2/K \leq 10$.

In the context of pollution minimisation from sudden discharges of pollutants, Daish (1985) used piecewise linear depth profiles to construct a wide range of test problems. The following three sub-sections concern the linear depth profile (3.15), but with decay profiles corresponding to uniform consumption by bacteria, to evaporation and to break up by turbulence. The diffusion centre y_1 is found to deviate by $\pm B/8$ from the non-decaying reference case (3.18).

3.5.1 Constant decay

Radioactive decay or consumption by bacteria (at a rate unaffected by sunlight or turbidity) are examples of constant temporal decay $\lambda = \Lambda$ (that is, $m = -\frac{1}{2}$) .

The exact solutions for the pollutant modes (not normalised) have an explicit solution

proportional to a Whittaker function with first and third arguments imaginary:

$$\phi_n = (-1)^n \frac{Whittaker\,M\left(\mathrm{i}\,\Lambda/(\mu_n U),\, \frac{3}{2},\, 4\,\mathrm{i}\,(\mu_n\,U\,B\,y/K)^{\frac{1}{2}}\right)}{(y/B)} \,. \tag{3.20}$$

The sign switching $(-1)^n$ is included so that, for compatibility with Figure 3.2, $\phi_1(y)$ exhibits a change from positive for small y to negative for large y. The no-flux boundary condition (3.14) at $y = B$ yields an equation satisfied by the eigenvalues μ_n:

$$\begin{aligned}\left(2 + \frac{\mathrm{i}\,\Lambda\,B}{(\mu_n U\,K)^{\frac{1}{2}}}\right) \Bigg[& Whittaker\,M\left(\mathrm{i}\,\Lambda\,B/(\mu_n U\,K)^{\frac{1}{2}},\, \frac{3}{2},\, 4\,\mathrm{i}\,(\mu_n\,U\,B^2/K)^{\frac{1}{2}}\right) \\ & - Whittaker\,M\left(\mathrm{i}\,\Lambda/(\mu_n U) + 1,\, \frac{3}{2},\, 4\,\mathrm{i}\,(\mu_n\,U\,B^2/K)^{\frac{1}{2}}\right)\Bigg] \\ = \; 2\,\mathrm{i}\,\left(\mu_n\,U\,B^2/K\right)^{\frac{1}{2}} & \; Whittaker\,M\left(\mathrm{i}\,\Lambda/(\mu_n U),\, \frac{3}{2},\, 4\,\mathrm{i}\,(\mu_n\,U\,B^2/K)^{\frac{1}{2}}\right) \,. \end{aligned} \tag{3.21}$$

Once an eigenvalue μ_n is evaluated, the shape of the mode $\phi_n(y)$ is given by equation (3.20). Figure 3.3 shows the normalized first mode shapes for three values of the decay parameter. For zero decay the first mode $\phi_1(y)$ and discharge centre y_1 are identical with those in Figure 3.2 and equation (3.18). The effects of decay on $\phi_1(y)$ are most marked near the beach. For a fixed distance downstream, the slower flow in shallow water gives more time for the contaminant to be depleted.

$\Lambda B^2/K$	y_1/B
0	0.608
2	0.637
4	0.657
6	0.673
8	0.685
10	0.696

Table 3.1: Optimal discharge positions for linearly increasing depth and constant decay.

From a $\phi_1(y)$ curve it is straightforward to compute the root y_1. Table 3.1 lists $\Lambda B^2/K$, y_1/B pairings including those appropriate to the curves shown in Figure 3.3. Constant

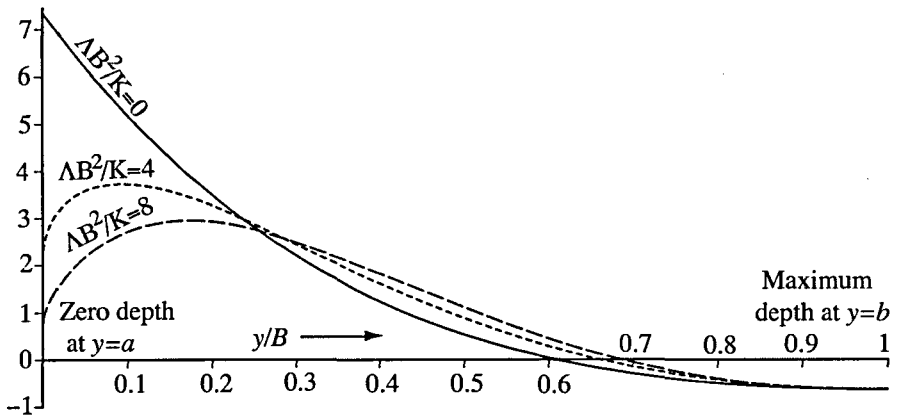


Figure 3.3: First mode $\phi_1(y)$ for constant decay Λ and linearly increasing depth.

decay shifts the diffusion centre towards the deeper water by an amount proportional to Λ.

3.5.2 Decay that decreases with depth

The decay can decrease with depth if $c(y,t)$ is a number count of bacteria which are killed by sunlight (Gould and Munro, 1981) only in the top few metres of the water column. A second example is removal at the bed (feeding by marine micro-organisms, fungi or yeasts). A third example is air-water contaminant exchange at the surface. For example, evaporation accounts for largest loss in oil volume during the early stages (Overstreet and Galt, 1995; Reddy and Brunet, 2003). Fingas (Fingas, 1994a; Fingas, 1985) notes that light crude oils can lose as much as 75 per cent of their original volume within the first few days after a spill; medium-weight crudes might lose as much as 40 per cent of the original volume. Heavy crude or residual oils, on the hand, will probably only lose about 10 per cent of their volume in the first few days.

An exactly solvable model problem that illustrates decay decreasing with depth is $\lambda = \Lambda(h/H)^{-\frac{1}{2}}$ (that is, $m = -1$) . The modes (not normalised) are proportional to a Bessel

function of non-integer-order:

$$\phi_n = \frac{Bessel\,J\left((\frac{9}{4}+4\Lambda B^2/K)^{\frac{1}{2}}, 2\,(\mu_n U B y/K)^{\frac{1}{2}}\right)}{(y/B)^{\frac{3}{4}}} \,. \tag{3.22}$$

The no-flux boundary condition (3.14) at $y = B$ yields the eigenvalue equation with roots μ_n:

$$\begin{aligned}
&(\frac{9}{4}+4\Lambda B^2/K)^{\frac{1}{2}}\ Bessel\,J\left((\frac{9}{4}+4\Lambda B^2/K)^{\frac{1}{2}}, 2\,(\mu_n U B^2/K)^{\frac{1}{2}}\right) \\
&-2\,(\mu_n U B^2/K)^{\frac{1}{2}} Bessel\,J\left((\frac{9}{4}+4\Lambda B^2/K)^{\frac{1}{2}}+1, 2\,(\mu_n U B^2/K)^{\frac{1}{2}}\right) \\
&= \frac{3}{2}\,Bessel\,J\left((\frac{9}{4}+4\Lambda B^2/K)^{\frac{1}{2}}, 2\,(\mu_n U B^2/K)^{\frac{1}{2}}\right) \,.
\end{aligned} \tag{3.23}$$

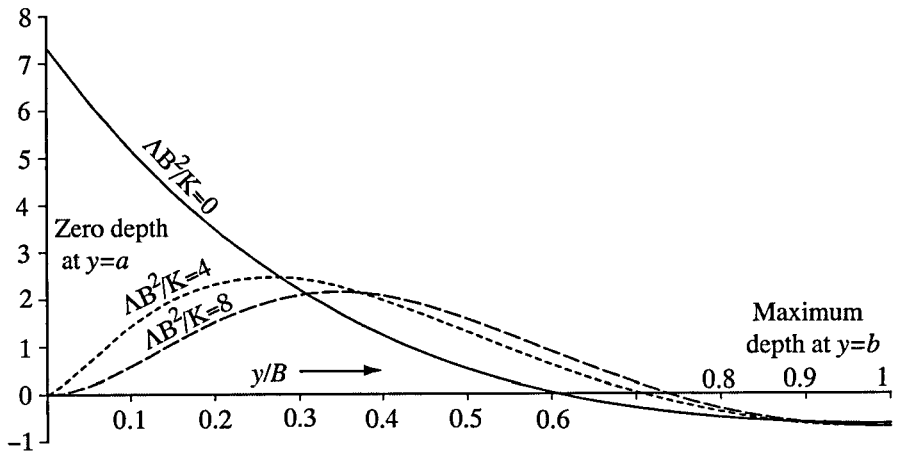


Figure 3.4: First mode $\phi_1(y)$ for decay that decreases with depth.

Figure 3.4 and table 3.2 respectively show the effects of the strength of the decay on the ϕ_1 pollutant mode and upon the diffusion centre. Again, for zero decay the first mode $\phi_1(y)$ and discharge centre y_1 are identical with those in Figure 3.2 and equation (3.18). For non-zero decay, the singularity in $\lambda(y)$ at the beach $y = 0$, gives a jump to zero for $\phi_1(0)$. Also, the displacement of the optimal discharge site towards the deeper part of the channel scales as the square-root of Λ.

$\Lambda B^2/K$	y_1/B
0	0.608
2	0.676
4	0.705
6	0.723
8	0.736
10	0.747

Table 3.2: Discharge positions for decay that decreases with depth.

3.5.3 Decay that increases with depth more than the velocity

The dissolution of oils or break up of clay flocs is most rapid in regions of the flow where the turbulence is energetic. In this sub-section, the decay is modelled $\lambda = \Lambda\,(h/H)^{\frac{3}{2}}$, as proportional to the turbulent mixing (that is, $m = 1$) and increasing with depth more strongly than the velocity (3.11).

The pollutant modes (not normalised) are proportional to Whittaker function modes with all three arguments real:

$$\phi_n = \frac{Whittaker\,M(\frac{1}{2}\mu_n\,U\,B/(\Lambda\,K)^{\frac{1}{2}},\,\frac{3}{4},\,2(\Lambda/K)^{\frac{1}{2}}y)}{(y/B)^{\frac{5}{4}}}\,. \tag{3.24}$$

The no-flux boundary condition (3.14) at $y = B$ yields an equation satisfied by the eigenvalues μ_n:

$$\left(\frac{5}{4}+\frac{\mu_n\,U\,B}{2\,(\Lambda\,K)^{\frac{1}{2}}}\right)\left[Whittaker\,M\left(\frac{1}{2}\mu_n\,U\,B/(\Lambda\,K)^{\frac{1}{2}},\,\frac{3}{4},\,2(\Lambda/K)^{\frac{1}{2}}B\right)\right.$$
$$\left. - Whittaker\,M(\frac{1}{2}\mu_n\,U\,B/(\Lambda\,K)^{\frac{1}{2}}+1,\,\frac{3}{4},\,2(\Lambda/K)^{\frac{1}{2}}B)\right]$$
$$= (\Lambda/K)^{\frac{1}{2}}B\;Whittaker\,M(\frac{1}{2}\mu_n\,U\,B/(\Lambda\,K)^{\frac{1}{2}},\frac{3}{4},\,2(\Lambda/K)^{\frac{1}{2}}B)\,. \tag{3.25}$$

Figure 3.5 and table 3.3 respectively show the first pollutant mode $\phi_1(y)$ and the optimum discharge site y_1 for a few values of $\Lambda B^2/K$. Once more, for zero decay the first mode $\phi_1(y)$ and discharge centre y_1 are identical with those in Figure 3.2 and equation (3.18).

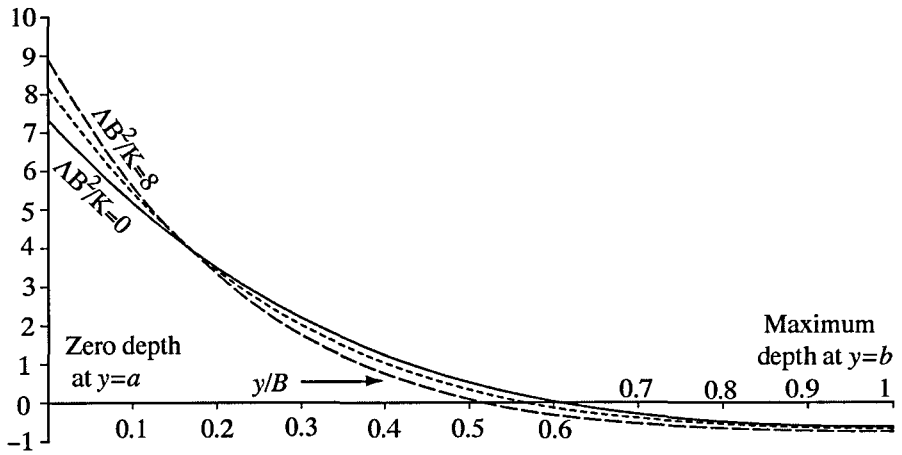


Figure 3.5: First mode $\phi_1(y)$ for decay that increases with depth.

$\Lambda B^2/K$	y_1/B
0	0.608
2	0.589
4	0.568
6	0.544
8	0.518
10	0.489

Table 3.3: Discharge positions for decay that increases with depth.

Contrary to the previous two sub-sections, the diffusion centre shifts to the shallower water.

3.6 Ratio λ/u as an indicator for changes in y_1

A physical interpretation of the ratio $\lambda(y)/u(y)$ is as the local spatial decay rate for the contaminant at the cross-channel location y. For the special case of linear depth, it was observed in §3.5 that if $\lambda(y)/u(y)$ is constant (that is, $m = 0$), then the modal shapes $\phi_n(y)$ are not effected by decay and the spatial decay rates μ_n for the modes are merely augmented by that constant spatial decay rate λ/u. It is evident from the square-bracketed terms in equation (3.4), that the same is true whatever the depth profile $h(y)$.

It is natural to investigate whether the depth-dependence of the ratio $\lambda(y)/u(y)$, or the sign and magnitude of the exponent m in the power-law model (3.12), can be used

as an indicator for changes to the position of the diffusion centre. In §3.5.1 and Figure (3.3), $\lambda(y)/u(y)$ decreases with negative exponent $m = -\frac{1}{2}$ and the diffusion centre shifts weakly to deeper water. In §3.5.2 and Figure (3.4), $\lambda(y)/u(y)$ decreases more strongly with negative exponent $m = -1$ and the diffusion centre shifts more strongly to deeper water. Finally, in §3.5.3 and Figure (3.5), $\lambda(y)/u(y)$ increases with positive exponent $m = 1$ and the diffusion centre shifts to shallower water. Hence, the diffusion centre is shifted to deeper or to shallower water accordingly as the ratio $\lambda(y)/u(y)$ decreases or increases with water depth (that is, m negative or positive).

3.7 Concluding remarks

Avoidable shoreline pollution excesses can be large for steady discharges close to shore. The special cases solved in this work sharpen insight about how loss mechanisms displace the best siting of steady discharges away from the site appropriate to non-decaying solutes. The mixing or diffusion centre is shifted to deeper or to shallower water accordingly as the spatial decay rate (that is, ratio $\lambda(y)/u(y)$) decreases or increases with water depth.

The three families of exact modes (3.20, 3.22, 3.24) together with the exact series solution (3.3) and weights (3.8) permit the construction of exact solutions that include decay. Such exact solutions extend the scope for the benchmark testing (Nassehi and Passone, 2005) of numerical computation schemes for environmental impacts in rivers.

Commonly, a steady discharge will comprise a mixture of pollutants with different decay processes and rates. The chosen discharge site will be a compromise between the diffusion centre for the constituent pollutants. For the wide range of cases considered in this work, the optimal discharge position for the different decay processes is never found to be more than one eighth of a channel breadth from the site appropriate to non-decaying solutes. For each decaying constituent the displacement between the discharge site and the diffusion centre for that constituent, corresponds to shoreline pollution excesses less than a factor of 0.4 above optimal (as contrasted to the factor of 4.0 excess at which Figure 3.1 is truncated).

The variety of exact solutions in this chapter illustrate the robustness of the commonsense policy that, to avoid large shoreline pollution excesses from any of the constituents in a mixture of pollutants, the discharge should be sited more or less in the middle of the river.

3.8 References

1. Bikangaga, J. H. and Nassehi, V.: 1995, Application of Computer Modelling Techinques to the Determination of Optimum Efluent Discharge Policies in Tidal Water Systems. *Wat. Res.*, **29**, 10, 2367 - 2375.

2. Daish, N. C.: 1985, The Optimal discharge profiles for sudden contaminant releases in steady, unform open-channel flow. *J. Fluid Mech.*, **159**, 303 - 321.

3. Elder, J. W.: 1959, The dispersion of marked fluid in turbulent shear flow. *J. Fluid Mech.*, **5**, 544 - 560.

4. Fingas, M.: 1994a, Studies on the evaporation of oil spills. Seventeenth Arctic Marine Oil Spill Program (AMOP) Tecnical Seminar, Vancouver, Canada, June 8-10, 1994, Vancouver, British Columbia: Environment Canada, 189-210.

5. Fingas, M.: 1985, A literature review of the physics and predictive modelling of oil spill evaporation. *Journal of Hazardous Materials*, **42**,157 - 175.

6. Fox, L.: 1957, The numerical solution of two-point boundary value problems, Oxford University Press, London UK.

7. Gould, D.J. and Munro, D.: 1981, Relevance of Microbial Mortality to outfall Design. *Coastal Discharges*, Thomas Telford, London, U.K., 45 - 50.

8. Kay, A.: 1987, The Effect of Cross-Stream Depth Variations upon Contaminant Dispersion in a Vertically Well-mixed Current. *Estuarine, Coastal and Shelf Science*, **24**, 2, 177 - 204.

9. Nassehi, V. and Bikangaga, J. H.: 1993, A mathematical model for the hydrodynamics and pollutants transport in long and narrow tidal rivers. *Appl. Math. Modelling*, **17**, 415 - 422.

10. Nassehi, V. and Passone, S.: 2005, Testing Accuracy of Finite Element and Random Walk Schemes in Prediction of Pollutant Dispersion in Coastal Waters. *Environmental Fluid Mechanics*, **5**, 199 - 214.

11. Overstreet, R. and Galt, J.A.: 1995, Physical Processes Affecting the Movement and Spresding of Oils in Inland Waters. NOAA/Hazardous Materials Response and Asssessment Division Seattle, Washingto, HAZMAT Report 95-7.

12. Reddy, G.S. and Brunet, M.: 2003, Numerical Prediction of Oil Slick Movement in Gabes Estuary, *www.fluidyn.com/Research.*

13. Rutherford, J. C.: 1994, River Mixing, Wiley, Chichester UK.

14. Smith, R.: 1981, Effect of non-uniform currents and depths variations upon steady discharges in shallow water. *J. Fluid Mech.*, **110**, 373 - 380.

15. Smith, R.: 1982, Where to put a steady discharge in a river. *J. Fluid Mech.*, **115**, 1 - 11.

16. Smith, R.: 1996, Horizontal fractionation of rising and sinking particles in wind-affected currents. *J. FLuid Mech..*, **316**, 325 - 334.

17. Smith, R.: 2004, Mixing Center of a Channel. *J. Hydraulic Engineering*, **130**, 2, 165 - 169.

18. Yoo, M. K., Cho, S. W., and Jun, K. S.: 2003, Unsteady Dispersion of Nonconservative Pollutants in Natural Rivers. *www.kfki.baw.de/conferences.*

19. Yotsukura, N. and Cobb, E. D.: 1972, Transverse diffusion of solutions in natural streams. *U. S. Geo. Survey Paper*, no.582 C.

20. Yotsukura, N. and Sayre, W.W.: 1976, Transverse mixing in natural channels. *U. S. Geo. Survey Paper*, no.582 C.

Chapter 4

Ray approximation for steady discharges in rivers

4.1 Introduction

One critical element in designing management strategies for rivers is the understanding of the dynamics of perturbations introduced into the water. Such perturbations include climatically forced variables (for example, changes in freshwater runoff) as well as spills of contaminants related to human activities along the river or in its watershed. For example, toxic contaminants could enter rivers by a variety of methods, including industrial and municipal wastewater discharges, urban runoff, accidental spills, landfill leachate, and tributary discharges (Fyrillas, 2000; Ho *et al.*, 2002; Baker *et al.*, 2003; Nedeau *et al.*, 2003). After the initial discharge, physical processes such as advective transport, dispersion and contaminant decay mechanisms (Mebine and Smith, 2006) play important roles in determining the movement and change in concentration of contaminants. Thus, they influence decision on methods used for detection, remediation, and treatment are likely to be most successful.

Kay (1987) demonstrated that depth topography has strong influence upon the horizontal spreading of a contaminant plume in vertically well-mixed currents. The method of solution of Kay's problem utilised the method of images, with real and virtual contaminant sources, and is therefore restricted to certain abrupt geometries. One objective of the present work is to investigate the effects of depth-dependent decay upon steady discharges in water of smoothly varying depth.

When advection dominates diffusion, there are special directions (rays), distinct from but closely related to the contaminant flux vector, along which information is carried (Smith, 1981). A second objective of this work is, therefore, to sharpen our intuition about the relative complementary role of decay upon such rays.

It is pertinent to note here that, undoubtedly, the ray method remains one of the most powerful and broadly used methods for investigating both forward and inverse wave propagation problems in modern exploration geophysics. Some fundamental ideas of the ray theory and its applications have been known in physics and the like for a long time

(Babich, 1956; Karal and Keller, 1959; Smith, 1970; Červený and Ravindra, 1971; Červený, Molotkov and Pšenčik, 1977; Hanyga, 1984; Kravtsov and Orlov, 1990).

The ray method has the following advantages. It provides a physical insight to the wave propagation phenomenon in rather complicated geophysical models, by describing the total wave field as a sum of different types of waves generated in the problem under consideration. It gives rise to rather effective and not so time consuming numerical algorithms when compared to the finite difference and finite element methods. On the other hand, the ray method is not without its limitations. The ray method does not correctly describe the wave field in the vicinity due to caustic problems.

Cohen and Lewis (1967) have shown that the mathematical methods of ray developed for wave problems can be applied for diffusion problems. Here we apply these methods to the two-dimensional advection-diffusion equation with contaminant decay. The outcome is a simple constructive procedure, which yields an accurate approximation to the concentration distribution.

4.2 Advection-diffusion equation

In keeping with the generality of the dispersion concept for horizontal spreading of a contaminant plume in vertically well-mixed currents and the loss of reactive contaminant by a first order reaction in the moving fluid, we start our mathematical analysis with the steady state depth-averaged advection-diffusion-reaction equation:

$$\lambda\, h\, c + \nabla\cdot(h\,\mathbf{u}c) - \nabla\cdot(h\,D\nabla c) = 0. \tag{4.1}$$

Here x and y are the longitudinal and transverse coordinates, $c(x,y)$ is the contaminant concentration in water of depth $h(x,y)$, $\mathbf{u}(x,y)$ is the vertically-averaged steady velocity vector, $D(x,y)$ is the vertically-averaged effective transverse diffusivity across the flow, $\lambda(y)$ is the first-order decay parameter, and ∇ is the horizontal gradient operator $(\partial_x\,,\partial_y)$. It

is the long-thin nature of steady contaminant plumes that gives predominance transverse diffusivity and permits a scalar rather than tensor characterisation of the dilution process.

Conservation of mass for the steady current implies that

$$\nabla \cdot (h\mathbf{u}) = 0. \tag{4.2}$$

4.3 The ray ansatz

In the spirit of the WKB approximation we shall assume that, with a suitable choice for the amplitude and phase (decay) functions $A(x, y), \Phi(x, y)$, the classical geometrical optics solution

$$c = A \exp(\pm \Phi) \tag{4.3}$$

can be constructed. If $\pm$ is replaced by i, where i is an imaginary unit, then the equation (4.3) becomes a specification of any local property of wave train (that is, pressure, velocity, displacement) in coastal zones (Massel, 1989) and also known as Fresnel representation (Iglesias and Negro, 2003). The representation (4.3) is due to Cohen and Lewis (1967) and has been widely used in the study of contaminant discharges in river systems by Smith(1981, 1983). If the steady flow were reversed (that is, $+\mathbf{u}$ replaced by $-\mathbf{u}$), then the direction of the plume would likewise be reversed. The $\pm$ sign is a technical device to ensure that this property is preserved exactly.

4.3.1 Eikonal and Transport equations

If we substitute the ansatz (4.3) into the advection-diffusion-reaction equation(4.1), with flow velocity $\pm\mathbf{u}$, then we generate terms proportional to

$$\exp(\pm \Phi) \quad \text{and} \quad \pm \exp(\pm \Phi).$$

Equating these groups of terms separately to zero, we have

$$h\lambda + h\mathbf{u}\cdot\nabla\Phi - hD(\nabla\Phi)^2 = \frac{1}{A}\nabla\cdot(hD\nabla A) \tag{4.4}$$

and

$$\nabla\cdot(h\mathbf{u}A) - hD\nabla A\cdot\nabla\Phi - \nabla\cdot(hDA\nabla\Phi) = 0. \tag{4.5}$$

The first, equation (4.4), governs the phase function Φ and is designated in analogy with geometrical optics, an *Eikonal* equation. The second, equation (4.5), is referred to as the *Transport* or the *Energy* equation, for it expresses mathematically the transmission of energy associated with wave propagation in wave dynamics.

The equations (4.4) and (4.5) are coupled. These equations can be decoupled by considering the essential features for the WKB-type approximation such that the phase Φ varies more rapidly than does the amplitude A (that is, the long-thin nature of steady contaminant plumes). Therefore, the corresponding approximation of equation (4.4) becomes

$$\lambda + \mathbf{u}\cdot\nabla\Phi - D(\nabla\Phi)^2 = 0. \tag{4.6}$$

What has been achieved with the ray approximation is that the parabolic equation (4.1) has been replaced by the hyperbolic equations (4.5) and (4.6). Thus instead of the concentration at any one point being influenced by all other points, the influence only comes outwards from the source (along ray paths). For conserved contaminants Smith (1983) solved equations (4.5) and (4.6) by marching methods. The main limitation of the ray approximation is that it is only applicable for wide rivers or open coastlines. It fails to account for the reflection at any far shoreline, or abrupt depth change.

4.3.2 Exponential Decay

The equation (4.6) is a nonlinear first-order partial differential equation, but it can be presented as an ordinary differential equation along a ray. The method of solution is the well known method of characteristics or rays (Sneddon, 1957; Courant and Hilbert, 1962). To this end, let

$$x = x(s)\,,\; y = y(s)$$

be a curve in $2D$ and consider a function $f = f(x\,,y)$. Then the derivative along the curve is defined by the formula

$$\frac{df}{ds} = \frac{\partial f}{\partial x}\frac{dx}{ds} + \frac{\partial f}{\partial y}\frac{dy}{ds} = \nabla f \cdot \mathbf{t}, \tag{4.7}$$

where s is the arc length also referred to as the travel time (Benamou, 1996) along the curve and $\mathbf{t}$ is a unit tangent vector to the curve. The formal derivatives of equation (4.6) with respect to $\frac{\partial \Phi}{\partial x}$, $\frac{\partial \Phi}{\partial y}$ define the ray direction. Normalization yields the unit tangent vector

$$\mathbf{t} = \frac{\mathbf{u} - 2D\nabla\Phi}{\sqrt{|\mathbf{u}|^2 + 4\lambda D}}. \tag{4.8}$$

From equation(4.7), taking $f = \Phi$ the rate of the exponential decay or the phase function along a ray is defined via the formula

$$\frac{\partial \Phi}{\partial s} = \mathbf{t} \cdot \nabla\Phi. \tag{4.9}$$

By eliminating $(\nabla\Phi)^2$ by means of the Eikonal equation (4.6), we obtain

$$\frac{\partial \Phi}{\partial s} = \frac{\mathbf{u}\cdot\mathbf{t} - \sqrt{|\mathbf{u}|^2 + 4\lambda D}}{2D} = -\frac{\left(4\lambda D + |\mathbf{u}|^2 - (\mathbf{u}\cdot\mathbf{t})^2\right)}{2D\left(\mathbf{u}\cdot\mathbf{t} + \sqrt{|\mathbf{u}|^2 + 4\lambda D}\right)}. \tag{4.10}$$

Hence, we see that the phase function along a ray depends upon the rate of contaminant decay and the relative direction of the ray path, and current. Decay is least in the flow direction with $\mathbf{t}$ aligned with $\mathbf{u}$.

In order to extend a ray path away from the source, we must know both its direction $\mathbf{t}$ and its curvature $K(s)$. If $\mathbf{k}$ is the unit vertical vector, a ray normal unit vector $\mathbf{n}$ can be defined such that $\mathbf{t}$, $\mathbf{n}$ and $\mathbf{k}$ form a right-handed triad. The curvature $K(s)$ can be defined in terms of $\mathbf{n}$, s and $\mathbf{t}$ as follows:

$$K \equiv \mathbf{n} \cdot \frac{\partial}{\partial s}\mathbf{t} = \mathbf{n} \cdot [(\mathbf{t} \cdot \nabla)\mathbf{t}] = \mathbf{n} \cdot [(\nabla \times \mathbf{t}) \times \mathbf{t}], \tag{4.11}$$

since $\mathbf{t} \cdot \mathbf{t} = 1$. The equation (4.11) is also known as Frenet's formula. If we define the advection-diffusion vector $\mathbf{K}$ by

$$\mathbf{K} = \frac{\mathbf{u}}{2D}, \tag{4.12}$$

then it follows from equation (4.8) that

$$\mathbf{t} = \frac{\mathbf{K} - \nabla\Phi}{\sqrt{|\mathbf{K}|^2 + \frac{\lambda}{D}}}. \tag{4.13}$$

Now denoting

$$|\mathbf{M}| = \sqrt{|\mathbf{K}|^2 + \frac{\lambda}{D}}, \tag{4.14}$$

with some manipulation of vector products, it follows from equations (4.11) and (4.13) that

$$K = \frac{\mathbf{n} \cdot \nabla|\mathbf{M}| + \mathbf{k} \cdot (\nabla \times \mathbf{K})}{|\mathbf{M}|}. \tag{4.15}$$

Decay λ influences the ray curvature via the appearance of the decay-diffusivity ratio λ/D in the formula (4.14).

4.3.3 Amplitude Factor

The field of geometrical optics has been developed within the context of light wave transport, it is valid to a great extent for water waves. It is known that waves carry energy along with them. In fact, water waves are just energy being transported along the sea surface. The amount of energy at each point on the wave train is directly related to the amplitude of oscillation at the same point. Here we draw an analogy and derive, in this section, the formulation for the amplitude factor as an energy conservation principle. As the contaminants spread out over a shoaling bottom, the contaminants are dispersed along a larger area and the amplitude decreases correspondingly. In the opposite case, if the bottom causes the rays to approach each other, the contaminants are focused and the amplitude increases. When this amplitude increase is large enough, the ray description breaks down.

The derivatives of the amplitude factor $A(x, y)$ in the transport equation (4.5) exactly conform to the ray direction. Therefore, to complete our solution for the concentration distribution $c(x, y)$, we need to determine the amplitude factor $A(x, y)$. Again, the aid of the solution is by the use of ray paths. It can readily be observed that by the use of the equations (4.7) and (4.8), the transport equation (4.5) can be written as

$$\frac{1}{A}\frac{\partial A}{\partial s} + \frac{1}{h\sqrt{|\mathbf{u}|^2 + 4\lambda D}}[\nabla \cdot (h\mathbf{u}) - \nabla \cdot (hD\nabla\Phi] = 0. \tag{4.16}$$

Next, we introduce a parameter p which labels the individual rays, and we consider the ray separation

$$J(p, s) = \left|\frac{\partial(x, y)}{\partial(p, s)}\right|. \tag{4.17}$$

This is called the spreading of a ray tube or geometrical spreading. In terms of the geometrical sense of the spreading we can infer that if the ray tube becomes wider, J increases, and if the ray tube becomes narrower and rays are focusing, for example, at a certain point

J decreases and $J = 0$ precisely at that point.

If we take the s-derivative of the formula (4.17) and eliminate second derivatives with respect to p by means of the chain rule, relating $x-, y-$ and $p-, s-$ derivatives, for example,

$$\frac{\partial^2 x}{\partial s\, \partial p} = \left(\frac{\partial x}{\partial p} \frac{\partial}{\partial x} + \frac{\partial y}{\partial p} \frac{\partial}{\partial y} \right) \frac{\partial x}{\partial s}, \tag{4.18}$$

then we obtain the result:

$$\frac{1}{J} \frac{\partial J}{\partial s} = \nabla \cdot \mathbf{t}. \tag{4.19}$$

This result (4.19), together with equations (4.8) and (4.14), permits us to rewrite the transport equation (4.16) as

$$\frac{1}{A} \frac{\partial A}{\partial s} + \frac{1}{2} \frac{1}{J} \frac{\partial J}{\partial s} + \frac{1}{2} \frac{1}{h\, D\, |\mathbf{M}|} \frac{\partial}{\partial s} \left(h\, D\, |\mathbf{M}| \right) = -\frac{1}{4} \frac{\nabla \cdot (h\mathbf{u})}{h\, D\, |\mathbf{M}|}. \tag{4.20}$$

Conservation of mass (4.2) for the steady current implies that the right-hand side is zero. Thus, equation (4.20) reduces to a homogenous ordinary differential equation, whose solution is given by

$$A = \frac{\Psi(p)}{J^{\frac{1}{2}}\, h^{\frac{1}{2}}\, D^{\frac{1}{2}} |\mathbf{M}|^{\frac{1}{2}}} = \frac{\Psi(p)}{J^{\frac{1}{2}}\, h^{\frac{1}{2}} \left(|\mathbf{u}|^2 + 4\lambda D \right)^{\frac{1}{4}}}, \tag{4.21}$$

where $\Psi(p)$ is a constant along rays. An immediate implication is that the contaminant concentrations are greatest where the ray separation J is relatively small or where the water depth, flow, diffusion and contaminant decay are least.

4.4 Ray tracing algorithm

The ideas developed in the previous sections constitute the building blocks for the analytical computation of the phase function, the curvature and the amplitude factor. We now propose

an algorithm with minimum computational demands for the numerical solutions of the curvature.

Ray tracing is a well established rendering technique in optics and computer graphics employed to create convincing depictions of natural environments (Whitted, 1980). The steps involved in the algorithm for the present work are as follows: (a) Define a source point (x_0, y_0); (b) Shoot a given number of rays, N, in regularly spaced directions. Denote these rays by $(R_n)_{n=0\ N}$; (c) Define the components of the unit vector $\mathbf{t}$ in the x- and y-directions respectively as t_1 and t_2 such that $t_1 = \cos\theta_n\,, t_2 = \sin\theta_n$, with $\theta_n = (-\frac{1}{2} + \frac{n}{N})\pi$, where n is the number count of the rays; (d) Compute the curvature; (e) Advance the rays and the direction vector $\mathbf{t}$ (or the angle θ_n), then return to step (d). These processes evaluate the curvature numerically. The illustrative examples considered hereafter takes $N = 20$ and ray tracing has been performed using a code written in Maple to integrate the ray equations.

4.5 Model problems to determine the curvature

For any real topography, the ray curvature would have to be calculated numerically and the previous section gives steps of the algorithm for the computation. However, it is of interest to consider some simple illustrative examples to sharpen our intuition about the relative roles of water depth, current strength, turbulence intensity and contaminant decay.

For steady, unstratified, plane parallel flow in water of non-uniform depth $h(y)$, Elder (1959) gave the scalings for the velocity and turbulent diffusivity respectively as

$$u = U\left(\frac{h}{H}\right)^{\frac{1}{2}}\,, \quad \kappa = \kappa_0\left(\frac{h}{H}\right)^{\frac{3}{2}}. \tag{4.22}$$

Therefore, the advection-diffusion vector is modelled as

$$\mathbf{K} = \text{constant}\,(1/h\,, 0\,, 0). \tag{4.23}$$

For the contaminant decay, power-law models with respect to the non-uniformity of the depth is employed:

$$\lambda = \Lambda \left(\frac{h}{H}\right)^{3/2+m}. \tag{4.24}$$

Accordingly, the decay-diffusivity ratio then becomes

$$\frac{\lambda}{D} = \frac{\Lambda}{\kappa_0} \left(\frac{h}{H}\right)^{m}, \tag{4.25}$$

where m is an integer relating to the nature of decay-diffusivity ratio with respect to the depth, H and Λ are respectively reference depth and decay. With the equations (4.23) and (4.25), the curvature (4.15) can be constructed for some powers of m in general:

$$K = \frac{1}{1+\beta\left(\frac{h}{H}\right)^{m+2}} \left[\sqrt{1+\beta\left(\frac{h}{H}\right)^{m+2}} - \left(1 - \frac{\beta m}{2}\left(\frac{h}{H}\right)^{m+2}\right)t_1\right] \frac{h'}{h}, \tag{4.26}$$

where $\beta = \frac{4\Lambda\kappa_0}{U^2}$. Much as Λ quantifies the strength of the decay, β the strength of the decay-diffusivity ratio.

4.5.1 Conserved contaminants

In the absence of decaying contaminants ($\beta = 0$), the curvature profile (Smith, 1981; equation (6.2)) becomes

$$K = (1 - t_1)\frac{h'}{h}. \tag{4.27}$$

Ray paths are closely related to the directions of contaminant flux. The results indicated that the rays and hence the contaminant flux, tend to curve towards the deeper water. Moreover, the variation in $h|\mathbf{u}|$ further exaggerates the asymmetry of the concentration distribution. Figure 4.1 shows the ray paths for equation (4.27) and it is observed that the

rays curve towards the deeper water, the ray at the middle is straight along and the lowest ray hits the bank at 1.

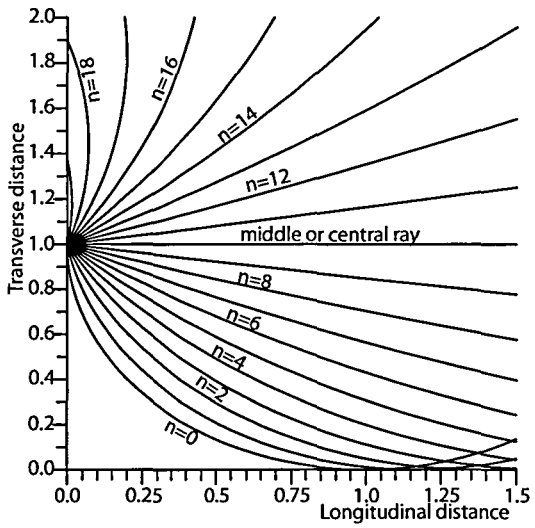


Figure 4.1: Ray paths for conserved contaminant spreading.

The following three subsections concern the same depth related velocity, turbulent diffusivity and decay profiles, but with decay-diffusivity ratio profiles corresponding to uniform consumption by bacteria, to evaporation and to break up by turbulence. For positive (or negative) m the ratio λ/D increases (or decreases) with depth and gives indication of changes to the curvature. Herein we consider three cases: (i) constant decay-diffusivity ratio, (ii) decay-diffusivity ratio that decreases with depth, and (iii) decay-diffusivity ratio that increases with depth.

4.5.2 Constant decay-diffusivity ratio

Radioactive decay or consumption by bacteria (at a rate unaffected by sunlight or turbidity) are examples that the temporal decay to diffusivity ratio is constant (that is, $m = 0$). For

this decay-diffusivity ratio model, from equation (4.26) it then follows that

$$K = \frac{1}{1+\beta\left(\frac{h}{H}\right)^2}\left(\sqrt{1+\beta\left(\frac{h}{H}\right)^2} - t_1\right)\frac{h'}{h}. \tag{4.28}$$

As our study is primarily intended to highlight the effect of decay actions via the decay-

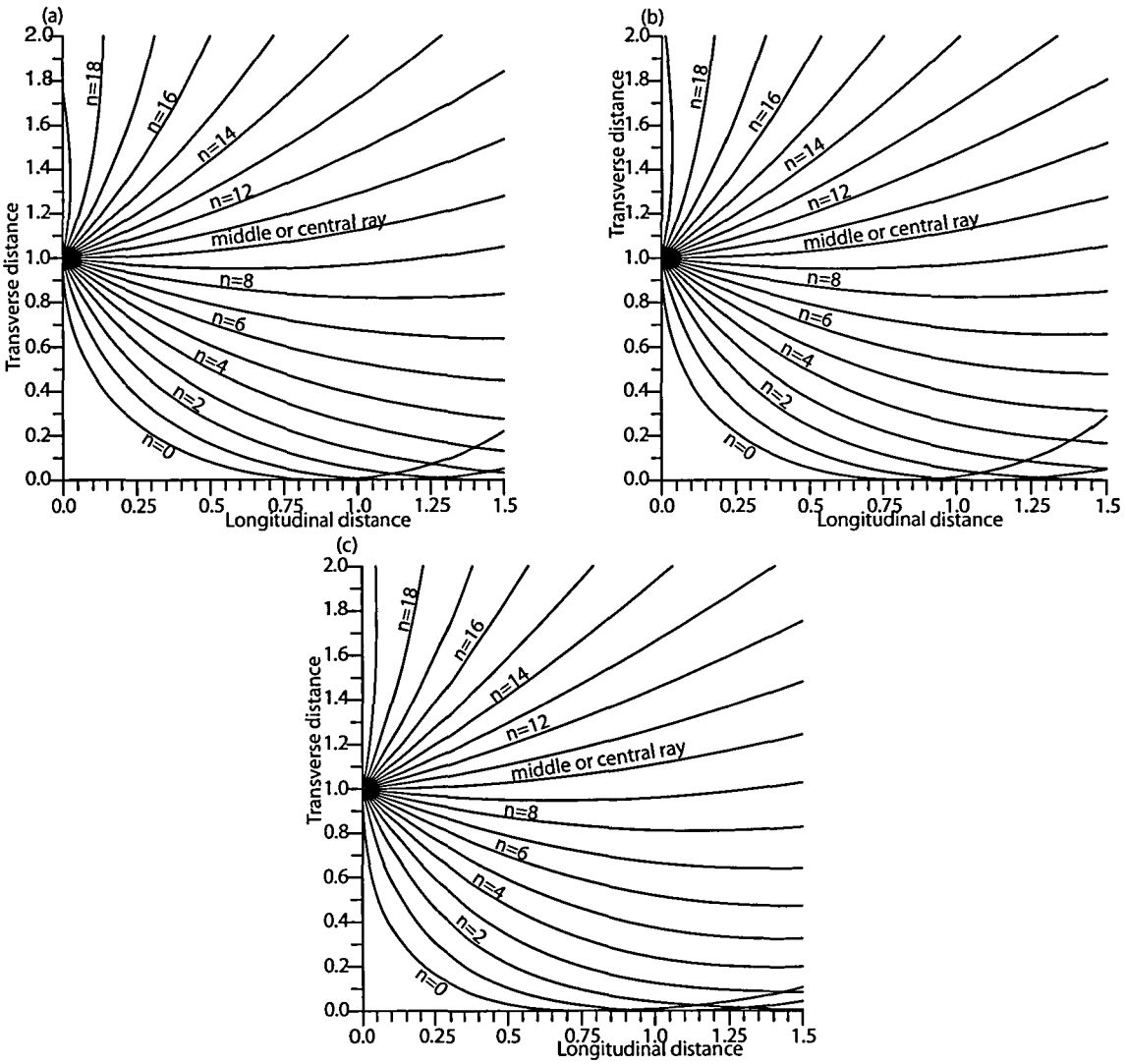


Figure 4.2: Ray paths for constant decay-diffusivity ratio: (a) $\beta = 2$; (b) $\beta = 4$; (c) $\beta = 8$.

diffusivity ratio, the illustrative decay-diffusivity strengths are taken to be 2, 4 and 8, and Figures 4.2 (a), (b) and (c), respectively show their effects for the curvature (4.28). From

each of the figures it is straightforward to compute the point where the lowest ray hits the bank. It is clearly observed from these figures that the ray paths curve towards the deeper water and the lowest ray hits the bank just before 1. For the ray that starts along x-direction, decay curves it up. For the ray that starts directly toward the shoreline, the point of hit shifts backwards as compared to the conserved case (see Figures 4.2). As h tends to zero, $t_1 = 1$ removes the singularity in curvature, but makes ray separation tend to zero.

4.5.3 Decay-diffusivity ratio that decreases with depth

The decay can decrease with depth if $c(y,t)$ is a number count of bacteria which are killed by sunlight (Gould and Munro, 1981) only in the top few metres of the water column. A second example is removal at the bed (feeding by marine micro-organisms, fungi or yeasts). A third example is air-water contaminant exchange at the surface. Here we illustrate the decay-diffusivity ratio that decreases with depth in three illustrative examples. In the first example, the degree of decay of the decay-diffusivity ratio is modelled $m = -2$. Here the curvature from equation (4.26) is given as

$$K = \frac{1}{\sqrt{1+\beta}}\left[\sqrt{1+\beta} - (1+\beta)t_1\right]\frac{h'}{h}. \tag{4.29}$$

Figures 4.3 (a), (b) and (c) depict a spectrum of twenty ray paths for the curvature (4.29) for each of the decay-diffusivity strengths $\beta = 2, 4$ and 8, respectively. The power law $m = -2$ gives a transition for shoreline behaviour of the ray paths. It can easily be observed from the Figures 4.3 (a), (b) and (c) that the rays hit the shore at approximately the same angle and the ray separation remains non-zero. Again, the lowest ray hits the shore far before 1 as compared to the conserved case (see Figure 4.1). The curvature of the rays significantly depend on the decay-diffusivity strength β. For each decay strength there is a threshold as to when the rays curve. In particular, for $\beta = 2, 4$ and 8 the ray paths

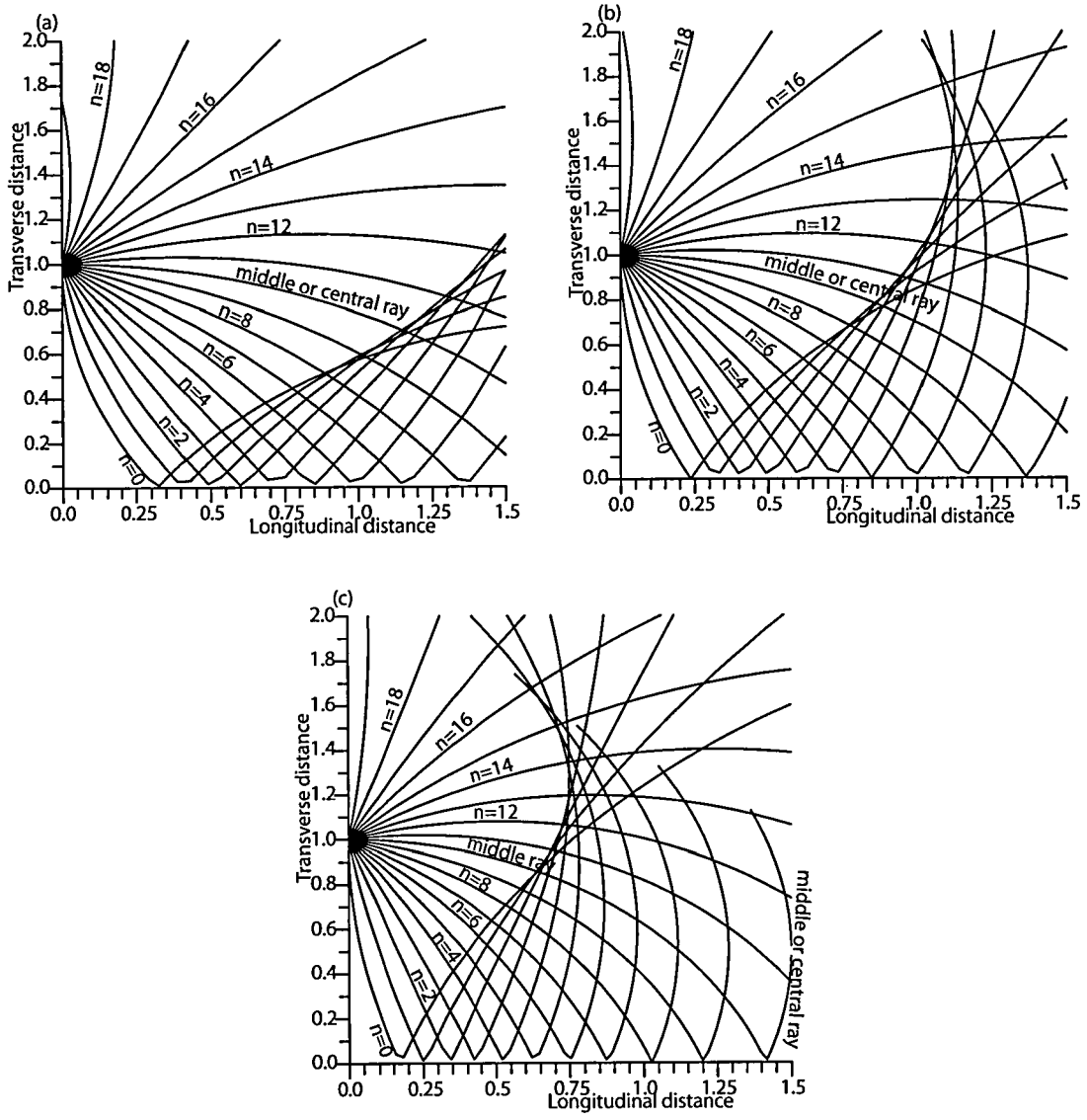


Figure 4.3: Ray paths for decay-diffusivity that decreases with depth, $m = -2$: (a) $\beta = 2$; (b) $\beta = 4$; (c) $\beta = 8$.

curve up if m exceeds $1-\sqrt{3}$, $1/2-1/2\sqrt{5}$, and $1/4-1/4\sqrt{9}$, respectively. The obvious shapes seen in the figures are due to small dropoffs, situations more often encountered when the rays are hyperbolic. This fact was emphasized by Musgrave (1990) who suggested that in this case the rays are best approximated by perfectly reflecting rays. The shapes of the rays confirm this suggestion (see Figures 4.3 (a), (b) and (c)). In this context the caustics do not render the ray solution invalid. The direct rays give the dominant contribution to the concentration. The reflected rays give an exponentially small contribution, by virture of the Φ exponent. The caustics makes the J tend to zero and the representation for the reflected contribution is not valid. The true reflected contribution remains exponentially small, but not as small as suggested by the ray calculation.

Another view of the ray crossings observed in the Figures 4.3 are due to the occurrence of complicated slowness profiles (symbolically these are $1/J, 1/h, 1/D$ and $1/M$) at the caustic line $x = 0$. Physically the ray crossings indicate multiple arc lengths occuring at the same location. In order to recover multivalued arc length field in the whole domain, the ray solutions have to be interpolated. Such considerations are reported in literature (Gjoystdal, Vinje, and Iversen, 1993; Kawanada and Asakawa, 1993; Hanyga, Lambare and Lucio, 1994).

We consider next under this subsection two specific examples where $m > -2$ and $m < -2$. The first of these is when $m = -3/2$. The resulting curvature to this power-law is given by

$$K = \frac{1}{1+\beta\left(\frac{h}{H}\right)^{1/2}}\left[\sqrt{1+\beta\left(\frac{h}{H}\right)^{1/2}} - \left(1+\frac{3\beta}{4}\left(\frac{h}{H}\right)^{1/2}\right)t_1\right]\frac{h'}{h}. \tag{4.30}$$

Figures 4.4 (a), (b) and (c) demonstrates the decay-diffusivity action for the curvature (4.30) with $\beta = 2, 4$ and 8, respectively. Here it is observed that at $t = 1$ the rays are tangent at the shoreline but renders the ray separation zero. Once again, the lowest ray hits the shore far before 1 as seen different from the conserved situation.

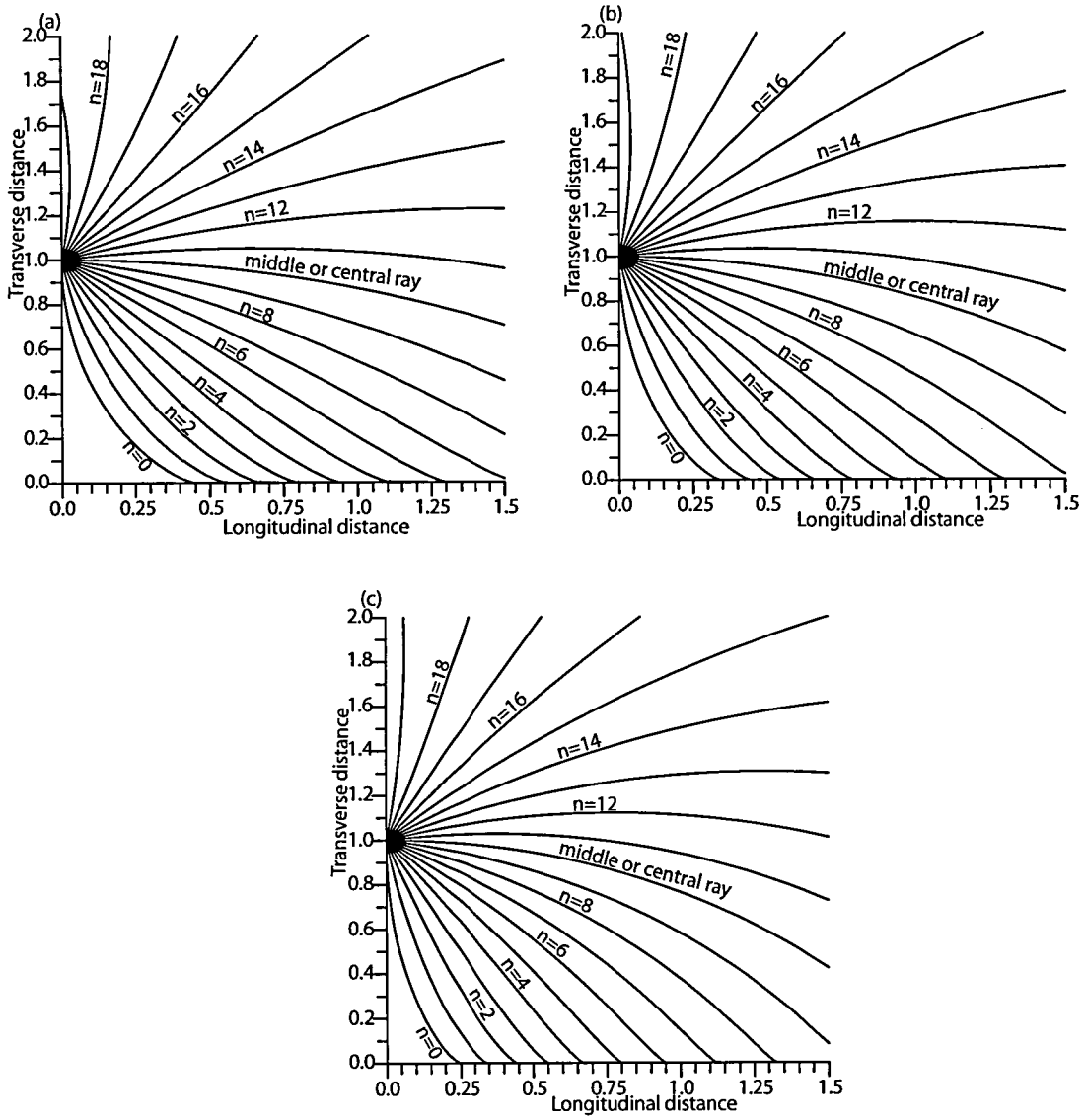


Figure 4.4: Ray paths for decay-diffusivity ratio that decreases with depth, $m = -3/2$: (a) $\beta = 2$; (b) $\beta = 4$; (c) $\beta = 8$.

The third illustrative example is when $m = -5/2$. Here the curvature from this power-law is given by

$$K = \frac{1}{\left(1+\beta\left(\frac{h}{H}\right)^{-1/2}\right.} \left[\sqrt{1+\beta\left(\frac{h}{H}\right)^{-1/2}} - \left(1+\frac{5\beta}{4}\left(\frac{h}{H}\right)^{-1/2}\right)t_1\right] \frac{h'}{h}. \tag{4.31}$$

Figures 4.5 (a), (b) and (c) show the ray paths for the curvature (4.31) with decay strengths $\beta = 2, 4$ and 8, respectively. The ray paths curve toward the shoreline and the lowest ray in each of the figures hits the shore far below 1. The decay strength shifts the point of hit of the lowest ray towards the origin. The ray separation remains non-zero.

Comparison of the models of decay-diffusitivity ratio that decreases with depth with the conserved case shows generally the expected decrease in contaminant concentration in the deeper water, and an overall decrease in the distance downstream for which high concentrations persist.

4.5.4 Decay-diffusivity ratio that increases with depth

The dissolution of contaminants or break up of clay flocs is most rapid in regions of the flow where the turbulence is energetic. Two illustative examples are considered here. In the first example, the decay-diffusivity ratio is modelled as proportional to the velocity (that is, $m = 1/2$). The curvature (4.15) is obtained as

$$K = \frac{1}{1+\beta\left(\frac{h}{H}\right)^{5/2}} \left[\sqrt{1+\beta\left(\frac{h}{H}\right)^{5/2}} - \left(1-\frac{\beta}{4}\left(\frac{h}{H}\right)^{5/2}\right)t_1\right] \frac{h'}{h}. \tag{4.32}$$

As can be seen in Figures 4.6 (a), (b) and (c) the rays and hence the contaminant flux, tend to curve towards the deeper water. In particular, the middle ray curves up and the lowest ray in each of the figures hits the shore before 1 and the decay ensure its gradual shift towards the origin.

The second example under the decay-diffusivity ratio that increases with depth is when

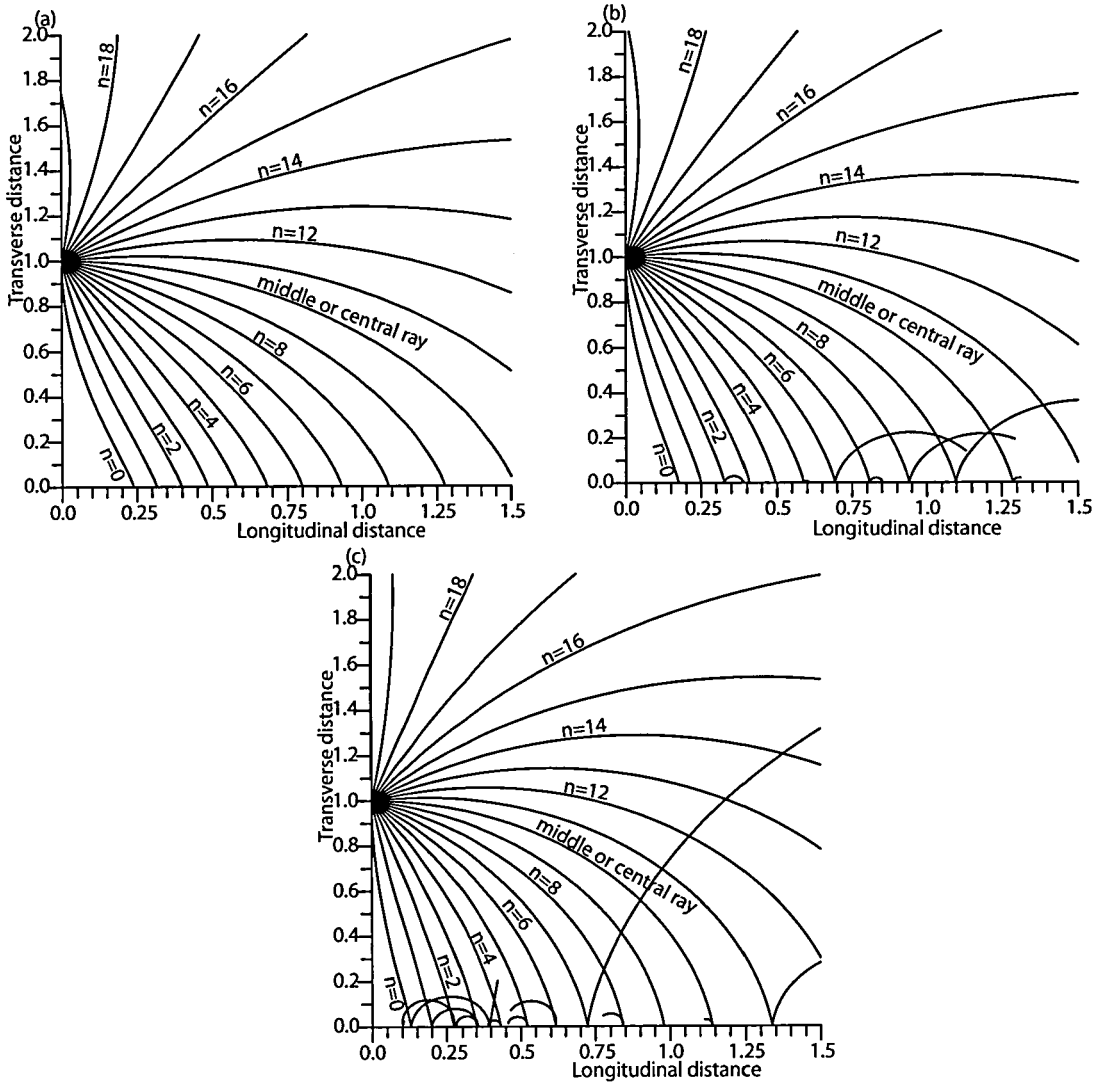


Figure 4.5: Ray paths for decay-diffusivity ratio that decreases with depth, $m = -5/2$: (a) $\beta = 2$; (b) $\beta = 4$; (c) $\beta = 8$.

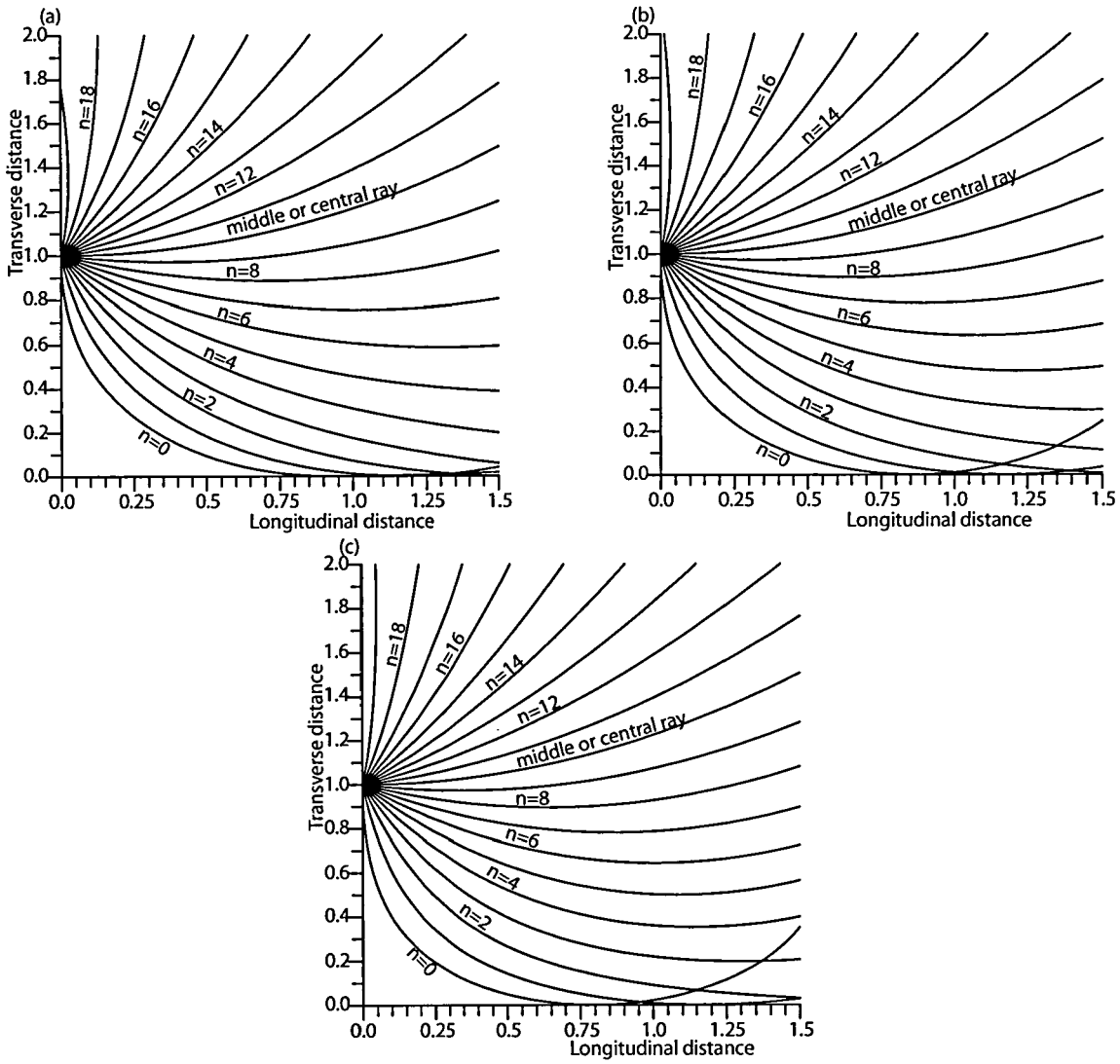


Figure 4.6: Ray paths for decay-diffusivity ratio that increases with depth, $m = 1/2$: (a) $\beta = 2$; (b) $\beta = 4$; (c) $\beta = 8$.

$m = 3/2$. This results in the following relation for the curvature:

$$K = \frac{1}{1+\beta\left(\frac{h}{H}\right)^{7/2}}\left[\sqrt{1+\beta\left(\frac{h}{H}\right)^{7/2}} - (1 - \frac{3\beta}{4}\left(\frac{h}{H}\right)^{7/2})t_1\right]\frac{h'}{h}. \tag{4.33}$$

Figures 4.7 (a), (b) and (c) compare the ray paths in the case of equation (4.33) for $\beta = 2, 4$ and 8. Although there are qualitative changes, the general features for the illustrative examples considered under decay-diffusivity ratio that increases with depth remain as before for the constant decay-diffusivity ratio model problems.

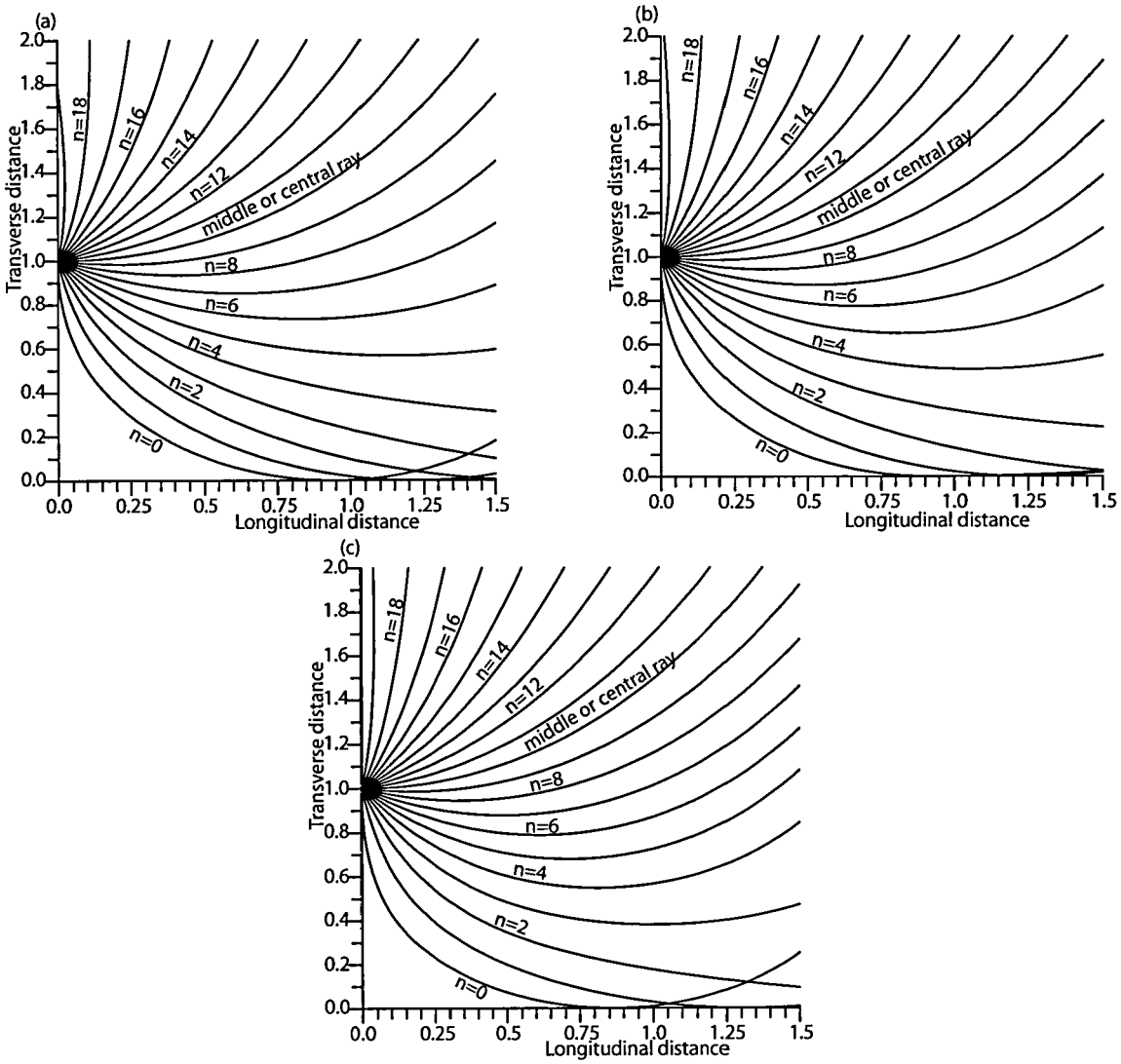


Figure 4.7: Ray paths for decay-diffusivity ratio that increases with depth, $m = 3/2$: (a) $\beta = 2$; (b) $\beta = 4$; (c) $\beta = 8$.

4.6 Sensitivity of curvature to decay-difffusivity ratio

In order to construct the sensitivity analysis of curvature to the decay-diffusivity ratio, we make use of the x-component of the unit vector $\mathbf{t}$, $t_1 = \cos\theta$, where θ is the angle between $\mathbf{t}$ and some fixed direction in the plane of motion. To this end, the sensitivity analysis of the curvature to the decay-difffusivity ratio can be investigated in terms of θ and for its derivative with respect to β for some powers of m in general. In particular, for the linear depth profile where $h(y) \propto y$ and by putting $y/B = 1$ (the point source plume), we obtain the curvature:

$$K = \frac{1}{1+\beta}\left[\sqrt{1+\beta} - \left(1 - \frac{\beta m}{2}\right)\cos\theta\right]. \tag{4.34}$$

A critical survey of equation (4.15) indicates that the curl gives the average curvature, as in rays pointing along or opposite to the gradient of decay-augmented absolute value, and the directional variation has tightest left curvature when large decay-augmented absolute value is on the left. The following Figures 4.8 (a), (b), (c) and (d) give illustrations of the sensitivity of curvature to decay using equation (4.34). Clearly, it can be observed that the rays at $y/B = 1$ point in all possible directions.

A second illustration of the sensitivity of curvature to decay is the derivative of the curvature (4.26) with respect to the strength of the decay-diffusivity ratio. At the point source plume, $y/B = 1$ using equation (4.34) we obtain

$$\frac{dK}{d\beta} = \frac{1}{2(1+\beta)^2}\left[(\beta m + 2)\cos\theta - \sqrt{1+\beta}\right]. \tag{4.35}$$

Generally, it can be observed that decay makes curvature negative (shore wards) (see Figures 4.9 (a), (b), (c) and (d)). In effect, the decay reduces the concentration of the contaminant downstream.

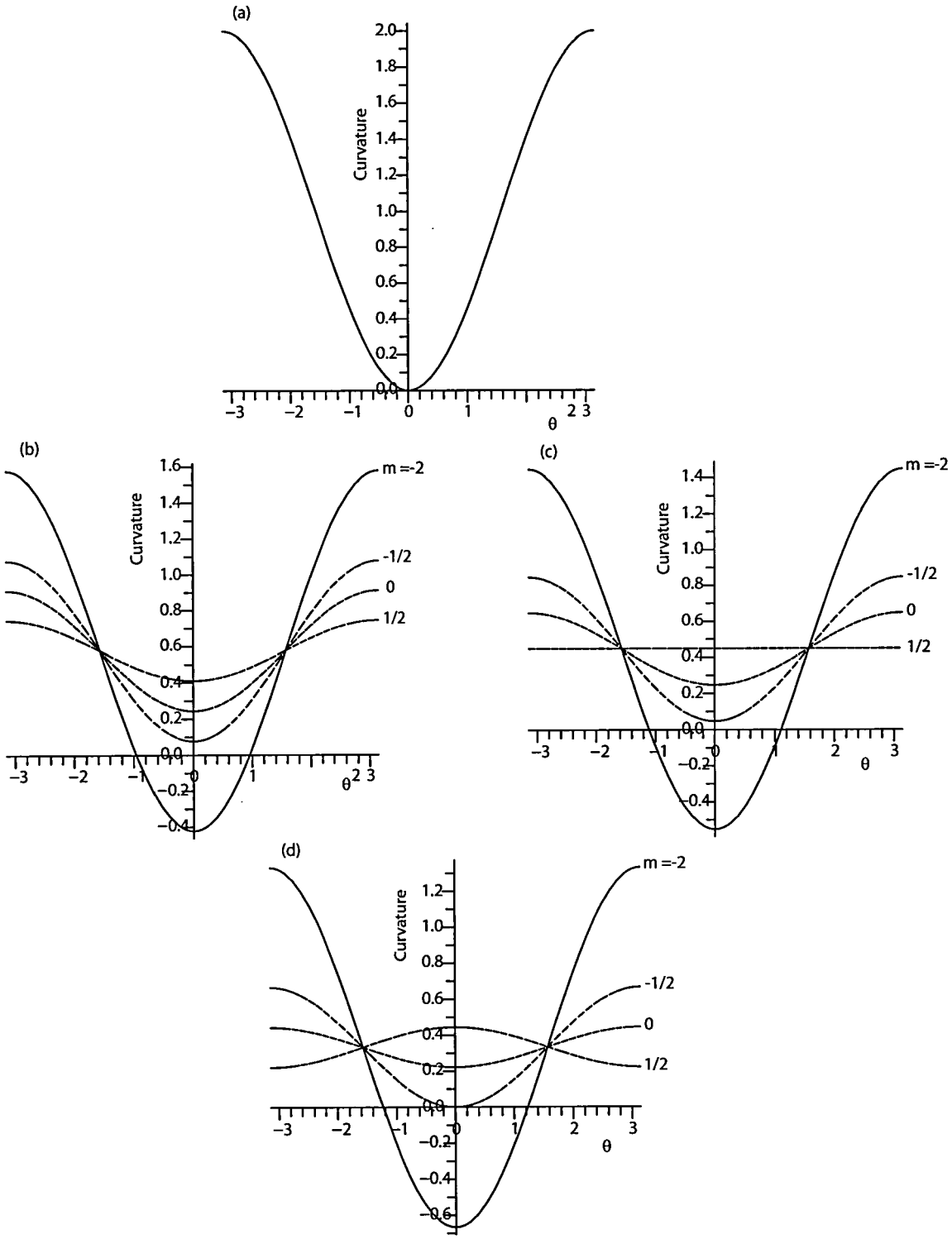


Figure 4.8: Curvature as a function of ray angle for different powers of m: (a) $\beta = 0$; (b) $\beta = 2$; (c) $\beta = 4$; (d) $\beta = 8$.

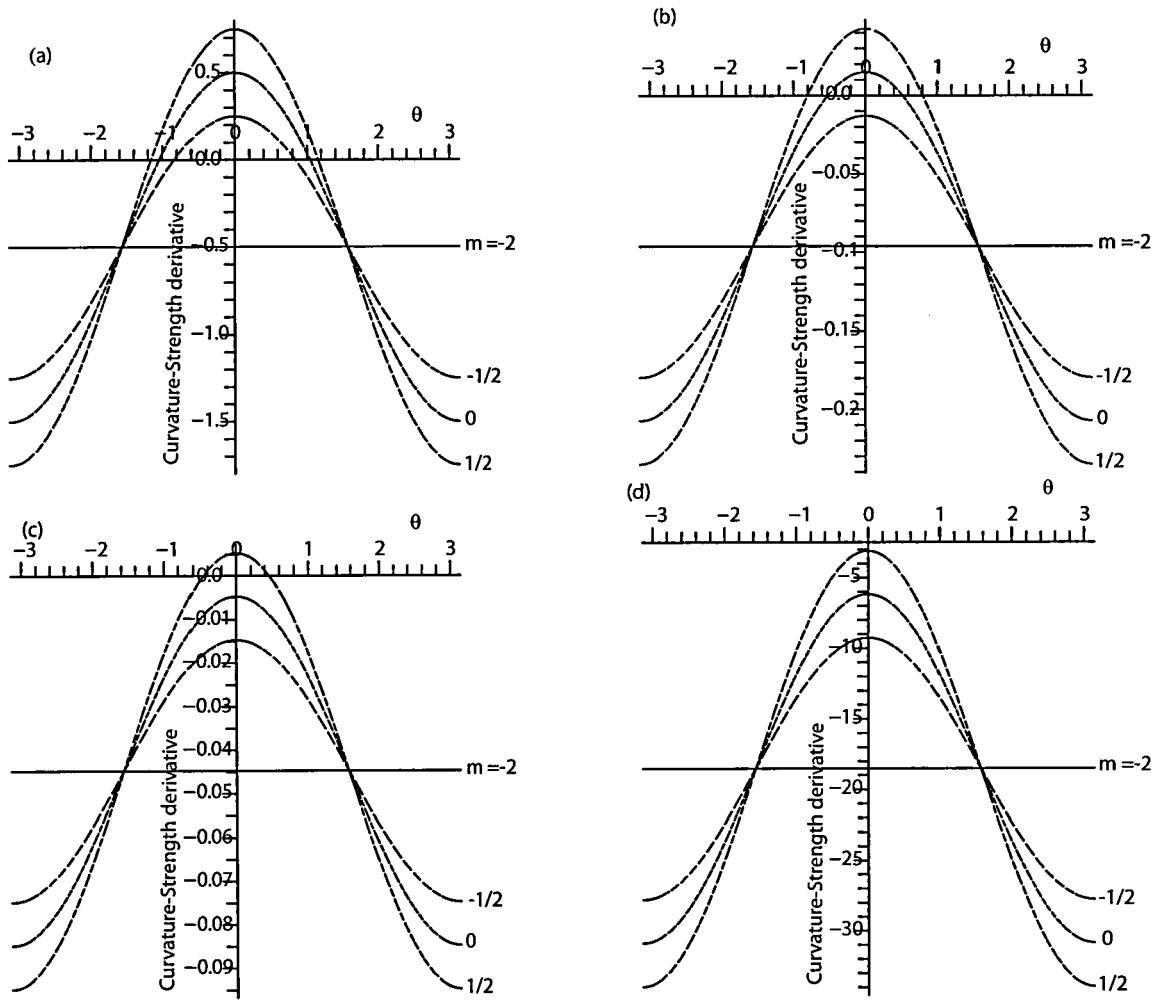


Figure 4.9: Curvature-strength derivative as a function of ray angle for different powers of m: (a) $\beta = 0$; (b) $\beta = 2$; (c) $\beta = 4$; (d) $\beta = 8$.

4.7 Caustic problems and other observed phenomena

The ray tracing algorithm of the curvature was intended to construct continuous and smoothly varying rays. However, during the course of testing the algorithm for the model problems, we came across situations where it did not work as expected. These situations are due to physical phenomena that had been overlooked in the implementation of the algorithm. Here two transport mechanisms that are being triggered by some terrain configurations are identified: caustics and reflection-refraction processes.

4.7.1 Caustics

A caustic is a geometrical object in which at each point the geometrical spreading or ray separation J vanishes. In other words, a caustic arises in regions where the rays intersect. A caustic creates a singularity which invalidates the computation of the amplitude A, while the real contaminant field remains to be finite on the caustics. This means that the ray method applied here does not properly describe the real contaminant field in a vicinity of caustics. This is precisely what is called caustic problems in ray theory.

Caustics are most likely to appear over underwater steps or channels. Our current algorithm is not capable of handling caustics properly because it cannot prevent the amplitude from going to infinity at caustics. Some corrective measures of handling caustics exist in literature. In particular, Chao (1971) constructed a uniformized asymptotic representation which is valid everywhere. Another approach to the caustic problem, based on the stationary phase method, was proposed by Lighthill (1978). Other simple approximate treatment of detecting and handling the caustic region to some extent are given in Mei (1983) and Benamou (1997). The method of parabolic approximation is suggested elsewhere in literature (Massel, 1989).

4.7.2 Reflection-refraction processes

The relevance of the above solutions is based upon certain assumptions in the shallow water environment. These include among others (i) the contaminant concentration gradients based upon the ray contours must be very small; (ii) under the assumption of a smoothly varying water depth within a characteristic contaminant plume length, any reflection can be neglected; (iii) the rays can be defined as a family of curves such that the amplitude at given points is conserved between two adjacent rays. There are, however, some difficulties in using and interpreting the results based on these assumptions, (for example see Figures 4.3). The solutions obtained give rays which are crossing. Any initial contaminant front which is concave in the direction of propagation leads to crossed rays and the algebraic amplitude factor then disappears to have a singularity. As the contaminant propagates into shallower water its concentration gradient becomes steeper because the phase decreases. In order to maintain the flux, the amplitude increases at the same time as the contaminant plume length shortens, the contaminant eventually becomes too steep for the simple ray approximation to handle.

4.8 Concluding remarks

In this work extension has been made of the investigation of Smith (1981) to the effects of contaminant decay. The ray approximation technique is employed to solve the advection-diffusion equation with spatially variable coefficients, proving itself as a useful analytical-numerical method. The special models considered sharpen insight about how loss mechanisms displace the ray paths and the consequent effects upon the curvature. In the absence of the decay and depth variations, the curvature of the ray paths is the same as the curvature of the current. This has the nice consequence that the central ray from the contaminant source continues along the changing flow direction. For the inclusion of the decay, the orientation of the curvature of the ray paths depend on accordingly as the spatial decay rate

(that is, ratio λ/D) decreases or increases with water depth. In general, the curvature of the ray paths are effected by spatial non-uniformity in the decay, depth, mixing, flow speed and flow direction. The corresponding results for the amplitude and the spatial rate of decay along rays together, permit the development of secure general principles for analysing water quality in rivers and channels and admit qualitative prediction for the different concentration distributions corresponding to different decay processes, up to the limit imposed by the phenomena of caustics and reflection-refraction processes. A consequence of this level of accuracy is to devise a new set of investigation of reflection and transmission phenomena for which no solutions yet exist in the effects of sharp changes in water depth, flow speed or diffusivity including contaminant decay upon diffusion problems. It is hoped that this work provides a sound theoretical framework and an implementation testbed where these new phenomena can be investigated further.Therefore, the next chapter concerns the investigation of the effects of sharp changes in contaminant decay, water depth, flow speed and diffusivity upon diffusion problems in rivers.

4.9 References

1. Babich, V. M.: 1956, Ray method of computation of the intensity of wave fronts. *Doklady Akademii Nauk SSSR*, **110 N3**, 355 - 357.

2. Baker, A., Inverarity, R., Charlton, M., and Richmond, S.: 2003, Detecting river pollution using fluorescence spectrophotometry: case studies from the Ouseburn, NE England. *Environmental Pollution*, **124**, 57 - 70.

3. Benamou, J-D.:1996, Big Ray Tracing: Multivalued Travel Time Field Computation Using Viscosity Solutions of the Eikonal Equation. *J. Comp. Physics*, **128**, 463 - 474.

4. Benamou, J-D.:1997, Multivalued Solution and Viscosity Solutions of the Eikonal Equation. Tech. Rep. 3281, INRIA Rocquencourt, available at http: //www.inria.fr/rrrt/rr-3281.html.

5. Červený, V., Molotkov, I. A. and Pšenčik, I.: 1977, Ray method in seismology. Praha, Universita Karlov.

6. Červený, V. and Ravindra, R.: 1971, Theory of seismic head waves. University of Toronto Press, Toronto.

7. Chao, Y. Y.: An asymptotic evaluation of the wave field near a smooth caustic. *Jour. Geoph. Res.*, **76**, 7401 - 7408.

8. Cohen, J. K. and Lewis, R. M.: 1967, A ray method for the asymptotic solution of the diffusion equation. *J. Inst. Math. Applic.*, **3**, 266 - 290.

9. Courant, R. and Hilbert, D.: 1962, Methods of Mathematical Physics, vol. 2. Interscience, New York.

10. Fyrillas, M. M.: 2000, Advection-dispersion mass transport associated with a non-aqueous-phase liquid pool. *J. Fluid Mech.*, **413**, 49 - 63.

11. Gjoystdal, H., Vinje, V. and Iversen, E.: 1993, Traveltime and amplitude estimation using wavefront construction. *Geophysics*, **58**, 1157 - 1166.

12. Gould, D.J. and Munro, D.: 1981, Relevance of microbial mortality to outfall design. *Coastal Discharges*, Thomas Telford, London, U.K., 45 - 50.

13. Hanyga, A.: 1984, Seismic Wave Propagation in the Earth. In: Hanyga, A.(Ed.); Physics and Evolution of the Earth's Interior 2. *Elsevier*, Amsterdam-Tokyo.

14. Hanyga, A., G. Lambare, G. and Lucio, P.: 1994, 2-D Asymptotic Green's Functions. *Proceedings of the 64th SEG annual meeting.*

15. Ho, D. T., Schlosser, P. and Caplow, T.: 2002, Determination of longitudinal dispersion coefficient and net advection in the tidal Hudson River with a large-scale, high resolution SF_6 tracer release experiment. *Environ. Sci. Technol.*, **36**, 3234 - 3241.

16. Iglesias, G. and Negro, V.: 2003, An engineering approach to wave propagation. *Water and Maritime Engineering*, **156**, 165 - 174.

17. Karal, F. C. and Keller, J. B.: 1959, Elastic Wave Propagation in Homogeneous and Inhomogeneous Media. *J. Acoust. Soc. Am.*, **31**, 694 - 705.

18. Kawanada, T and Asakawa, E.: 1993, Seismic ray tracing using linear traveltime interpolatioon. *Geophysical Prospecting*, **41**, 99 - 111.

19. Kay, A.:1987, The effect of cross-stream depth variations upon contaminant dispersion in a vertically well-mixed current. *Estuarine, Coastal and Shelf Science* **24**, 2, 177 - 204.

20. Kravtsov, Y. and Orlov, Y.: 1990, Geometrical Optics of Inhomogeneous Media. *Spring-Verlag*, New York.

21. Lighthill, J.: 1978, Waves in fluids. Camb. Univ. Press.

22. Massel, S. R.: 1989, Hydrodynamics of Coastal Zones. Elsevier Oceanography series, Elsevier Science Publishers B.V.

23. Mebine, P. and Smith, R. : 2006, Effects of contaminant decay on the diffusion centre of a river. *Environmental Fluid Mechanics,* **6**, 101 - 114.

24. Musgrave, F. K.: 1990, A Note on Ray Tracing Mirages. *IEEE Computer Graphics and Applications*, **10**(6): 1012.

25. Nedeau, E. J., Merritt, R. W. and Kaufman, M.G.: 2003, The effect of an industrial effluent on an urban stream benthic community: water vs. habitat quality, *Environmental Pollution*, **123**, 1 - 13.

26. Smith, R.: 1970, Asymptotic solutions for high-frequency trapped wave propagation. *School of Mathematics, University of Bristol*, **268**, A. 1189, 289 - 324.

27. Smith, R.: 1981, Effect of non-uniform currents and depth variations upon steady discharges in shallow water. *J. Fluid Mech.*, **110**, 373 - 380.

28. Smith, R.: 1983, The dependence of shoreline contaminant levels upon the siting of an effluent outfall. *J. Fluid Mech.*, **30**, 153 - 164.

29. Sneddon, I.: 1957, Elements of Partial Differential Equations. McGraw-Hill Book Company, Inc.

30. Whitted, T.: 1980, An Improved Illumination Model for Shaded Display. *Communications of the ACM*, **23**, 6, 343 - 349.

Chapter 5

Decay and depth discontinuity effects upon steady discharges in rivers

5.1 Introduction

Downstream of a steady point discharge of a variety of contaminants into a moderately sized river, it can take several kilometres travel, or several hours transit, for the overlapping plumes to mix across the river (Yotsukura and Cobb, 1972). On such time scales evaporative heat loss (Macqueen and Preston, 1983) or bacterial decay (Gould and Munro, 1981) can be significant. The losses differ in mechanism and in lateral distribution. Could the consequent differences in concentration distributions be substantial enough to amount to lateral separation between plumes for contaminants with different decay mechanisms while a significant fraction of the contaminant remains in the flow?

In real rivers or coastal waters, properties (such as depth, velocity, mixing and decay) vary continuously. For computational modelling or for developing understanding, those properties are often considered to be piecewise constant with abrupt jumps. On a sufficiently small length scale any curve of discontinuity can be regarded as being locally straight. Kay (1987) gave exact solutions for non-decaying solutes from a point source in an idealised river where the depth discontinuity is aligned with the flow (see Figure 5.1). The aim of the present work is to illuminate the effects of a jump in decay, by means of an appropriate modification to Kay's (1987) ray-tracing interpretation of his generalised Gaussian solutions.

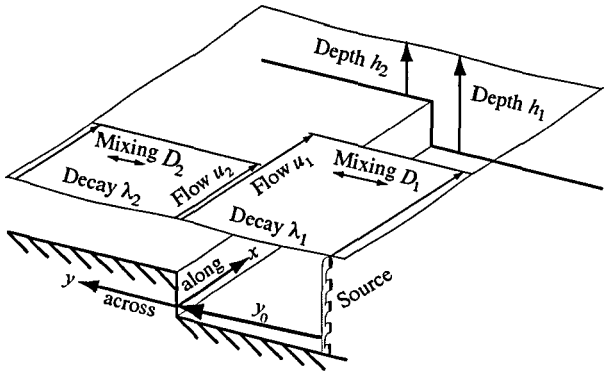


Figure 5.1: Steady source in flow along a depth discontinuity with a jump in decay.

Instead of ray reflection and refraction depending just on the depth ratio r (Kay, 1987),

for each decaying contaminant there is a second non-dimensional parameter M proportional to the change across the jump in the longitudinal decay (quotient of temporal decay rate and flow speed). Appropriate scaling permits the variation of the ray patterns with r and M to be collapsed into just two cases depending upon whether the discharge takes place at the side of the jump with greater or lesser longitudinal decay for the particular contaminant. Likewise, there are just two alternatives for the scaled ray amplitudes and phases.

The variety of contaminant plumes stems from the reconstruction of the concentration from the two alternative sets of ray ingredients. A position factor P (proportional to $|M|^{\frac{1}{2}}$ and to the distance from the source to the jump) quantifies both the tendency for plumes to migrate to the respective low-decay side of the jump and the amount of decay experienced in that migration. For small P there is little migration and for large P there is little contaminant remaining in the flow after the migration. The interesting regime is P of order unity. It is demonstrated that for $P = 1$ there can be lateral separation between the two plumes associated with an anti-symmetric pair of contaminants with $1:2$ and $2:1$ changes of longitudinal decay across the jump, while a significant fraction of the contaminant remains in the flow.

5.2 Advection-diffusion equation and flux matching

As a starting point for our mathematical analysis, we consider the steady-state horizontal spreading of the plume for one of the contaminants in a vertically well-mixed current with the loss modelled as a first order process. In the region i of constant depth h_i, decay rate λ_i, longitudinal flow u_i, and transverse diffusivity D_i, this corresponds to the advection-diffusion-reaction equation:

$$\lambda_i \, c_i + u_i \frac{\partial c_i}{\partial x} - D_i \frac{\partial^2 c_i}{\partial y^2} = 0. \tag{5.1}$$

Here $c_i(x, y)$ is the contaminant concentration, x is along-flow distance and y is cross-flow distance. It is the long-thin nature of steady contaminant plumes that gives predominance to transverse diffusivity and permits a scalar rather than tensor characterisation of mixing. Far downstream, as the plume widens and transverse diffusion reduces in importance, the effective longitudinal rate of decay in each region is λ_i/u_i.

For brevity, this work restricts attention to the case of two regions: $i = 1$ denotes the region $y < 0$ which contains a contaminant point source at $(0, -y_0)$ and $i = 2$ denotes the region $y > 0$. The transport between those regions is modelled through boundary conditions which ensure matching both of concentrations and of diffusive fluxes across $y = 0$:

$$c_1 = c_2\,, \quad h_1 D_1 \frac{\partial c_1}{\partial y} = h_2\, D_2 \frac{\partial c_2}{\partial y}. \tag{5.2}$$

5.3 Exponential solutions

For the piecewise constant pollution problem as sketched in Figure 5.1, we shall represent the concentration as a superposition of generalised Gaussian exponential solutions (Cohen and Lewis, 1967; Smith, 1981; Kay, 1987) with incident, reflected and transmitted contributions:

$$c_1 = A_I \exp(-\phi_I) + R\, A_R \exp(-\phi_R) \quad \text{for} \quad y < 0\,, \tag{5.3a}$$

$$c_2 = (1 + R) A_T \exp(-\phi_T) \quad \text{for} \quad y > 0\,. \tag{5.3b}$$

The long thin nature of the plumes makes the exponential phases vary rapidly by comparison to the spatial rate of change of the amplitudes. The discharge originates from $(0, -y_0)$ with zero incident phase $\phi_I(0, -y_0) = 0$. Along the discontinuity, there is matching of all three phases upstream of any limit point x_L (see §5.6)

$$\phi_I = \phi_R = \phi_T \quad \text{for} \quad x < x_L \quad \text{along} \quad y = 0\,. \tag{5.4}$$

It is convenient to impose similar matching for the amplitudes:

$$A_I = A_R = A_T \quad \text{for} \quad x < x_L \quad \text{along} \quad y = 0\,. \tag{5.5}$$

The reflection coefficient R is used to quantify immediate changes across the discontinuity. The transmission coefficient is $(1 + R)$. Absence of transmission implies $R = -1$.

For the incident contribution, we seek to split a single equation (5.1) into a pair of equations for $\phi_I(x, y)$ and $A_I(x, y)$. To do this we follow Smith (1981) and assume that flow reversal $\pm u_i$ has unchanged A_I but phase reversal $\pm\phi_I$. Writing

$$\frac{\partial \phi_I}{\partial x} = k_I(x, y)\,, \quad \frac{\partial \phi_I}{\partial y} = \ell_I(x, y)\,, \tag{5.6}$$

the non sign-changing incident terms in equation (5.1) give

$$\lambda_1 - u_1 k_I - D_1 {\ell_I}^2 = \frac{D_1}{A_I}\frac{\partial^2 A_I}{\partial y^2}\,. \tag{5.7}$$

The ray approximation, of neglecting the right hand side term in equation (5.7), yields an algebraic dispersion relation between k_I, ℓ_I. Phase matching (5.4) has k-matching counterparts

$$k_I = k_R = k_T \quad \text{for} \quad x < x_L \quad \text{along} \quad y = 0\,. \tag{5.8}$$

The $\pm$ terms from equation (5.1) give a transport equation for the incident amplitude

$$u_1 \frac{\partial A_I}{\partial x} + 2\, D_1 \ell_I \frac{\partial A_I}{\partial y} + D_1 \frac{\partial \ell_I}{\partial y} A_I = 0\,, \tag{5.9}$$

There are similar reflected and transmitted dispersion relations and transport equations.

Cohen and Lewis (1967, §2.2) point out that the ray representation (5.3a,b) can be interpreted as a steepest descent approximation to an integral representation for the con-

centration.

5.4 Incident rays

The formal derivatives of the dispersion relation (5.7) with respect to (k_I, ℓ_I) defines the ray or bi-characteristic direction along which the phase ϕ_I is directly computable (Sneddon, 1957). Normalisation yields the directional vectors:

$$\mathbf{t}_I = \frac{u_1 \hat{\mathbf{x}} + 2 D_1 \ell_I \hat{\mathbf{y}}}{\sqrt{{u_1}^2 + 4 {D_1}^2 {\ell_I}^2}}, \tag{5.10}$$

where $\hat{\mathbf{x}}$ and $\hat{\mathbf{y}}$ are unit vectors along the x and y axis, respectively. The constancy of λ_1, u_1, D_1 within region $i = 1$ implies that moving along a ray keeps k_I, ℓ_I unchanged, the rays are straight lines and the change in phase along the ray conforms with the expression

$$\phi_I = k_I x + \ell_I y + \text{constant}. \tag{5.11}$$

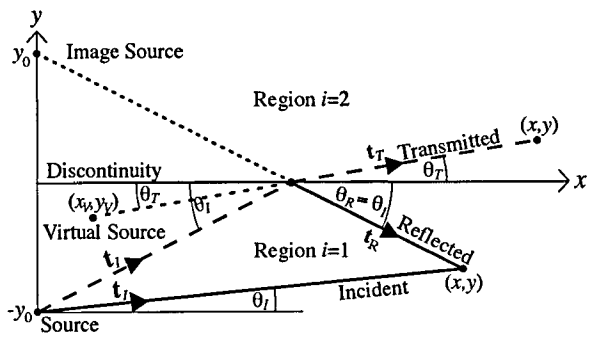


Figure 5.2: The variety of rays (continuous and dashed) either side of a discontinuity.

If θ_I denotes the incident angle between the incident ray and the x-axis (see Figure 5.2),

then from the $\hat{\mathbf{x}}$ and $\hat{\mathbf{y}}$ components equation (5.10) we infer that

$$\frac{u_1}{\sqrt{{u_1}^2 + 4\,{D_1}^2\,{\ell_I}^2}} = \cos\theta_I\,, \quad \frac{2\,D_1\,\ell_I}{\sqrt{{u_1}^2 + 4\,{D_1}^2\,{\ell_I}^2}} = \sin\theta_I\,, \tag{5.12a}$$

$$\ell_I = \frac{u_1\tau_I}{2\,D_1}\,, \quad k_I = \frac{\lambda_1}{u_1} - \frac{u_1\tau_I^2}{4\,D_1} \quad \text{with} \quad \tau_I = \tan\theta_I\,. \tag{5.12b}$$

The larger the slope τ_I of the rays the larger the lateral decay rate ℓ_I. Ray trigonometry gives $y = x\,\tau_I - y_0$. In incident ray co-ordinates (x, τ_I) or Cartesian co-ordinates $(x,\, y)$, the incident phase (5.11) has the alternative representations

$$\phi_I = \frac{\lambda_1 x}{u_1} + \frac{u_1\tau_I^2 x}{4D_1} = \frac{\lambda_1 x}{u_1} + \frac{u_1(y+y_0)^2}{4D_1 x}\,, \tag{5.13}$$

corresponding to a decaying Gaussian plume from the source $(0, -y_0)$.

In the ray co-ordinates (x, τ_I) the transport equation (5.9) becomes

$$\frac{\partial A_I}{\partial x} + \frac{1}{2\,x} A_I = 0\,. \tag{5.14}$$

For a point source at $(0, -y_0)$ with volume flux q, the solution for the incident amplitude is the standard Gaussian amplitude

$$A_I(x, \tau_I) = \frac{q}{2\,h_1\,(\pi\,D_1 u_1 x)^{\frac{1}{2}}}\,. \tag{5.15}$$

The Cartesian counterpart $A_I(x, y)$ has the same formula, with zero second y-derivative. Thus, no error was made in neglecting the right hand side of equation (5.7). The incident plume contribution to the solution (5.3a) is exact, rather than approximate.

5.5 Reflected rays

By analogy to equation (5.12b), for reflected rays coming at downward angle $\theta_R > 0$, we have

$$\ell_R = -\frac{u_1 \tau_R}{2\,D_1} \quad , \quad k_R = \frac{\lambda_1}{u_1} - \frac{u_1^2 \tau_R^2}{4\,D_1} \quad \text{with} \quad \tau_R = \tan\theta_R \,. \tag{5.16}$$

Ray trigonometry gives $y = y_0 - x\,\tau_R$. Matching $k_R = k_I$ along the discontinuity implies mirror-like reflection $\tau_R = \tau_I$ (Kay, 1987). The incident and reflected rays through a point (x, y) below the discontinuity have tangents related by

$$\tau_R = \tau_I - \frac{2y}{x} \,. \tag{5.17}$$

The solution for the reflected phase has the ray (x, τ_R) or Cartesian (x, y) equivalents

$$\phi_R = \frac{\lambda_1 x}{u_1} + \frac{u_1 \tau_R^2 x}{4D_1} = \frac{\lambda_1 x}{u_1} + \frac{u_1 (y - y_0)^2}{4 D_1 x} \,, \tag{5.18}$$

corresponding to a decaying Gaussian plume from the image source position $(0, y_0)$.

In reflected ray co-ordinates (x, τ_R) the reflected transport equation becomes

$$\frac{\partial}{\partial x}\,(R\,A_R) + \frac{R\,A_R}{2\,x} = 0 \quad \text{for} \quad \frac{\mathrm{y_0}}{\tau_\mathrm{R}} \leq \mathrm{x} \,. \tag{5.19}$$

The product $R\,A_R$ has $x^{-\frac{1}{2}}$ decay. If the reflection coefficient $R(x, \tau_R)$ does <u>not</u> vary along a ray (see §5.10), then at the discontinuity $x = y_0/\tau_R$, matching $A_R = A_I$ leads to the solution

$$A_R(x, \tau_R) = \frac{q}{2\,h_1\,(\pi\,D_1 u_1 x)^{\frac{1}{2}}} \,. \tag{5.20}$$

The Cartesian counterpart $A_R(x, y)$ is unchanged. For the reflected plume contribution to the solution (5.3a) to be exact (for example, Kay, 1987), it suffices that $R(\tau_R)$ be linear in τ_R.

5.6 Transmitted rays and decay-jump parameter M

If θ_T denotes the transmitted angle into $y > 0$, then the counterpart to equation (5.12b) is

$$\ell_T = \frac{u_2 \tau_T}{2\, D_2}\,, \quad k_T = \frac{\lambda_2}{u_2} - \frac{u_2 \tau_T^2}{4\, D_2} \quad \text{with} \quad \tau_T = \tan\theta_T\,. \tag{5.21}$$

Again, k_T, ℓ_T are constant along a ray, the rays are straight and the change in phase along the ray conforms with the expression

$$\phi_T = k_T x + \ell_T y + \text{ constant}\,. \tag{5.22}$$

Matching $k_T = k_I$ along the discontinuity $y = 0$ gives the refraction equation

$$\frac{\lambda_1}{u_1} - \frac{u_1 \tan^2\theta_I}{4\, D_1} = \frac{\lambda_2}{u_2} - \frac{u_2 \tan^2\theta_T}{4\, D_2}\,. \tag{5.23}$$

We introduce two parameters M and Λ to classify respectively, the jump and uniformity in longitudinal decay:

$$M = \frac{4\, D_1}{u_1}\left(\frac{\lambda_2}{u_2} - \frac{\lambda_1}{u_1}\right), \qquad \Lambda = \frac{\min(\lambda_2/u_2\,,\, \lambda_1/u_1)}{|\lambda_2/u_2 - \lambda_1/u_1|} \geq 0\,, \tag{5.24a}$$

$$\frac{\lambda_1}{u_1} = \frac{u_1|M|}{4\, D_1}\left\{\Lambda + H(-M)\right\}, \qquad \frac{\lambda_2}{u_2} = \frac{u_1|M|}{4\, D_1}\left\{\Lambda + H(M)\right\}, \tag{5.24b}$$

where the pair of Heaviside functions $H(-M)$ and $H(M)$ switch 0 or 1 depending upon the sign of M. If the longitudinal decay is greater in the upper region $i = 2$, then the jump parameter M is positive. For the illustrative case of a factor of two variation in the longitudinal decay rates λ_i/u_i, the uniformity parameter has the value $\Lambda = 1$.

The refraction equation (5.23) can be used to express τ_T in terms of τ_I:

$$\tau_T \;=\; \left(\frac{D_2\, u_1}{D_1\, u_2}\right)^{\frac{1}{2}} \tau_I \left\{1 + \frac{M}{\tau_I^2}\right\}^{\frac{1}{2}}. \tag{5.25}$$

There is an implicit restriction to $\tau_I > 0$ for positive M and to

$$x \le x_L = \frac{y_0}{|M|^{1/2}}, \quad |M|^{1/2} \le \tau_I \quad \text{for transmission with} \quad M < 0. \tag{5.26}$$

Downstream of x_L, the limiting ray for $M < 0$ transmits along the discontinuity with $\tau_T = 0$. It is convenient to use $\tau_I > 0$, rather than τ_T, to label the transmitted rays:

$$y = \left(\frac{D_2\, u_1}{D_1\, u_2}\right)^{\frac{1}{2}} \left\{1 + \frac{M}{\tau_I^2}\right\}^{\frac{1}{2}} (\tau_I x - y_0)\,. \tag{5.27}$$

The virtual source (x_V, y_V) corresponds to where adjacent transmitted rays meet, that is, the mathematical solution of equation (5.27) by setting its τ_I-derivative to zero. In terms of τ_I, a parametric representation for the virtual source is

$$x_V = -\frac{y_0 M}{\tau_I^3}, \quad y_V = -y_0 \left(\frac{D_2\, u_1}{D_1\, u_2}\right)^{\frac{1}{2}} \left\{1 + \frac{M}{\tau_I^2}\right\}^{\frac{3}{2}}. \tag{5.28}$$

For M positive (negative), as τ_I decreases from infinity, the virtual source moves upstream (downstream) and further from (closer to) the discontinuity. The position of the virtual source in Figure 5.2 corresponds to negative M.

In (x, τ_I) co-ordinates, the phase along a transmitted ray can be written

$$\phi_T = \frac{\lambda_1 x}{u_1} + \frac{u_1 \tau_I^2 x}{4D_1} + \frac{M\, u_1}{2\, D_1}\left(x - \frac{y_0}{\tau_I}\right) \quad \text{for} \quad \frac{\mathrm{y_0}}{\tau_\mathrm{I}} \le \mathrm{x}. \tag{5.29}$$

For $M < 0$, the limiting ray along the discontinuity has phase

$$\phi_T = \frac{\lambda_2}{u_2} x + \frac{u_1}{2\, D_1} |M|^{1/2} y_0 \quad \text{for} \quad \mathrm{x} \ge \frac{\mathrm{y_0}}{|\mathrm{M}|^{1/2}}. \tag{5.30}$$

In (x, τ_I) co-ordinates the transmitted transport equation becomes

$$\frac{\partial}{\partial x}\left((1+R)A_T\right) + \frac{(1+R)A_T}{2\,(x - x_V)} = 0 \quad \text{for} \quad \frac{\mathrm{y_0}}{\tau_\mathrm{I}} \le \mathrm{x}. \tag{5.31}$$

Along rays, there is $(x - x_V)^{-\frac{1}{2}}$ decay. If the reflection coefficient $R(x, \tau_I)$ does not vary along a ray (see §5.10) then matching $A_T = A_I$ at $\tau_I = y_0/x$ leads to the solution

$$A_T = \frac{q\left\{1 + M/\tau_I^2\right\}^{\frac{1}{2}}}{2\,h_1\left(\pi\, D_1 u_1[x + y_0 M/\tau_I^3]\right)^{\frac{1}{2}}}. \tag{5.32}$$

In (x, y) co-ordinates the transmitted amplitude has y-dependence via τ_I. It is only for $M = 0$ (Kay, 1987) that the transmitted contribution to the solution (5.3b) is exact. For $M < 0$ the limiting transmitted ray along the discontinuity has zero amplitude.

Alas, rapid variations in the transmitted amplitude (5.32) and reflection coefficient (5.44) render the ray approximation (5.3a,b) inapplicable near $(x_L, 0)$. Downstream, the ray solution exhibits a abrupt jump in concentration across the reflected ray through $(x_L, 0)$, akin to the shortcoming of the abrupt model of a shadow boundary in optics (Peatross and Ware, 2004). The present work does not investigate whether, as in higher-order optics, a suitable integral superposition over a secondary fan of rays might represent the smooth transition, that is, a ray description for leakage of concentration back from region $i = 2$ into region $i = 1$.

5.7 Reduction to two scaled ray patterns

To compress the variety of ray patterns, we scale the incident tangent $T_I = \tau_I/|M|^{1/2}$ and introduce non-dimensional scaled distances :

$$X = \frac{x|M|^{1/2}}{y_0}, \quad Y = \frac{y}{y_0} \text{ for } \mathrm{y} < 0, \quad \mathrm{Y} = \frac{\mathrm{y}}{\mathrm{y_0}}\left(\frac{\mathrm{D_1\,u_2}}{\mathrm{D_2\,u_1}}\right)^{\frac{1}{2}} \text{ for } \mathrm{y} > 0. \tag{5.33}$$

The disparity in y-scalings at the two sides of the discontinuity eliminates the $M = 0$ ray refraction investigated by Kay (1987), leaving just the decay contribution to the ray bending. The Cartesian (X, Y) formulas for scaled incident, reflected and transmitted rays

(indexed with the scaled incident tangent $T_I = T_R$ at the discontinuity) become:

$$Y_I = T_I X - 1\,,\quad Y_R = 1 - T_R X\,,\quad Y_T = \left\{1 + \frac{\text{sign(M)}}{T_I^2}\right\}^{\frac{1}{2}} (T_I X - 1)\,. \qquad (5.34)$$

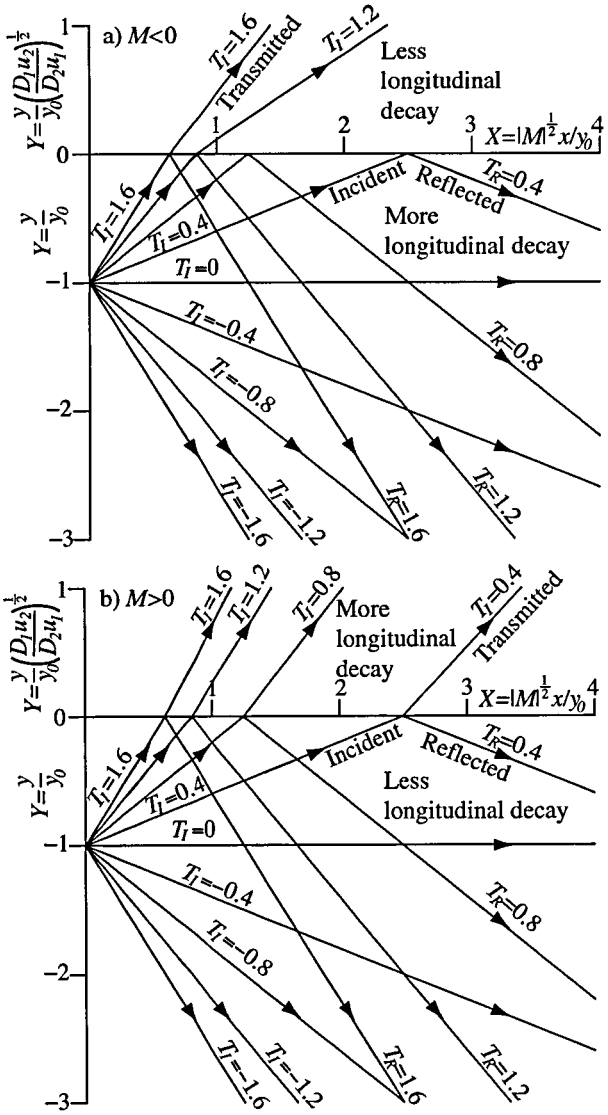


Figure 5.3: There are only two possible scaled ray patterns: a) $M < 0$ and b) $M > 0$.

Figure 5.3a shows the scaled ray pattern at intervals of 0.4 in T_I or T_R with lower decay in $Y > 0$. The transmitted rays are restricted to $T_I > 1$ and are at a lower angle than the incident rays. For $0 < T_I < 1$ the incident rays reflect but do not transmit.

Figure 5.3b shows the scaled ray pattern with greater decay in $Y > 0$. The transmitted rays are at a higher angle than the incident rays.

The incident and reflected rays through a point (X, Y) below the discontinuity have tangents related by

$$T_R - T_I = \frac{2Y}{X}. \tag{5.35}$$

For example, there is intersection between the rays $T_I = -0.8$ and $T_R = 1.6$ at the location $X = 2.5$, $Y = -3$ along the bottom of Figures 5.3a, b.

5.8 Decay-adjusted phases and position factor P

Far downstream, most of the remaining contaminant will be at the side of the discontinuity with lower longitudinal decay. For the incident phase, we extract that lower decay:

$$\phi_I(x,y) = \min\left(\frac{\lambda_1}{u_1}, \frac{\lambda_2}{u_2}\right) x + P\Phi_I(X,Y) = P\left\{\tfrac{1}{2}\Lambda X + \Phi_I(X,Y)\right\}, \tag{5.36a}$$

$$\text{with} \qquad P = \frac{y_0 u_1 |M|^{1/2}}{2D_1} = y_0 \left\{\frac{u_1}{D_1}\left|\frac{\lambda_2}{u_2} - \frac{\lambda_1}{u_1}\right|\right\}^{1/2}, \tag{5.36b}$$

with similar reflected and transmitted decay adjustments. P is a position factor proportional to the lateral distance y_0 between the discharge and the discontinuity. The zero-decay work of Kay (1987) corresponds to P and X tending to zero at the same $|M|^{1/2}$ rate.

Diffusive mixing over the lateral distance y_0 between the source to the discontinuity, can be estimated as requiring a longitudinal distance $\frac{1}{2}y_0^2 u_1/D_1$ and can be associated with the standard Gaussian e-folding of $\frac{1}{2}$. On that longitudinal distance, the difference in e-foldings either side of the discontinuity can be estimated $\frac{1}{2}P^2$. Comparability between mixing and the variability of non-uniform decay can be characterised by $P = 1$.

Larger P gives more emphasis to Φ_I and to migration of the contaminant plume to the region of lower longitudinal decay. However, larger P also gives more mean e-folding loss $\frac{1}{4}P^2\Lambda$ in that migration, possibly making the concentrations too small for the structure to

be of interest. For small P there is neither much migration nor much loss and the zero-decay work of Kay (1987) would be applicable. The interesting regime is P of order unity.

The M, Λ, P three-parameter continuum for $\phi_I(x,y)$ is collapsed to just two cases for $\Phi_I(X,Y)$. In $(X,\, T)$ co-ordinates, the decay-adjusted phases for $M < 0$ are:

$$\Phi_I = \tfrac{1}{2}X\left(T_I^2+1\right)\,,\quad \Phi_R = \tfrac{1}{2}X\left(T_R^2+1\right)\,,\quad \Phi_T = \tfrac{1}{2}X\left(T_I^2-1\right)+\frac{1}{T_I}\,. \tag{5.37a}$$

There is the requisite matching of phases along $X\,T_I = 1$ where $T_I = T_R$. For $M > 0$, the different decay adjustment gives the different phase expressions

$$\Phi_I = \tfrac{1}{2}XT_I^2\,,\quad \Phi_R = \tfrac{1}{2}XT_R^2\,,\quad \Phi_T = X(\tfrac{1}{2}T_I^2+1)-\frac{1}{T_I}\,. \tag{5.37b}$$

For $M < 0$, Figure 5.4a gives composite contours at $1/4$ intervals of the decay-adjusted incident and transmitted phase. The matching of phases across the line of discontinuity is restricted to $X < 1$. In region $i = 1$ with $Y < 0$, the contours are exactly circular and mutually tangential at the source $(0,-1)$. The decay-adjusted reflected phase contours correspond to an upwards displacement, from source to image source, of the exactly circular contours of incident phase. Far downstream $(X > 2)$ in Figure 5.4a the lowest values of the decay-adjusted phase and highest concentration occur in the upper region, as a consequence of the smaller longitudinal decay.

For the other case $M > 0$ of larger longitudinal decay in region $i = 2$, Figure 5.4b gives contours of the decay-adjusted phase. There is matching of phases all along the line of discontinuity. In region $i = 1$ the phase contours are exact parabolas through the source $(0,-1)$. Again, the contours of the decay adjusted reflected phase correspond to an upwards displacement, from source to image source, of the contours of incident phase. Far downstream in Figure 5.4b the contours in region $i = 2$ become lines of constant y, that is, the route for arriving contaminant is principally carried along by flow in the low-decay

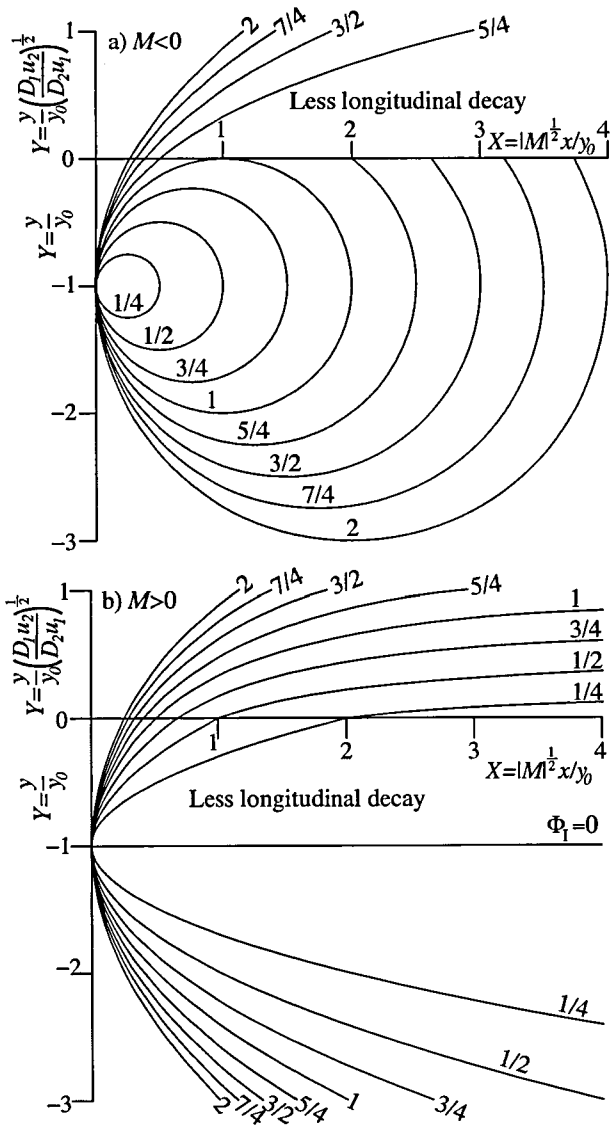


Figure 5.4: The two decay-adjusted phase patterns: a) $M < 0$ and b) $M > 0$.

region followed by a shorter span of transverse diffusion into the high-decay region.

5.9 Transmitted amplitude

To scale the discharge strength we define

$$Q = \frac{q|M|^{\frac{1}{4}}}{h\,(2\,D_1 u_1 y_0)^{\frac{1}{2}}}, \tag{5.38}$$

with the sequels

$$A_I = A_R = \frac{Q}{(2\,\pi X)^{\frac{1}{2}}}, \quad A_T = \frac{Q\left\{1 + \text{sign(M)}/\text{T}_\text{I}^2\right\}^{\frac{1}{2}}}{\left(2\,\pi\left[X + \text{sign(M)}/\text{T}_\text{I}^3\right]\right)^{\frac{1}{2}}} \tag{5.39}$$

Only the transmitted amplitude A_T exhibits Y-dependence and contours that deviate from being perpendicular to the discontinuity. Figures 5.5a , b show the A_T contours, corresponding to unit scaled strength $Q = 1$. For $M < 0$ (Figure 5.5a) there is rapid variation near the limit point $(1, 0)$. Further downstream, the contours give the appearance of pivoting about the limit point and the transmitted amplitude tends to zero as the line of discontinuity is approached. For $M > 0$ (Figure 5.5b) the contour shapes tilt gradually more as X increases. In the non-plotted region $Y < 0$, the $A_I = A_R$ contours are straight down extensions from where the A_T contours intersect $Y = 0$.

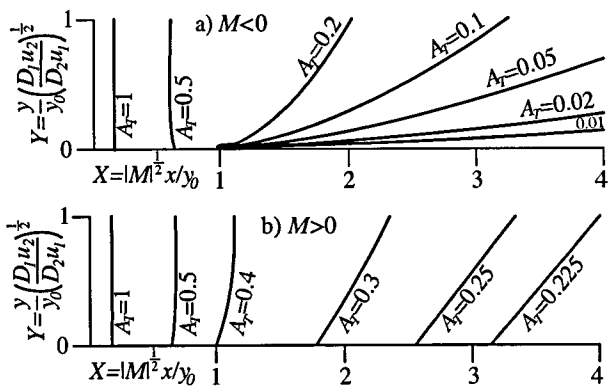


Figure 5.5: The two transmitted amplitude patterns: a) $M < 0$ and b) $M > 0$.

5.10 Reflection coefficient

The R-structure of the ansatz (5.3a,b) is designed to guarantee concentration matching $c_1 = c_2$. For the flux matching (5.2), we neglect y-derivatives of A_I, RA_R, $(1+R)A_T$ and solve for the reflection coefficient

$$R = \frac{h_1 D_1 \ell_I - h_2 D_2 \ell_T}{h_1 D_1 \ell_I + h_2 D_2 \ell_T}. \tag{5.40}$$

Such coefficients are extensively used in the contexts of water waves (Mei, 1983; Massel, 1989) and optics (Peatross and Ware, 2004). The expressions (5.12b, 5.21) permit the reflection coefficient to be expressed in terms of the ray tangents at the discontinuity:

$$R = \frac{h_1 u_1 \tau_I - h_2 u_2 \tau_T}{h_1 u_1 \tau_I + h_2 u_2 \tau_T}. \tag{5.41}$$

This expression for R only depends on the transition and does not vary along a ray.

If r denotes the depth ratio across the discontinuity, then the turbulent open-channel flow scalings noted by Elder (1959) and used by Kay (1987) link the flow quantities in region $i = 2$ to those in $i = 1$:

$$h_2 = r\, h_1\,, \quad u_2 = r^{\frac{1}{2}} u_1\,, \quad D_2 = r^{\frac{3}{2}} D_1\,. \tag{5.42}$$

In particular, the non-dimensional scaled lateral distances (5.33) are

$$Y = \frac{y}{y_0} \text{ for } y<0\,, \quad Y = \frac{y}{r^{\frac{1}{2}} y_0} \text{ for } y>0\,. \tag{5.43}$$

With the above scalings, the reflection coefficient (5.41) becomes

$$R = \frac{1 - r^2 \left\{1 + M/\tau_R^2\right\}^{\frac{1}{2}}}{1 + r^2 \left\{1 + M/\tau_R^2\right\}^{\frac{1}{2}}} = \frac{1 - r^2 \left\{1 + \text{sign}(M)/T_R^2\right\}^{\frac{1}{2}}}{1 + r^2 \left\{1 + \text{sign}(M)/T_R^2\right\}^{\frac{1}{2}}}. \tag{5.44}$$

Since R only depends on the transition, in evaluating the transmission coefficient $1 + R$ for the transmitted rays, it suffices to replace τ_R by τ_I or to replace T_R by T_I. Negative M increases the reflection coefficient, while positive M decreases the reflection coefficient. The $M = 0$ limit gives the result obtained by Kay (1987, equation 18a):

$$R = \frac{1 - r^2}{1 + r^2} \quad \text{for} \quad M = 0\,. \tag{5.45}$$

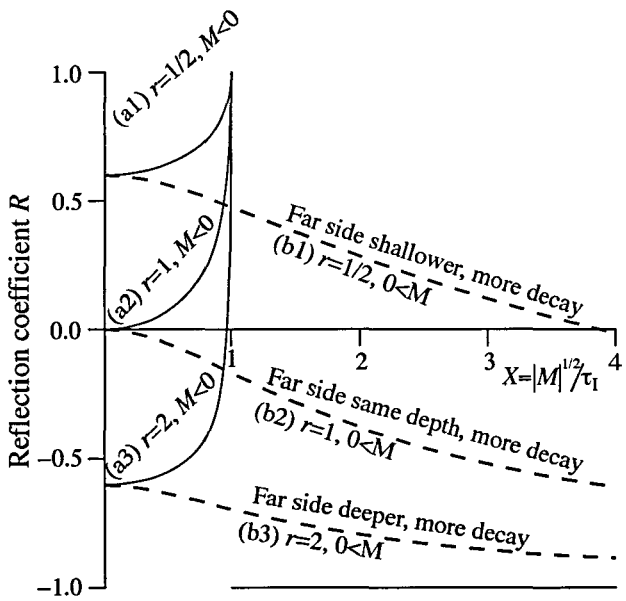


Figure 5.6: Reflection coefficient as function of reflection point for three depth ratios.

For compatibility with the three pairs of previous figures, Figure 5.6 plots the reflection coefficient for both signs of M as a function of the ray intersection point $X = 1/T_I$ for depth ratios $r = \frac{1}{2}$, 1, 2. At small non-dimensional distances X downstream of the source, the reflection coefficient has the constant value as given by the Kay (1987) result (5.45). Moving downstream for $M < 0$, there is a rise in R as more of the arriving contaminant is transmitted, escalating to $R = 1$ at the limit point $X = 1$, beyond which the transmission ceases and the reflection coefficient has been extended as $R = -1$. By contrast, for $M > 0$ the reflection coefficient reduces smoothly with asymptote $R = -1$.

5.11 Concentrations

The two alternative scaled rays, phases, amplitudes and reflection coefficients plotted in Figures 5.3-5.6, give all the ingredients needed to construct the ray approximation (5.3a,b) to the concentrations.

As the first pair of illustrative examples, we consider anti-symmetric pair of contaminants with $2:1$ or $1:2$ changes of longitudinal decay across the jump. For opposite signs of M the two contaminants share the dimensionless specification

$$\Lambda = 1, \quad r = 0.5, \quad Q = 1, \quad P = 1. \tag{5.46}$$

Thus, region $i = 2$ has water depth half that of region $i = 1$, the two contaminants have equal rates of discharge, and the position factor is taken to be unity. In X units, the e-folding distance in the lower decay region is two and the figures only extend to two e-foldings. Figures 5.7a, b show the ray approximation (5.3) to the concentration contours. By $X = 0.5$ the contours have already begun to differ, for example, the extent to which the 0.2 contour crosses the discontinuity line $Y = 0$.

In Figure 5.7a, by $X = 1$ (one e-folding in region $i = 1$) there is a clear separation into a more rapidly-decaying plume in region $i = 1$ and a less rapidly-decaying plume in region $i = 2$. The erroneously sharp jump in concentration across the reflected ray through the limit point $(1, 0)$ is revealed from the displacements in the concentration contours either side of the -45^o line down to the bottom right-hand corner of Figure 5.7a. It is evident that the ray approximation fails to include a contribution of magnitude 0.02 that switches on at the limit point.

In Figure 5.7b only a single plume is evident, that is principally in the less longitudinal-decay region $i = 1$. In region $i = 2$ the concentrations for the anti-symmetric pair of contaminants are of similar magnitudes. However, in region $i = 1$ the disparity in concentrations becomes marked as X increases.

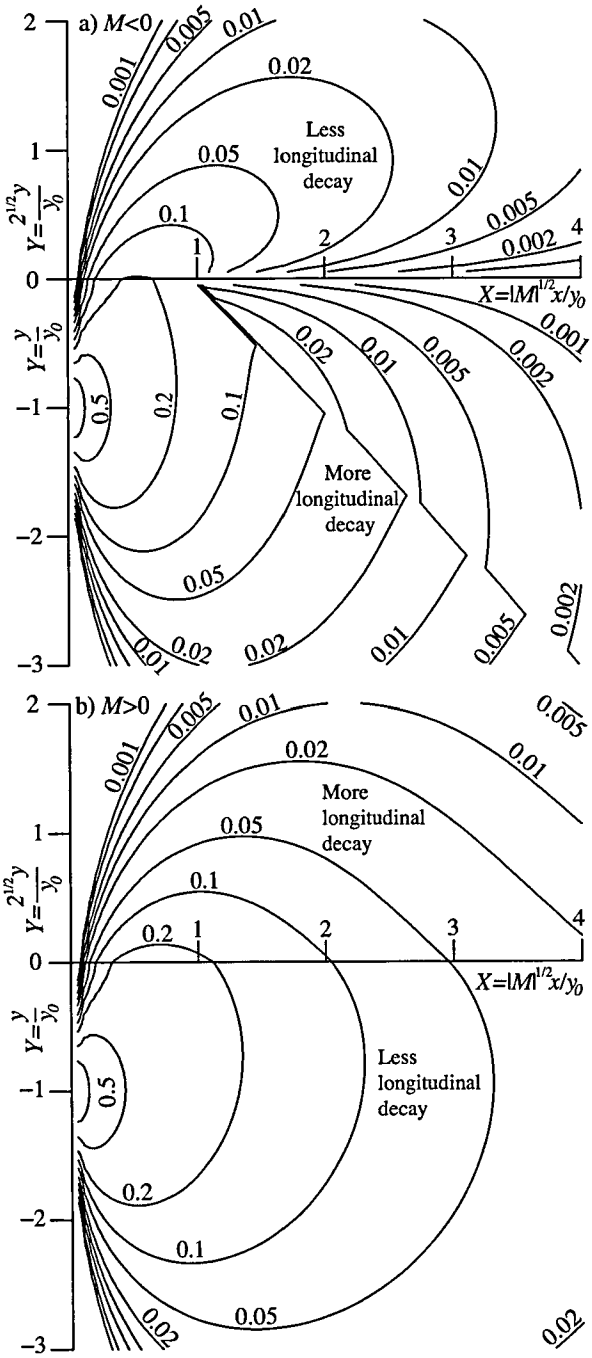


Figure 5.7: Ray approximations to concentration for half-depth far side.

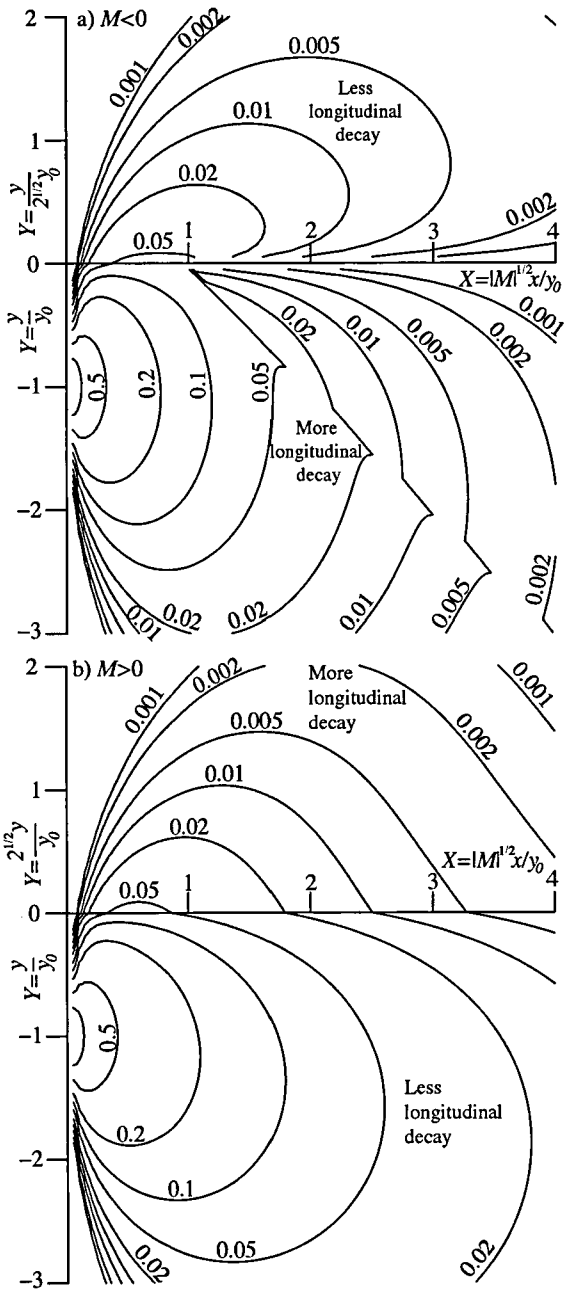


Figure 5.8: Ray approximation to concentration for double-depth far side.

For the second pair of illustrative examples, we change the depth ratio to $r = 2$, that is, for example, region $i = 2$ has water depth twice that of region $i = 1$. The other parameters are unchanged:

$$\Lambda = 1, \quad r = 2, \quad Q = 1, \quad P = 1. \tag{5.47}$$

Figures 5.8a, b show the ray approximation (5.3) to the concentration contours. Similarity to the first pair of examples is evident. Strict equality is restricted to the triangular sector, where the ray approximation fails, between the discontinuity and the -45^o line down to the bottom right-hand corner of Figures 5.7a and 5.8a. For fixed properties in region $i = 1$, the water depth in region $i = 2$ for Figure 5.8 is four times that for Figure 5.7. Consequently, region $i = 2$ in Figure 5.8 has approximately a factor of four concentration reduction as compared to Figure 5.7 whatever the side of less longitudinal decay. Again, the disparity in concentrations between the anti-symmetric pair of contaminants is most marked in region $i = 2$.

In translating the collapsed variety of (X, Y) ray solutions into the greater variety of (x, y) physical quantities, it needs to be recalled that for each contaminant the longitudinal X scaling (5.33) depends upon the $|M|$ value for that contaminant. Also, at the far side of the jump there is r-dependent Y scaling (5.43). For fixed properties in region $i = 1$, the physical y range into region $i = 2$ for Figure 5.8 is twice the physical y-range for Figure 5.7.

5.12 Concluding remarks

A mathematical topic requiring further study is the inadequacy of the ray approximation across the reflected ray through the limit point $(x_L, 0)$ for $M < 0$. The derivatives of the reflection coefficient and of the transmitted amplitude become singular at the limit point. The jump from reflection coefficient $R = 1$ at the left of the dividing reflected ray, to $R = -1$ to the right, gives a shadow-like drop in concentration. Also, the ray solution gives

zero concentration along both sides of the discontinuity downstream of the limit point. A possible way to resolve the inadequacy would be first to seek an integral representation for the exact solution using a Laplace transform in x, then to investigate why steepest descent (Cohen and Lewis, 1967) ceases to be accurate, and finally to seek a tractable improvement upon steepest descent. The desired outcome would be an addition to the ray solution that yields rapid but smooth drop in concentration across the dividing reflected ray, with non-zero concentrations smoothly matched across the discontinuity downstream of the limit point.

One revelation from the present work is that in the ray approximation there are just two scaled ray pattern (phase and amplitude), depending upon which side of the jump has less longitudinal decay. Another revelation is that the position factor P quantifies both the migration of contaminant to the side of less longitudinal decay and the amount of decay experienced in that migration. It is for P of order unity that migration and concentrations are both large enough to be important. Two illustrative examples revealed that for a pair contaminants with $P = 1$ and interchanged decay rates either side of a depth jump, plume separation to the respective low-decay sides takes place while a significant fraction of both contaminants remain in the flow.

5.13 References

1. Cohen, J. K. and Lewis, R. M.: 1967, A ray method for the asymptotic solution of the diffusion equation. *J. Inst. Math. Applic.*, **3**, 266 - 290.

2. Elder, J. W.: 1959, The dispersion of marked fluid in turbulent shear flow. *J. Fluid Mech.*, **5**, 544 - 560.

3. Gould, D.J. and Munro, D.: 1981, Relevance of microbial mortality to outfall design. *Coastal Discharges*, Thomas Telford, London, U.K., 45 - 50.

4. Kay, A.:1987, The effect of cross-stream depth variations upon contaminant dispersion

in a vertically well-mixed current. *Estuarine, Coastal and Shelf Science* **24**, 2, 177 - 204.

5. Macqueen, J. F. and Preston, R. W.: 1983, Cooling water discharges into a sea with sloping bed. *Water Research*, **17**, 4, 389 - 395.

6. Massel, S. R.: 1989, Hydrodynamics of Coastal Zones. Elsevier Science Publishers B. V., Amsterdam.

7. Mei, C. C.: 1983, Applied Dynamics of Ocean Surface Waves. John Wiley and Sons, Inc., New York.

8. Peatross, J. and Ware, M.: 2004, Physics of Light and Optics. Addison-Wesley, online draft.

9. Smith, R.: 1981, Effect of non-uniform currents and depth variations upon steady discharges in shallow water. *J. Fluid Mech.*, **110**, 373 - 380.

10. Sneddon, I.:1957, Elements of Partial Differential Equations. McGraw-Hill Book Company, Inc.

Chapter 6

Computational scheme for steady discharges in rivers

6.1 Introduction

The possibility of a contaminant being accidentally or intentionally spilled upstream from a water supply is a constant concern to those diverting and using water from streams and rivers (Jobson, 1997). The effects of variability of depth, flow, mixing, decay, and irregular boundaries or boundary conditions in rivers pose problems for the construction of accurate modelling techniques and prediction of mixing processes. Except for some special initial and boundary conditions, the partial differential equations governing the very many mathematical models of the physical, chemical and biological phenomena are not easily amenable to closed form analytical solutions. Instead, to investigate the predictions of these models it is often necessary to approximate the solutions numerically. Examples that use the finite-difference method are presented in this work. Several mathematical models, which exhibit decay of pollutants, are present in literature (Nassehi and Bikangaga, 1993; Bikangaga and Nassehi, 1995; Smith, 2000; Yoo *et al.*, 2003; Araújo *et al.*, 2005). However, numerical investigations of the effects of the variability of decay with depth in the advection-diffusion of pollutants has not been attempted. Thus, the overall goal of this work is intended to provide efficient numerical methods for the solution of advection-diffusion-reaction equations that include the effects of the variability of decay together with the complexity of the changed coefficients and of the geometry in river systems.

6.2 Background and model equation

A significant proportion of the contaminant sources introduced into waterways approximate to steady state conditions, such as cooling water returns or sewage treatment outfalls. Under steady state conditions, modelling transverse mixing is critical in assessing the impacts of pollutants, or establishing discharge/loading levels such that water quality criteria are complied with (Yotsukura and Cobb, 1972; Boxall, Guymer and Marion, 2003). Longitudinal mixing becomes less significant under these conditions. Fischer (1969) showed that

there is an inverse relationship between the transverse and longitudinal mixing. Transverse mixing is important with steady state sources in the near and mid-field prior to complete cross-sectional mixing, and to quantify longitudinal mixing in the far-field. Recent developments of this theory and models are summarized by Rutherford (1994). For a channel that is much wider than it is deep, the timescale for cross-sectional mixing is much greater than that for vertical mixing. Thus, in a study of the even slower process of longitudinal dispersion, the contaminant can be regarded as being transversely well-mixed. Studies of steady contaminant plumes in natural channels has shown to have a large length to width ratio, which implies that transverse turbulent diffusion is more important than longitudinal shear dispersion (Elder, 1959).

Hence, as the starting point of the mathematical analysis, the depth-averaged model advection-diffusion-reaction equation,

$$\lambda h c + h u \frac{\partial c}{\partial x} - \frac{\partial}{\partial y}\left(h \kappa \frac{\partial c}{\partial y}\right) = 0. \tag{6.1}$$

with

$$h \kappa \frac{\partial c}{\partial y} = 0 \quad \text{on} \quad y = a, b, \text{ for all } x, \tag{6.2}$$

will form the basis of application for the numerical analysis. Here x and y are longitudinal and transverse coordinates, $c(x, y)$ is the contaminant concentration between the shorelines $y = a, b$ in water of depth $h(y)$, vertically-averaged steady velocity $u(y)$, vertically-averaged effective transverse diffusivity $\kappa(y)$. Macqueen and Preston (1983) and Gould and Munro (1981) noted that even within a single application, the magnitudes of the decay rate $\lambda(y)$ (evaporative heat loss or bacterial decay), the flow velocity and the diffusivity can vary significantly. For the predictions of the effectiveness of pollutant dispersal in rivers in order to enhance water-quality the process can involve flows ranging from droughts to floods, and biochemical constituents with widely differing decay rates. Therefore, the intended

numerical method is to achieve high-order accuracy with stability over a wide (h, λ, u, κ) range of parameters.

6.3 Flow profiles

In order to illustrate the validity of the shallow water assumption (that is, all horizontal length scales are much greater than the water depth), the flow profiles (the power-law velocity and diffusivity appropriate to turbulent flow) for linearly sloping straight channels as provided by Elder (1959) is presented as a single severe test case for the variable coefficients (see Figure 6.1(a)):

$$u = U\left(\frac{h}{H}\right)^{\frac{1}{2}}, \quad \kappa = K\left(\frac{h}{H}\right)^{\frac{3}{2}}. \tag{6.3}$$

For the variability of decay, use is made of depth-dependent power-law models (Mebine and Smith, 2006) (see Figure 6.1(b)):

$$\lambda = \Lambda\left(\frac{h}{H}\right)^{m}. \tag{6.4}$$

The capital letters H, U, K and Λ denote the depth, flow, transverse mixing and contaminant decay at some reference position in the channel. The parameter m is a number that quantifies the degree of contaminant decay. The chosen scalings (6.3) are not unduly complicated, but are nevertheless of interest in their own rights in linearly sloping beach, and they are used to illustrate the problem of contaminant dispersion in a vertically well-mixed channel of transverse cross-section where the presence of contaminant decay (6.4) in river flows play a vital role. It is pertinent to note here that the variables c, y and x in the equations (6.1) and (6.2) have their appropriate scales.

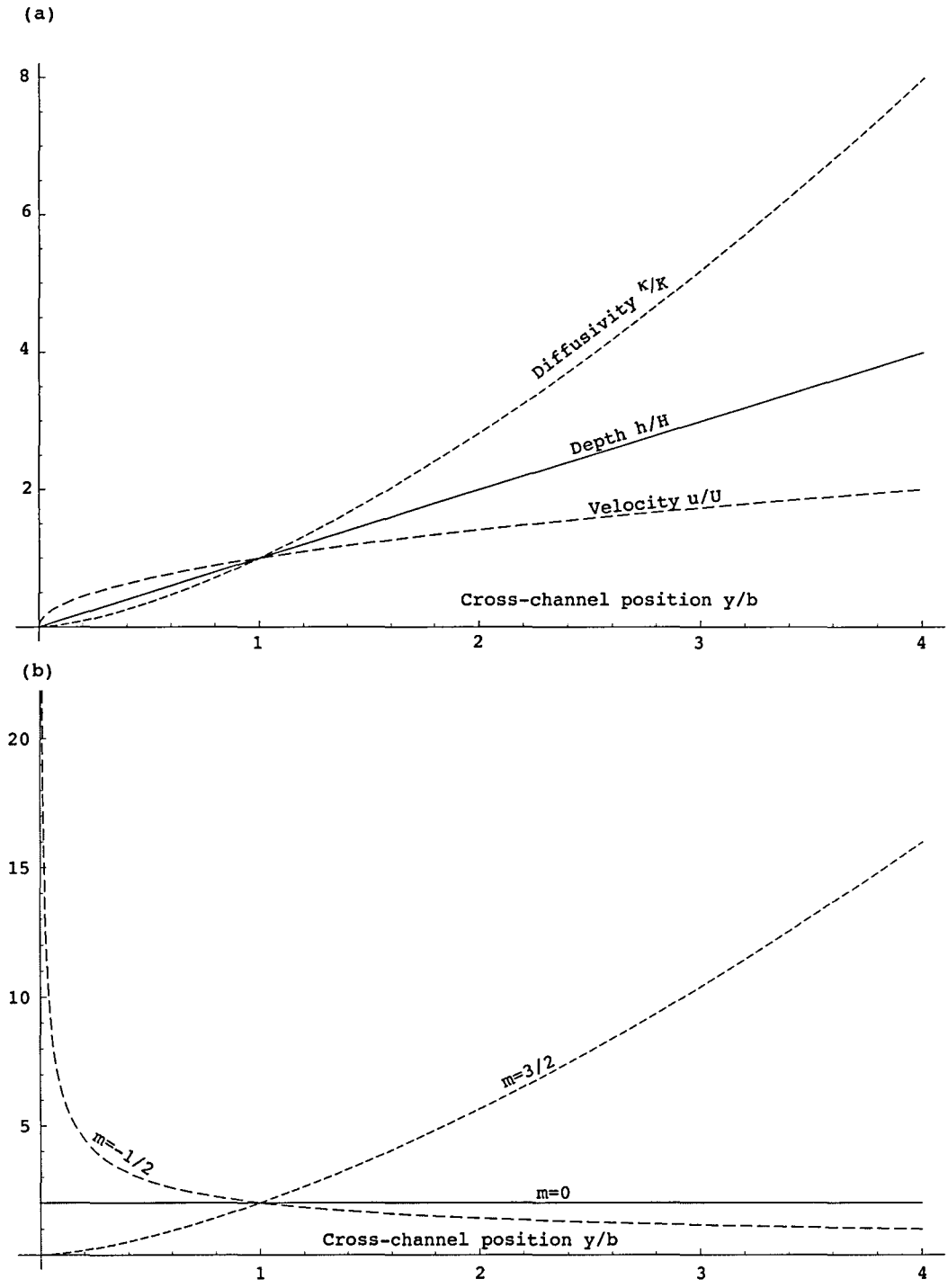


Figure 6.1: (a) Variable depth, velocity and diffusivity profiles; (b) Decay profiles for (i) constant decay $m = 0$, (ii) decay that decreases with depth $m = -1/2$, (iii) decay that increases with depth more than the velocity $m = 3/2$.

6.4 Finite-difference scheme

In order to discuss the prediction of pollutant dispersion phenomena from steady discharges, the finite difference technique would be applied to solve equation (6.1) numerically together with the specified boundary conditions (6.2). The transverse spatial grid will be indexed by the subscript j, while the superscript n indexes the longitudinal spatial grid. If at the nth longitudinal spatial level the transverse grid points are the locations y_j, then the corresponding numerical approximations to the concentration are denoted C_j^n. Richtmyer and Morton (1967) pointed out that, if on advancing to the $(n+1)$th longitudinal spatial-step, only three successive spatial mesh points are used in the local approximation scheme, then the tri-diagonal matrices linking the numerical approximations to the concentrations C_{j-1}^{n+1}, C_j^{n+1}, C_{j+1}^{n+1} are straightforward to solve. Bowen and Smith (2005) introduced maximal accuracy three-point approximations to c, $\partial_y c$, $\partial_y^2 c$ at the computational module, that is, $\overline{y_j} = \frac{1}{3}(y_{j-1} + y_j + y_{j+1})$ - the centroid:

$$\begin{aligned} D_0^y[C^n] &= \frac{(y_j - \overline{y_j})(y_{j+1} - \overline{y_j})}{(y_{j-1} - y_j)(y_{j-1} - y_{j+1})} C_{j-1}^n + \frac{(y_{j-1} - \overline{y_j})(y_{j+1} - \overline{y_j})}{(y_j - y_{j-1})(y_j - y_{j+1})} C_j^n \\ &\quad + \frac{(y_j - \overline{y_j})(y_{j+1} - \overline{y_j})}{(y_{j-1} - y_j)(y_{j-1} - y_{j+1})} C_{j+1}^n , \end{aligned} \tag{6.5a}$$

$$\begin{aligned} D_1^y[C^n] &= -\frac{(y_j + y_{j+1} - 2\overline{y_j})}{(y_{j-1} - y_j)(y_{j-1} - y_{j+1})} C_{j-1}^n - \frac{(y_{j-1} + y_{j+1} - 2\overline{y_j})}{(y_j - y_{j-1})(y_j - y_{j+1})} C_j^n \\ &\quad - \frac{(y_{j-1} + y_j - 2\overline{y_j})}{(y_{j-1} - y_j)(y_{j-1} - y_{j+1})} C_{j+1}^n , \end{aligned} \tag{6.5b}$$

$$\begin{aligned} D_2^y[C^n] &= \frac{2}{(y_{j-1} - y_j)(y_{j-1} - y_{j+1})} C_{j-1}^n + \frac{2}{(y_j - y_{j-1})(y_j - y_{j+1})} C_j^n \\ &\quad + \frac{2}{(y_{j-1} - y_j)(y_{j-1} - y_{j+1})} C_{j+1}^n . \end{aligned} \tag{6.5c}$$

The use of the centroid as the reference point makes the numerical scheme particularly neat (and easy to program). The equations (6.5) are connected together through the relationships:

$$D_1^y[C^n] = \frac{\partial D_0^y[C^n]}{\partial \overline{y_j}}, \tag{6.6a}$$

$$D_2^y[C^n] = \frac{\partial^2 D_0^y[C^n]}{\partial \overline{y_j}^2}. \tag{6.6b}$$

The accuracy of the three-point approximations is studied in detail by Bowen and Smith (2005).

A combined scheme of equations (6.5) and the weighted average or θ- method (Morton and Mayers, 1994) has been employed. The advection term has been discretised using forward difference technique but for the decay and the diffusion terms the three-point approximations (6.5) are appropriately applied. Therefore, equation(6.1) becomes

$$\begin{aligned} & D_0^y[h\,\lambda]\left(\theta\, D_0^y[C_j^{n+1}] + (1-\theta) D_0^y[C_j^n]\right) + D_0^y[h\,u]\left(\frac{C_j^{n+1} - C_j^n}{\Delta x}\right) \\ & - D_1^y[h\,\kappa]\left(\theta\, D_1^y[C_j^{n+1}] + (1-\theta) D_1^y[C_j^n]\right) \\ & - D_0^y[h\,\kappa]\left(\theta\, D_2^y[C_j^{n+1}] + (1-\theta) D_2^y[C_j^n]\right) = 0. \end{aligned} \tag{6.7}$$

The resulting system of equations from equation(6.7) is tri-diagonal; equation number j in the system only involves unknowns with numbers $j-1, j$ and $j+1$, so that the matrix of the system has non-zero elements only on the diagonal and in the positions immediately to the left and to the right of the diagonal. The Thomas algorithm is therefore employed to solve the system most efficiently. For constant coefficients, the scheme has the desirable attributes of being unconditionally stable, second-order accurate, economical to formulate, cost minimal computer time and applicable to both regular and irregular grid points. The

parameter controlling the degree of implicitness, θ, is such that $0 \leqslant \theta \leqslant 1$; $\theta = 0$ gives the explicit scheme, $\theta = \frac{1}{2}$ the Crank-Nicolson (1947) scheme and $\theta = 1$ the fully implicit scheme.

Specific examples are presented to illustrate and demonstrate the proposed finite difference scheme. Recognising that a real test of any newly proposed numerical method lies in the ability to handle efficiently, robustly and accurately solute transport in non-uniform and truly variable coefficients, the scheme is applied to simulate solute transport in turbulent flow with variable contaminant decay with respect to the depth of the river. The scheme is, therefore, applied to both constant and non-constant coefficients with regular grid spacings. The Fourier analysis of error and the plots of error are equally discussed in the following sections.

6.5 Regular grid spacing with constant coefficients

A direct method for verifying the accuracy of a numerical scheme is to compare the predictions with non-trivial exact solutions. Therefore, the numerical test considered herein apparently utilises a regular grid spacing with constant coefficients. Here, $C(n, j)$ is the value of C at the mesh point $(n, j) : x = n\,\Delta x$ and $y = j\,\Delta y$, Δx and Δy are grid spacings along the x- and y-axis, respectively. The D notations of (6.5) of the three-point approximation now reduces to

$$D_0^y[C^n] \;=\; C_j^n\,, \tag{6.8a}$$

$$D_1^y[C^n] \;=\; \frac{-C_{j-1}^n + C_{j+1}^n}{2\Delta y}\,, \tag{6.8b}$$

$$D_2^y[C^n] \;=\; \frac{C_{j-1}^n - 2C_j^n + C_{j+1}^n}{(\Delta y)^2}. \tag{6.8c}$$

The Crank-Nicolson and Crandall (1955) implicit schemes are employed for the test cases. The later scheme uses the choice of $\theta = \frac{1}{2} - \frac{1}{12\nu}$, where $\nu = \frac{\kappa \Delta x}{(\Delta y)^2}$ is a dimensionless diffusion parameter. The Crandall scheme is often known as an optimum scheme (Smith, 1999). The application of the equations (6.8) yields the following discrete approximation to (6.1):

$$\begin{aligned} &-\theta\,\nu\,C_{j-1}^{n+1} + (u + 2\,\theta\,\nu + \lambda\,\theta\,\Delta x)C_j^{n+1} - \theta\,\nu\,C_{j+1}^{n+1} \\ &= (1-\theta)\,\nu\,C_{j-1}^{n} + [u - 2\,(1-\theta)\,\nu - \lambda\,(1-\theta)\Delta x]C_j^{n} + (1-\theta)\,\nu\,C_{j+1}^{n}. \end{aligned} \tag{6.9}$$

Giving j the values $1, 2, \ldots, (J-1)$, a system of $J-1$ linear equations in the $J-1$ unknowns $C_j^{n+1}, j = 1, 2, \ldots, J-1$ are obtained. The Thomas algorithm is applied to solve the system of equations (6.9) efficiently.

A separation-of-variables exact solution for the constant coefficients of the equation (6.1) together with (6.2) is given by

$$c(x,y) = \cos\left(\frac{\pi\,y}{b}\right) \exp\left\{-\left(\frac{\lambda}{u} + \frac{\pi^2\,\kappa}{b^2\,u}\right)x\right\}. \tag{6.10}$$

Any other solution of the advection-diffusion-reaction equation (6.1) can be regarded as being built from a superposition of the solution (6.10). In general, the superposition will tend to reduce errors.

The benefits of an accurate numerical scheme could be lost with the use of an inaccurate boundary condition. In order to ensure that to a high order the exact solution fits the discrete boundary condition, the following boundary condition generating function is employed

$$g = \exp(-k^2\,\kappa\,\Delta x) - P\,\exp(-k^2\,\kappa\,\Delta x)\cos(k\,\Delta y) + Q_w - R\cos(k\,\Delta y), \tag{6.11}$$

where $k = \pi/b$ and P, Q_w and R are weights. Optimal selection of the weights as Δx and

Δy tend to zero is

$$P = 1 - \frac{6\,(\Delta y)^2}{6\,k\,\Delta x\, +\, 5\,(\Delta y)^2}\,, \tag{6.12a}$$

$$Q_w = 1 - \frac{10\,(\Delta y)^2}{6\,k\,\Delta x\, +\, 5\,(\Delta y)^2}\,, \tag{6.12b}$$

$$R = 1 - \frac{4\,(\Delta y)^2}{6\,k\,\Delta x\, +\, 5\,(\Delta y)^2}. \tag{6.12c}$$

Sufficient conditions for computational accuracy are that the grid spacings Δy and Δx are small enough. Therefore, the chosen parameter values are

$$\Delta x = \frac{1}{4\,\pi^2}\,, \quad \Delta y = \frac{1}{J-1}\,, \quad \frac{\kappa\,\Delta x}{(\Delta y)^2} = 0.633\,, \quad \lambda\,\Delta x = 0.0253\,, \quad u = 1, \tag{6.13}$$

where J denotes the number of transverse grid points.

Figure 6.2 shows the discrete Crank-Nicolson numerical solutions with $J = 6$ obtained with the initial condition $c(0, y) = \cos\left(\frac{\pi y}{b}\right)$ and the exact solutions for the first and second longitudinal-steps, $n = 1$ and $n = 2$, respectively. Figure 6.3 demonstrates the errors at these longitudinal steps. The error maximum is 4×10^{-3}, and is a vast improvement on explicit schemes at such low resolution.

The numerical method is designed to give the best possible results. Figure 6.4 pertains to the Crandall scheme for the first and second longitudinal-steps, $n = 1$ and $n = 2$, respectively. The error maximum is 1.3×10^{-3} (see Figure 6.5). The superiority of the Crandall scheme is clear.

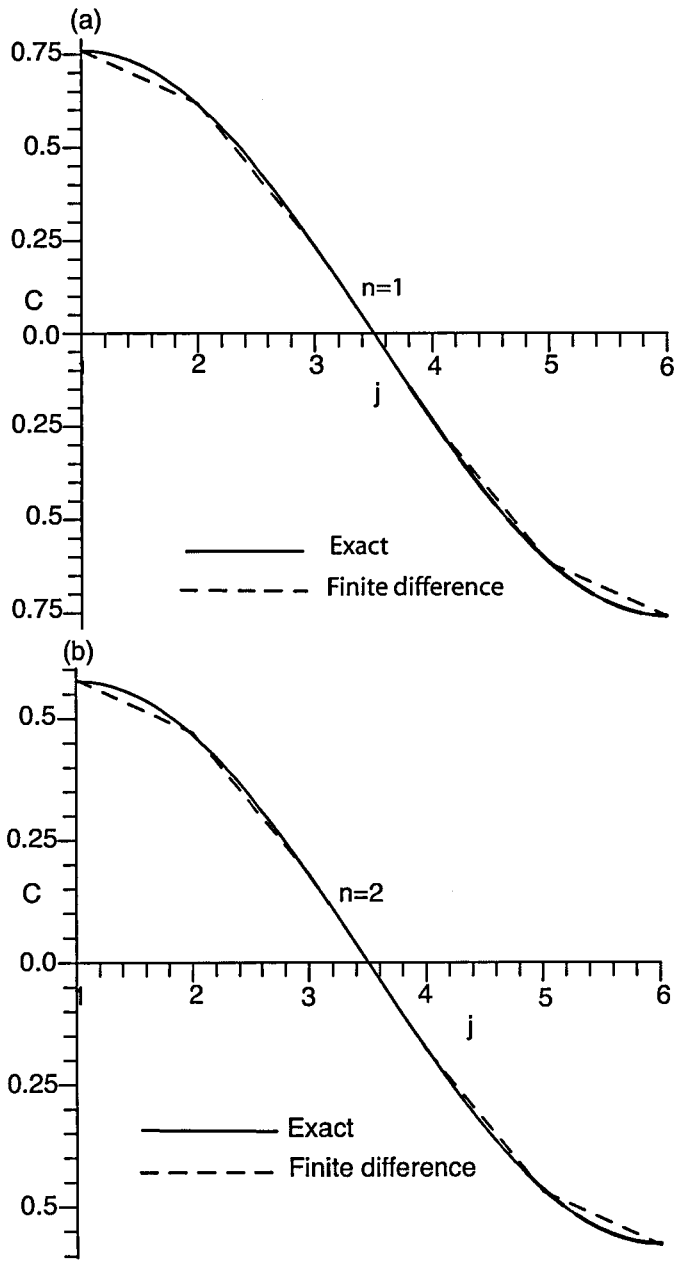


Figure 6.2: Crank-Nicolson finite difference solutions at the first and second longitudinal steps.

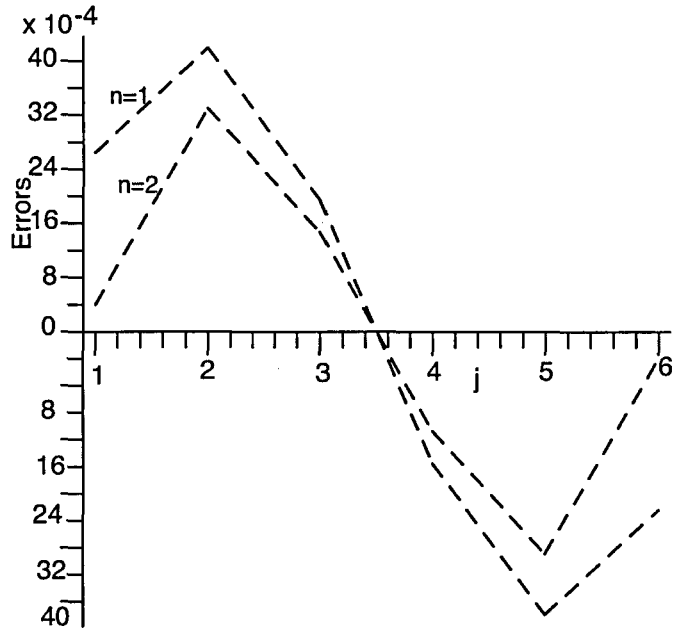


Figure 6.3: Error plots of Crank-Nicolson finite difference solutions at the first and second longitudinal steps.

6.6 Regular grid spacing with non-constant coefficients

In natural channels the behaviour of the discharged pollutant is influenced by a number of factors including: (i) the properties of the effluent being discharged, that is, its physical, chemical, and biological transformations, (ii) the rate at which the effluent is being discharged, that is, the total mass of pollutant injected in a given time, (iii) the spacing and orientation of the discharge outlets, that is, the height of the injection point above the outfall of the shoreline, and (iv) the characteristics of the river, that is, its depth, width and flow velocity. Thus, this section considers the numerical computation of equation (6.1) with the no-flux boundary conditions (6.2) and the prescribed variable coefficients (6.3) and (6.4). In the present problem, contaminant is injected at the point $x = 0$ in the form:

$$c(0, y) = Q\,\delta(y - y_0), \tag{6.14}$$

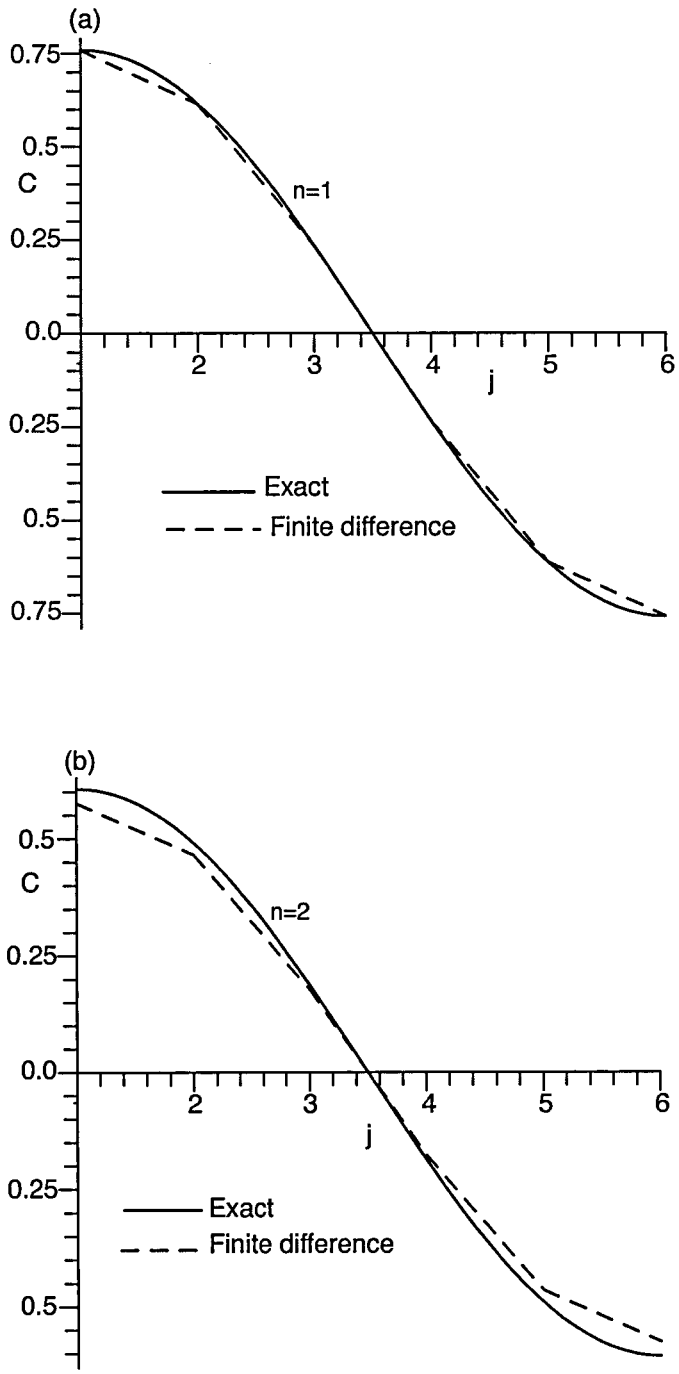


Figure 6.4: Crandall finite difference solutions at the first and second longitudinal steps.

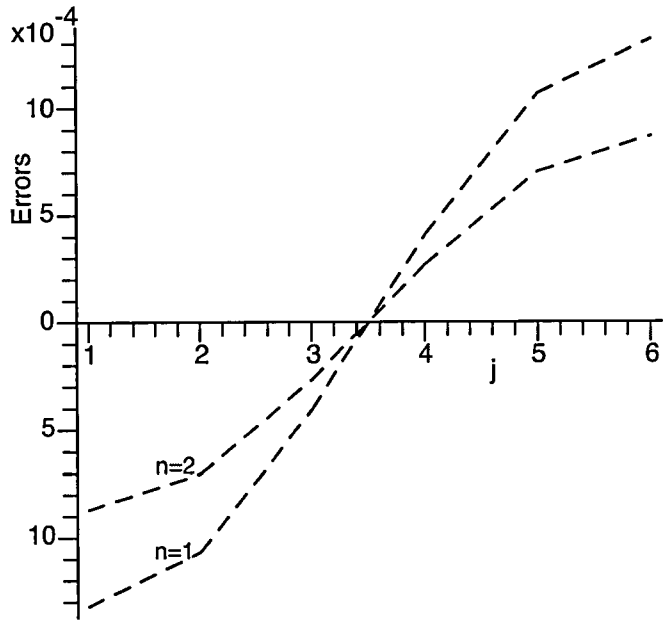


Figure 6.5: Error plots of Crandall finite difference solutions at the first and second longitudinal steps.

where Q is the contaminant discharge rate or the total volume flow rate, y_0 is the height of the injection point above the outfall of the shoreline and $\delta(y - y_0)$ is the Dirac delta function. Normalizing the concentration with respect to the volume flux Q:

$$\int_a^b h\,u\,c\,dy = \int_a^b h\,u\,dy = Q\ , \tag{6.15}$$

ensures a unit average concentration when there is no decay.

We note here that the numerical scheme is constructed to give the highest-order accuracy at long length-scales. This is of particular importance in real river situations where the fate of contaminant dispersion downstream is monitored. For the purpose of insights, the non-dimensional domain length and width are chosen as 4×1 and the number of grids in x- and y- directions are chosen respectively as 2020 and 201. The grid spacings applied here

are $\Delta x = 0.0005$ and $\Delta y = 0.02$, and the initial concentrations used for the computations are deduced from the relation (6.15) such that

$$c = \frac{1}{{y_0}^{3/2}\,\Delta y}\,\frac{2}{5}\,{y_b}^{5/2}, \tag{6.16}$$

where y_b denotes the width of the river.

6.6.1 Kay benchmark problem

Benchmark problems with known exact solutions permit stringent assessment of the numerical methods. Section 6.5 considered such an exact solution for constant coefficients. This section considers an exact solution for non-constant coefficients.

For conserved contaminants, Kay (1987) investigated the effect of cross-stream depth variations upon contaminant dispersion in a vertically well-mixed current. Applying similar scaling conditions (6.3) for the current speed and lateral eddy diffusivity, he obtained an exact solution of the variable-coefficient advection-diffusion equation that corresponds to a constant-rate point discharge in steady flow along a sloping beach. The exact solution derived by Kay (1987, equation 36) can be written in non-dimensional variables as

$$c_\star = {y_\star}^{-3/4}\,{x_\star}^{-1}\,\exp\Big(-\frac{y_\star+1}{x_\star}\Big)\,I_{3/2}\Big(\frac{2\,{y_\star}^{1/2}}{x_\star}\Big), \tag{6.17}$$

where $I_{3/2}$ is a modified Bessel function. Figure 6.6 (with solid lines) (Kay, 1987; Figure 8) is based upon the exact solution (6.17) and shows concentration contours, with contours at intervals of 0.2, up to 2.0 units, in the $(x\,,y)$ plane for the benchmark case $Q' = 1$, $x_\star = 0$, $y_\star = y_0$. For uniformly sloping natural beaches the ratio of the distance from the outfall to the shoreline (reference off-shore distance) and the distance which contaminant will have been advected downstream before it meets the shoreline (reference long-shore distance) is about 0.001 and pollutant plumes are elongated 1000 times relative according to Figure 6.6 (with solid lines). The most striking feature is the high concentration tongue from source

to shoreline, which may be due to the higher velocity gradient near the shoreline. As the velocity is low near the shoreline, the solute concentration in the lower velocity region disperses slowly, where in the higher velocity region, it disperses faster. This reveals that the contaminant remains at high concentrations further downstream in the shallower water near the shoreline than in the deeper water. Thus, the solute disperses to a great extent downstream as seen from the figure.

The exact analytical result (6.17) has been widely used as benchmark problem for validating experiments, the testing and comparison of random walk and Galerkin finite element schemes (Potter *et al.*, 1996; Scott, 1997; Nassehi and Passone, 2005). Figure 6.6 (a) shows the contour plots of the exact versus the numerical result obtained using the no-flux boundary conditions. The Figure 6.6 (a) has acceptable level of evidence that the numerical results give reasonable approximations to the exact solution near the lower boundary or shoreline. The numerical solution fails along the upper boundary where low solute concentrations are expected. This failure is observed at about 0.2 units downstream. Beyond this point, the numerical solution overestimates the analytical solution near the upper boundary. Again, the comparisons (Figure 6.6 (a)) indicate that the numerical approximation gives mismatch with the analytical result in the leading concentration tongue with unit 1.4. The overestimation near the upper boundary could be attributed to the difference between the boundary conditions used in the analytical and the numerical solutions. While the numerical solution uses no flux boundary conditions in both boundaries, the analytical solution uses no flux boundary in the lower boundary and zero concentration at great distances from the shoreline in the upper boundary. For curiosity and compatibility, a zero concentration far boundary condition is used giving the Figure 6.6 (b). Once again, the numerical solution represents the exact solution reasonably well near the lower boundary. The numerical results give an underestimation of the exact solution from the centerline of the plume toward the upper boundary. The discrepancies observed in the Figures 6.6 are attributed to the inherent weakness of numerical schemes to resolve properly the problems associated with

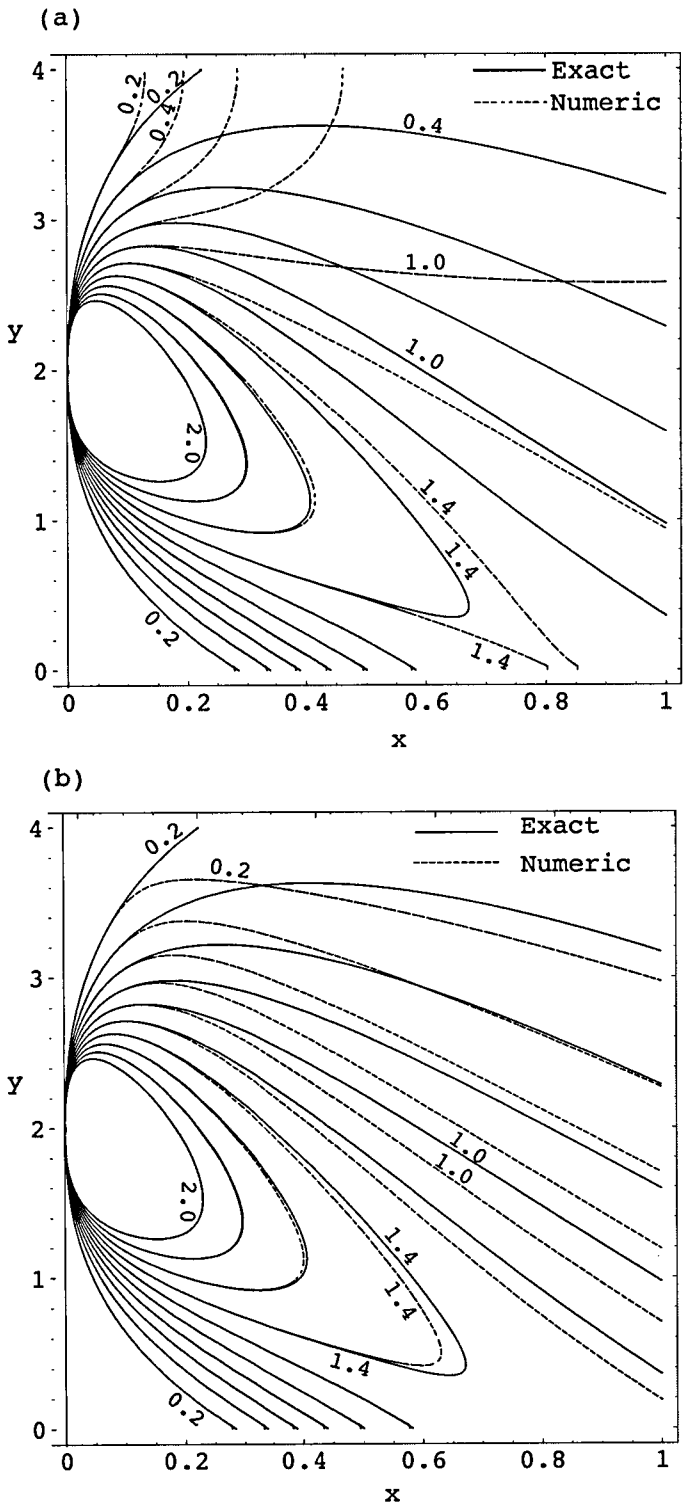


Figure 6.6: Concentration contours of midpoint discharge for the Kay exact solution (6.17) versus the numerical computation with (a) no-flux boundary conditions, (b) Zero concentration far boundary condition.

variable coefficients in the prediction of pollutant dispersion in coastal waters (Nassehi and Passone, 2005).

6.7 Optimal and non-optimal discharge

An optimal discharge site for a steady discharge in a river was obtained by Smith (1982) using the method of eigenmodes. The precise location of the optimal discharge site was found at the single zero crossing of the first advection-diffusion eigenmode. Simple examples revealed that this position tends to be weighted towards the deeper part of the channel, where it was determined as $y_1 = 0.607B$. The explanation is that contaminant plumes tend to curve towards the shallower water. It is to counteract this tendency that the siting of the discharge must be weighted towards the deeper water. Figure 6.7 (a) demonstrates contour plots of the computational scheme using the optimal discharge site with no-flux boundary conditions. For the zero concentration far boundary condition Figure 6.7 (b) gives the contour plots. It can readily be observed that the solute concentration is moderately dispersed near the origin than the midpoint discharge (see Figures 6.6 (a, b) with dashed lines) and the centre-line of the contaminant plume is reasonably far away from the shore. The high reduction in the concentration tongue from source to shoreline is a clear indication that the point of injection changes significantly the pattern of dispersion downstream.

To further illustrate the gains of using optimal discharge other than non-optimal discharge and the use of the no-flux and zero concentration far boundary condition, Figures 6.8 and 6.9 present the concentration contours of two scenarios of the point source taken to be halfway above and halfway below the midpoint discharge respectively with no-flux and zero concentration boundary condition. Evidently, putting the discharge site further out to the deeper water can drastically reduce the shoreline concentration (Figures 6.8 (a, b)) but gives peak concentration greater than 1 along the deep-water boundary. On the other hand, the Figures 6.9 (a, b) demonstrates high solute concentration in excess of 7 along the shoreline. This again emphasizes the existence of the physics of a higher velocity gradient near the

origin. The consequent effect is, therefore, the slow dispersion in this region due to the low velocity. In practice, the cost of using an optimal discharge site in relatively deep water, rather than a site closer to the bank, is justifiable only if there is a significant reduction in the pollution levels. To this end, from the Figures 6.8 and 6.9, it is conveniently observed that if the discharge site were too near one of the banks then the contaminant plume would reach that bank relatively soon with a concentration in excess of the eventual asymptote (Smith, 1982; figure 1). The remarkable differences between these two cases exemplifies further the significant importance of the need to use optimal discharge sites in rivers in order to make water quality management decisions. Therefore, it is for often-repeated water quality predictions, such as controlling environmental impact of discharges from sewage works, that the gains in using optimal discharge sites are potentially of greatest importance.

In natural river systems the cross-section is rarely of uniform depth, and the fall-line tend to meander. Therefore, it is usually the lateral shear rather than the vertical shear that plays the more important role. This affects the fate of an effluent discharged and ultimately the decay mechanisms. The following three subsections concern the same depth related velocity and turbulent diffusivity profiles (see Figure 6.1(a)), but with decay profile applications corresponding to uniform consumption by bacteria, to evaporation and to break up by turbulence (see Figure 6.1(b)). The no-flux boundary conditions are herein applied since the contaminant decay will effect the reduction in the overestimation of the numerical computations. The numerical computations uses the reference decay strength of $\Lambda B^2/K = 2$.

6.7.1 Constant decay

This is a situation where the contaminant is consumed by bacteria, that is, decay uniform across the flow. The decay profile for the constant case is quantified by $m = 0$. Figure 6.10 (a) depicts a midpoint injection concentration contours for the computation with the reference decay strength. Remarkable differences between the non-decaying (see Figure 6.6

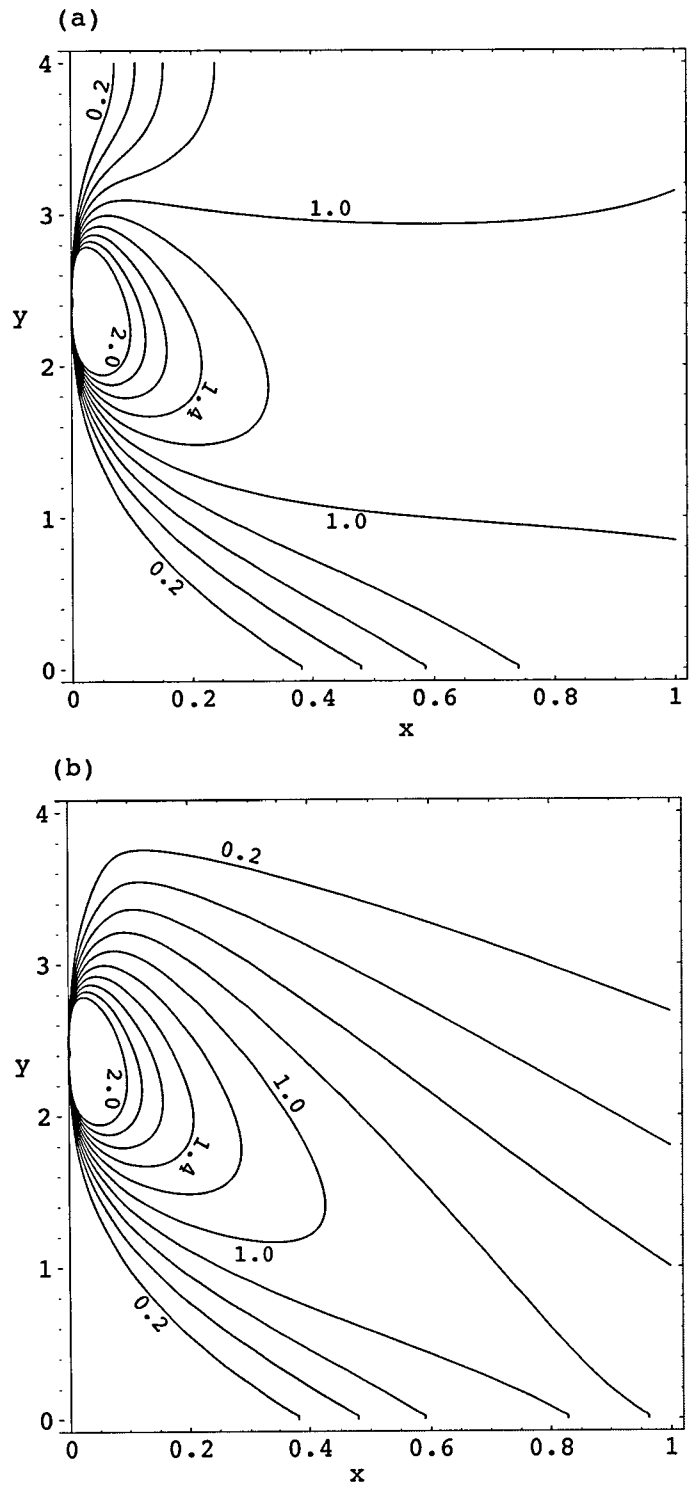


Figure 6.7: Concentration contours for optimal discharge with (a) no-flux boundary conditions, (b) zero concentration far boundary condition.

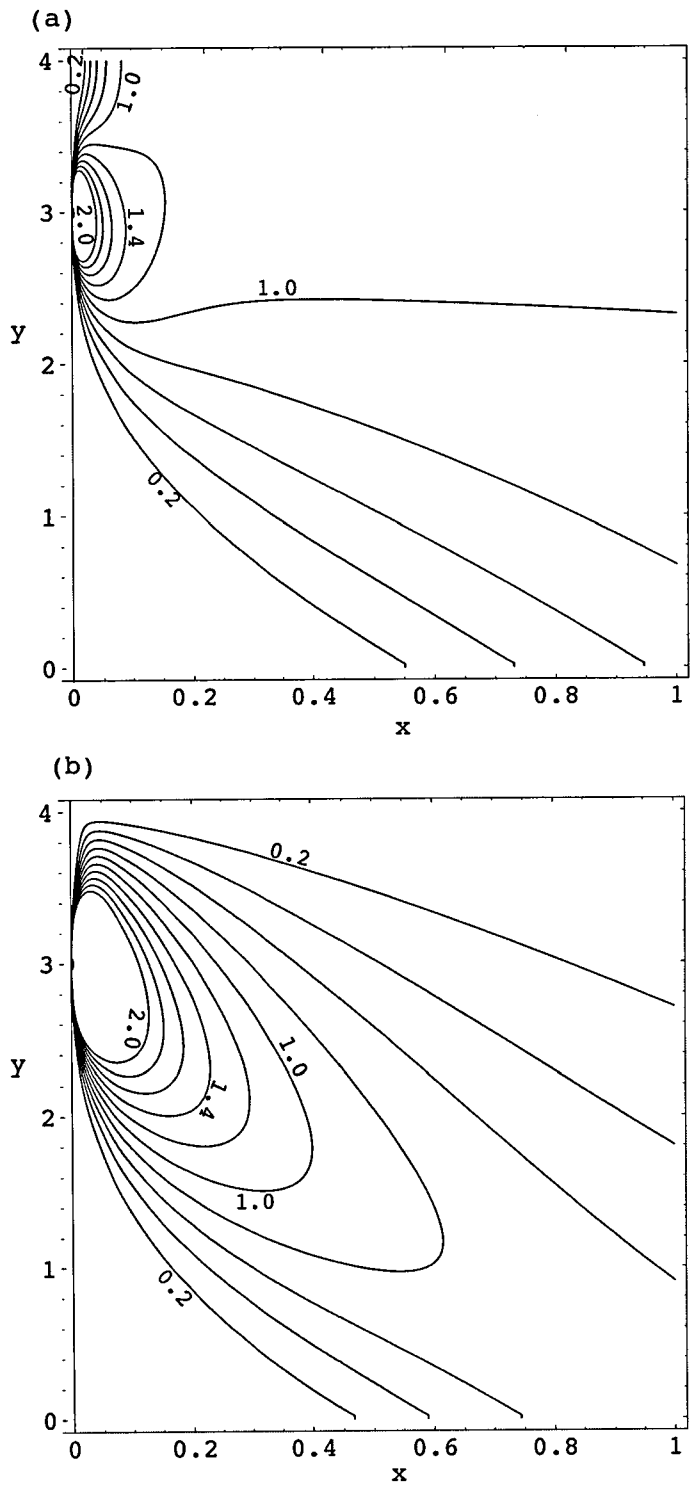


Figure 6.8: Concentration contours of discharge (a) halfway above the midpoint discharge with no-flux boundary conditions, (b) halfway above the midpoint discharge with zero concentration far boundary condition.

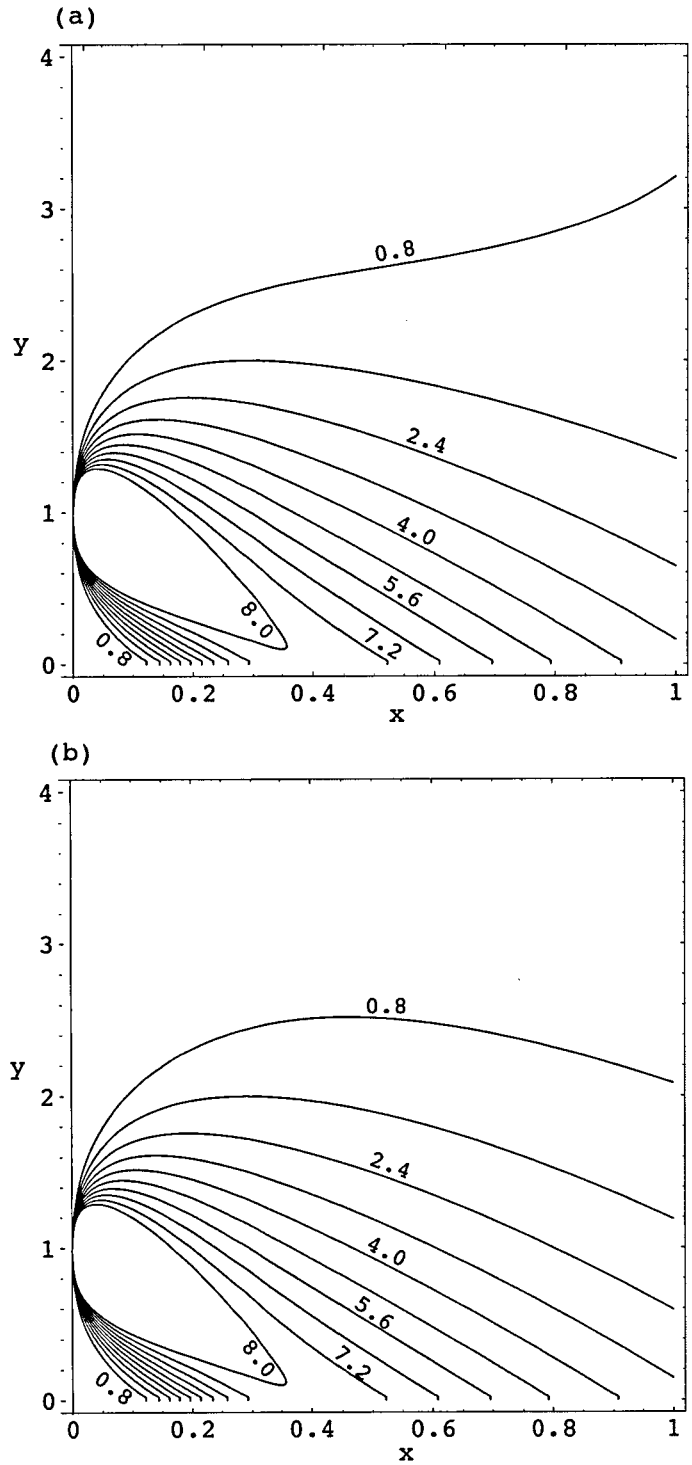


Figure 6.9: Concentration contours of discharge (a) halfway below the midpoint discharge with no-flux boundary conditions, (b) halfway below the midpoint discharge with zero concentration far boundary condition.

(a)) and the decaying contaminant for the midpoint discharge can clearly be examined from the contour patterns, for instance between the 1.4 unit contour. Therefore, the decay effects qualitatively the loss of the contaminant from the river flow. For the reference decay strength for constant decay, Mebine and Smith (2006) obtained the optimal discharge site $0.637B$, and Figure 6.10 (b) gives the plots of the concentrations. A distinctive contribution of the optimal discharge as compared to the midpoint discharge is the reduction in the tongues of the concentration contours.

Because the decay is not proportional to the flow velocity, the concentration far downstream is not uniform, but has structure $\phi_0(y)$ of the lowest eigenmode. It is $c(x,y)/\phi_0(y)$ that becomes uniform. Hence, the increase in $c(x,y)$ towards the deeper boundary echoes the structure of $\phi_0(y)$.

6.7.2 Decay that decreases with depth

The time rate of decay can be greater in shallower water if there is air-water contaminant exchange at the surface. Other removal processes that are more effective in shallower water are the killing of bacteria by sunlight (Gould and Munro, 1981) and feeding at the bed by marine micro-organisms, bacteria, fungi or yeasts. In this subsection, the degree of contaminant decay parameter is given by $m = -1/2$. Figure 6.11 (a) shows the numerical contour plots. The optimal discharge site for the decay that decreases with depth for the reference decay strength is $0.676B$ (Mebine and Smith, 2006). Figure 6.11 (b) illustrates the contour profiles of optimal discharge for decay that decreases with depth. Once again, it is observed the distinctive reduction of the tongues of the concentration contours of the optimal discharge as compared to the midpoint discharge. The stronger lateral concentration structure echoes that of $\phi_0(y)$ for this decay structure.

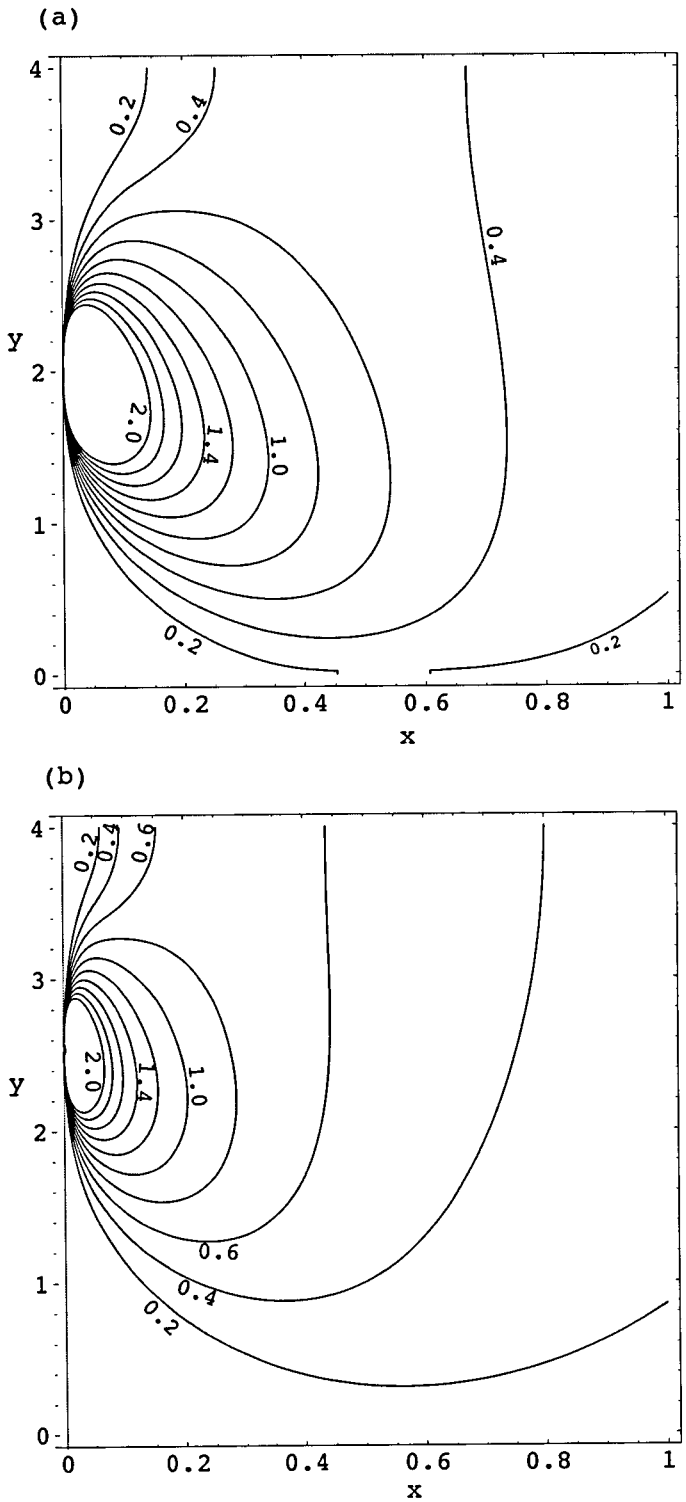


Figure 6.10: Concentration contours for constant decay with decay strength $\Lambda B^2/K = 2$ (a) midpoint discharge, (b) optimal discharge .

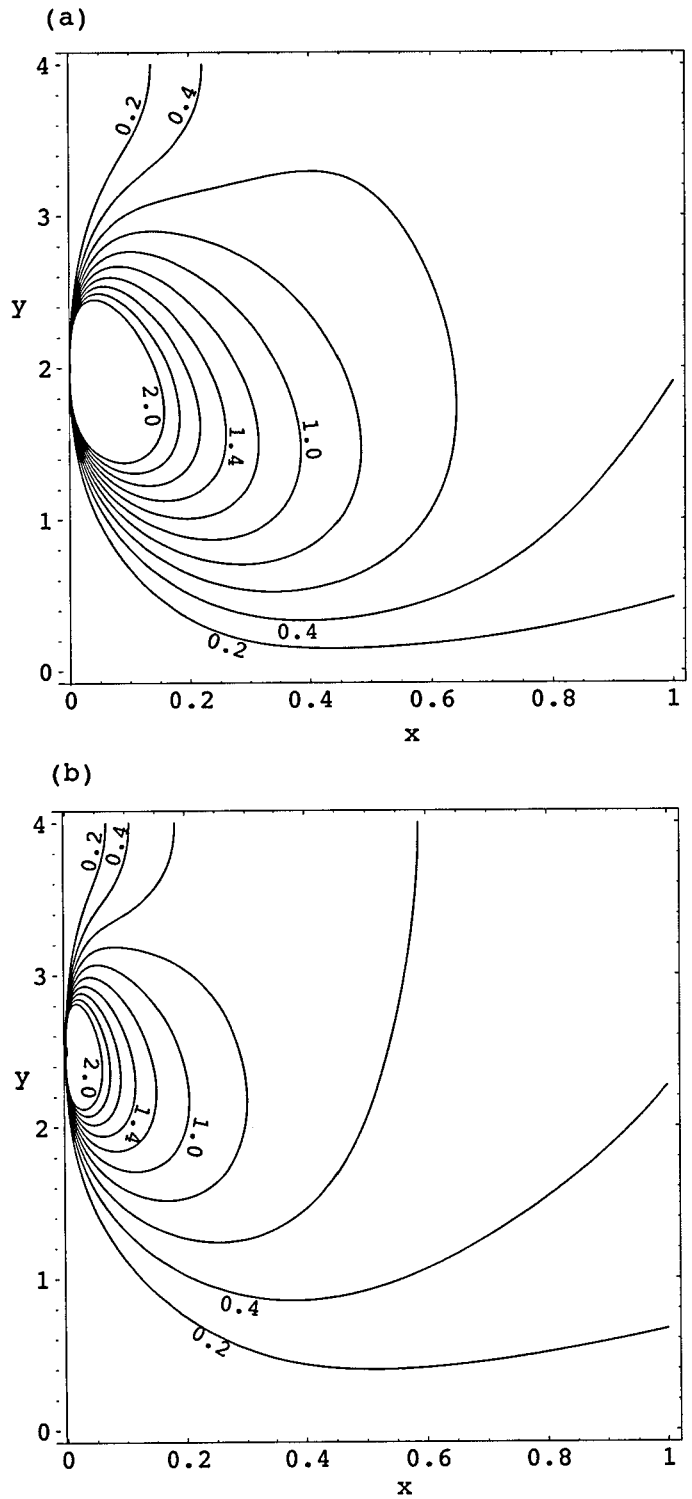


Figure 6.11: Concentration contours for decay that decreases with depth and with decay strength $\Lambda B^2/K = 2$ (a) midpoint discharge, (b) optimal discharge.

6.7.3 Decay that increases with depth more than the velocity

The dissolution of oils or flocs is most rapid in regions of the flow where the turbulence is energetic. It is worth noting that the level of turbulence affects flocculation in the near field, and therefore shear in the discharged plume. Increases in turbulence intensity tend to result in larger flocs due to an increase in the probability of collision between particles. In this subsection, the degree of decay is modelled $m = 3/2$. The centre-line of the contaminant plume is displaced towards the shore (see Figure 6.12 (a)). Using the optimal discharge site $0.589B$ (Mebine and Smith, 2006) reduces the extent of the displacement of the centre-line of the contaminant plume towards the shore (Figure 6.12(b)). The changed form of decay from the previous case, changes the lowest mode $\phi_0(y)$ to being largest in shallow water (where decay is least). Hence, the largest concentrations are along the shallow shoreline.

6.8 Evolution of Fourier modes and Stability Analysis

Insight in the solution of the advection-diffusion-reaction equation (6.1), or of any numerical approximation, can be obtained by Fourier decompositions. We consider the construction of a solution of the finite difference equations for Fourier modes of the form:

$$C_j^n = G^n \, e^{i\,k_j\,(j\,\Delta y)}, \tag{6.18}$$

where $i = \sqrt{-1}$, k_j is the wave number and denotes the number of waves that exist over a distance of 2π and G is a function of k_j and is known as the growth or amplification factor for the modes. For a flat channel (that is, $\kappa = 1$, $u = 1$, $\lambda = 1$), using equation (6.18) and similarly for the other terms, equation (6.9) results

$$G = \frac{1 - 4\,(1-\theta)\,\nu\,\sin^2\left(\frac{1}{2}\,k_j\,\Delta y\right) - (1-\theta)\,\Delta x}{1 + 4\,\theta\,\nu\sin^2\left(\frac{1}{2}\,k_j\,\Delta y\right) + \theta\,\Delta x}. \tag{6.19}$$

Fourier decompositions determines the stability of the solution of the finite difference

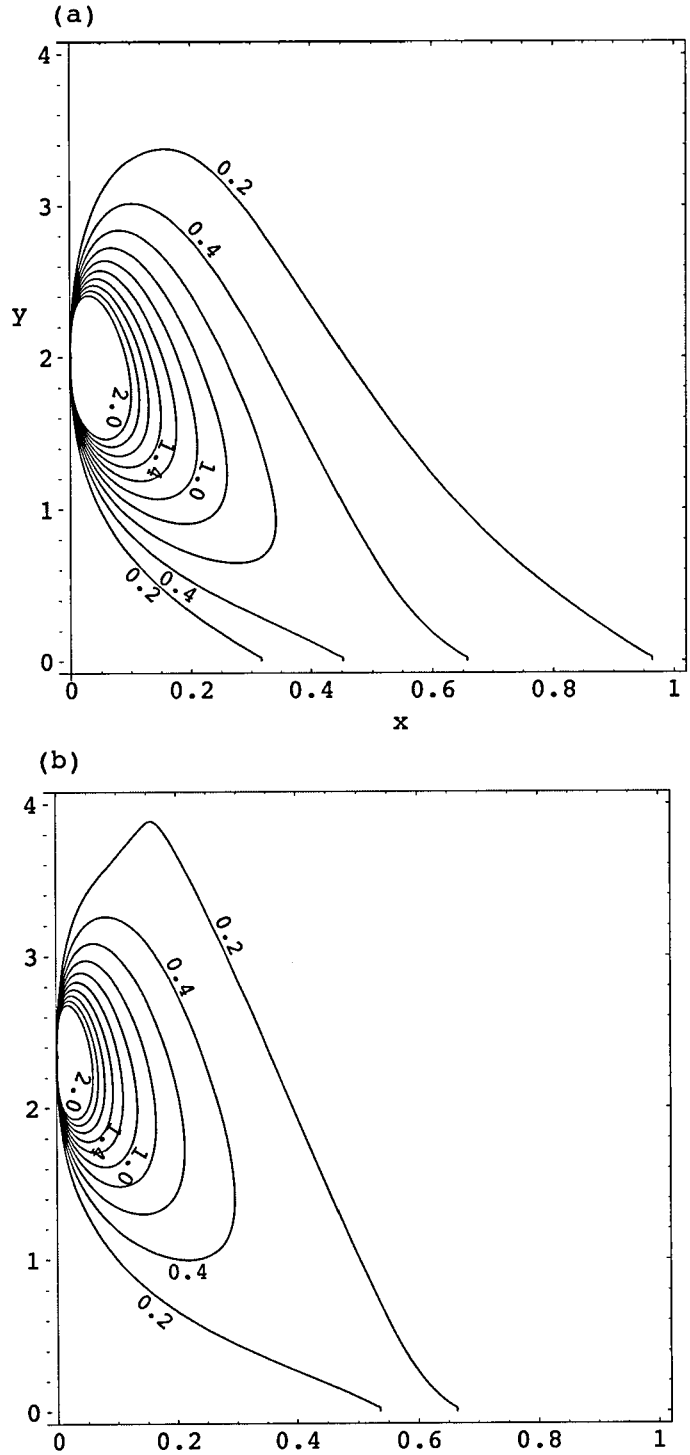


Figure 6.12: Concentration contours for decay that increases with depth and with decay strength $\Lambda B^2/K = 2$ (a) midpoint discharge, (b) optimal discharge.

equations. Decay or growth of an amplification factor indicates whether or not the numerical algorithm is stable. This is known as von Neuman stability analysis (Orthega and Rheinbolt, 1970). The computational scheme (6.9) is said to be stable if

$$| G | \leq 1 \quad \text{for all} \quad k_j \Delta y. \tag{6.20}$$

Evidently equation (6.19) can never have $G > 1$ for any positive choice of ν, assuming $0 \leq \theta \leq 1$. Thus, instability arises only through the possibility that $G < -1$, and hence

$$4\nu(1-2\theta)\sin^2\left(\frac{1}{2}k_j \Delta y\right) > 2 - (1-2\theta)\Delta x. \tag{6.21}$$

The mode most liable to instability is the one for which the left side is largest, and this occurs for $k_j \Delta y = \pi$. Hence, this is an unstable mode if

$$\nu(1-2\theta) > \frac{1}{2} - \frac{1}{4}(1-2\theta)\Delta x. \tag{6.22}$$

Therefore, a necessary and sufficient conditions for the stability of equation (6.9) are:

$$\text{when} \quad 0 \leq \theta < \frac{1}{2}, \quad \text{stable if and only if} \quad \nu \leq \frac{1}{2}(1-2\theta)^{-1} - \frac{1}{4}\Delta x, \tag{6.23a}$$

$$\text{when} \quad \frac{1}{2} \leq \theta \leq 1, \quad \text{for all} \quad \nu. \tag{6.23b}$$

These two cases are often referred to as conditional and unconditional stability respectively.

For variable coefficient problems, the von Neuman stability analysis can also be applied locally (with local values of the coefficients). Because instability is a local phenomenon, due to the high frequency modes being most unstable, the von Neuman stability analysis gives necessary stability conditions which can often be shown to be sufficient (Morton and Mayers, 1994). For the incorporation of the effect of boundary conditions, conservation

laws and the energy method analysis can sometimes be employed to yield sufficient stability conditions to complement the necessary conditions given by the von Neuman analysis.

6.9 Concluding remarks

The special cases solved broaden insight about a quantitative criterion for environmental impact of a contaminant released into rivers. The quantitative influence far downstream can be characterized in terms of the point of injection and the rate of contaminant decay, and hence changes significantly the pattern of dispersion. For an optimal discharge, the shear dispersion near the origin is greatest when there is both strong shear and strong turbulent mixing, while the velocity is least and the time-lag maximized for an injection close to the origin other than the middle of the transverse direction. As the contaminant moves faster for higher point of injection than for lower one, there is a tendency to develop an asymmetry in dispersion of material when it is injected near the origin. The major conclusion is that optimal discharges in the presence of a varying decay, current and diffusivity with depth can lead to the rapid attainment of the equilibrium lowest mode shape $\phi_0(y)$ of the cross-stream concentration profile. The computational results provide reasonable estimates and give pictorial illustrations of the concentration distributions and of the difference between discharging at non-optimal and optimal sites in rivers.

6.10 References

1. Araújo, A., Ferreira, J. A. and de Oliveira, P.: 2005, The role of abstract numerical properties in the change of character of reactive flows. *J. Math. Fluid Mech.*, **7**, S141 - S163.

2. Bikangaga, J. H. and Nassehi, V.: 1995, Application of computer modelling techinques to the determination of optimum efluent discharge policies in tidal water systems. *Wat. Res.*, **29**,10, 2367 - 2375.

3. Bowen, M. K. and Smith, R.: 2005, Derivative formulas and errors for non-uniformly spaced points. *Proc. Roy. Soc. Lond.* A, **461**, 1975 - 1997.

4. Boxall, J. B., Guymer, I. and Marion, A.: 2003, Transverse mixing in sinuous open channel flows. *Journal of Hydraulic Research*, **41**, 2, 153 - 165.

5. Crandall, S. H.: 1955, An optimum implicit recurrence formula for the heat conduction equation. *Quart. Appl. Math.*, **13**, 3, 318 - 320.

6. Crank, J. and Nicolson, P.: 1947, A practical method for numerical evaluation of solutions of partial differential equations of the heat-conduction type. *Proc. Camb. Philos. Soc.*, **43**, 50 - 67.

7. Elder, J. W.: 1959, The dispersion of marked fluid in turbulent shear flow. *J. Fluid Mech.*, **5**, 544 - 560.

8. Fischer, H. B.: The effects of bends on dispersion in streams. *Water Resources Research*, **5**, 2, 496 - 506.

9. Gould, D.J. and Munro, D.: 1981, Relevance of microbial mortality to outfall design. *Coastal Discharges*, Thomas Telford, London, U.K., 45 - 50.

10. Jobson, H.E.: 1997, Predicting travel time and dispersion in rivers and streams. *Journal of Hydraulic Engineering*, **123**, 11, 971 - 979.

11. Kay, A. : 1987, The effect of cross-steam depth variations upon contaminant dispersion in a vertically well-mixed current. *Estuarine, Coastal and Shelf Science*, **24**, 2, 177 - 204.

12. Macqueen, J. F. and Preston, R. W.: 1983, Cooling water discharges into a sea with sloping bed. *Water Research*, **17**, 4, 389 - 395.

13. Mebine, P. and Smith, R.: 2006, Effects of Contaminant Decay on the Diffusion Centre of a River. *Environmental Fluid Mechanics*, **6**, 101 - 114.

14. Morton, K. W. and Mayers, D. F.: 1994, Numerical Solution of Partial Differential Equations, Cambridge Univ. Press.

15. Nassehi, V. and Bikangaga, J. H.: 1993, A mathematical model for the hydrodynamics and pollutants transport in long and narrow tidal rivers. *Appl. Math. Modelling*, **17**, 415 - 422.

16. Nassehi, V. and Passone, S.: 2005, Testing Accuracy of Finite Element and Random Walk Schemes in Prediction of Pollutant Dispersion in Coastal Waters. *Envronmenatal Fluid Mechanics*, **5**, 3, 199 - 214.

17. Orthega, J. M. and Rheinbolt, W. C.: 1970, Iterative Solutions of Non-Linear Equations and Several Variables. Wiley, London.

18. Potter, R., Guymer, I., Pearson, J. M., West, J. R. and Croates, L. E.: 1996, Mixing Processes within open-channel flows containing transverse depth variations. *Proc. 2nd Int. Con. on Hydrodynamics*, Hong Kong, December 16 -19, 1996.

19. Richtmyer, R. D. and Morton, K. W.: 1967, Difference methods for initial-value problems. Second edition, Wiley.

20. Rutherford, J. C.: 1994, River Mixing, Wiley, Chichester UK.

21. Scott, C. F.: 1997, Particle tracking simulation of pollutant discharges. Journal of Env. Eng., **123**, 9, 919 - 927.

22. Smith, R.: 1981, The importance of discharge siting upon contaminant dispersion in narrow rivers and estuaries. *J. Fluid Mech.*, **108**, 45 - 55.

23. Smith, R.: 1982, Where to put a steady discharge in a river. *J. Fluid Mech.*,**115**, 1 - 11.

24. Smith, R.: 1999, Optimal and near-optimal advection-diffusion finite-difference Schemes I. Constant coefficient in one dimension. *Proc. R. Soc. Lond.* A, **455**, 2371 - 2387.

25. Smith, R.: 2000, Optimal and near-optimal advection-diffusion finite-difference Schemes II. Unsteadiness and non-uniform grid. *Proc. R. Soc. Lond.* A, **456**, 489 - 502.

26. Yoo, M. K, Cho, S. W., and Jun, K. S.: 2003, Unsteady Dispersion of Nonconservative Pollutants in Natural Rivers. *www.kfki.baw.de/conferences/ICHE/2000-Seoul/pdf/251/RAP-291.PDE*

27. Yotsukura, N. and Cobb, E. D.: 1972, Transverse diffusion of solutions in natural streams. *U. S. Geo. Survey Paper*, no.582 C.

Chapter 7

Conclusions and Further Work

7.1 Conclusions

In this dissertation both analytical and numerical developments for the study of steady discharges of contaminants in rivers have been performed. The fate and transport of contaminants have been analysed using depth-averaged partial differential equations of advection-diffusion-reaction models with appropriate initial and boundary conditions. The main motivation of the work was concerned with the development of mathematical ideas and computer programmes to make direct computations of best discharging for rivers principally considering the effects of loss mechanisms of contaminants.

The research done here has generally been written about in the order in which it was actually done. Hopefully, this has given both a flavour of what has been achieved and also serves as a good indication of how the research proceeded step-by-step.

Chapter 1 began by introducing the specific problem under consideration with some related literature and basic concepts of mixing and its importance.

The derivations of the equations governing contaminant transport with the discussions of some basic concepts were carried out in Chapter 2. All the techniques in formulating the model equations were taken from standard mathematical texts and literature.

Exact analytical results were presented in Chapter 3. Given that oil, chemical and biological waste will continue to be discharged into rivers, Chapter 3 posed the questions does it matter (a) where, and (b) what is discharged? For small discharges in a non-branching straight section of river, answer (a) yes, there is a well-defined best place to discharge (that is, the mixing or diffusion centre), and (b) yes, but the best place only depends weakly on the ratio of decay rate to flow speed. Three test problems were used to determine the effective role of the decay rate . Decay mechanisms included consumption by bacteria or radioactive decay (temporal decay uniform across the flow), heat loss or evaporation through the surface (decay decreasing with depth), and break up by turbulence (decay proportional to the product of velocity and depth). It was observed that for a mixture of pollutants with different decay processes and rates, the chosen discharge site will be a

compromise between the diffusion centre for the constituent pollutants. The variety of the exact analytical results illustrated the robustness of the commonsense policy that, to avoid large shoreline pollution excesses from any of the constituents in a mixture of pollutants, the discharge should be sited more or less in the middle of the river.

Chapter 4 introduced ray approximation for representing steady discharges in river flows. In this work extension was made of the investigation of Smith (1981) to include the effects of contaminant decay. The special models considered sharpened insight about how loss mechanisms displaced the ray paths and the consequent effects upon the curvature. Critically however, the results indicated that there was a dependence upon reflection and transmission phenomena at sharp changes in water depth, flow speed or diffusivity including contaminant decay upon diffusion problems.

Chapter 5 extended the findings of Chapter 4 to include reflection and transmission phenomena in steady discharges in river flows with depth discontinuities or sharp depth changes. The heuristic formulations predicted that by using characterisation of pollution levels by rays, ray bending indicated that the downstream propagation of pollutant is principally in the low-decay region.

The complexity of the changed coefficients and of the geometry in rivers, makes numerical computations inevitable. Therefore, Chapter 6 focused on the development of numerical schemes to handle the computations of steady discharges. The results indicated the ability of the proposed schemes to handle efficiently, robustly and accurately solute transport in non-uniform and truely variable coefficients. The computational results provided reasonable estimates and give pictorial illustrations of the concentration distributions and of the difference between discharging at non-optimal and optimal sites in rivers.

7.2 Further Work

The implementation of all the techniques developed in this research has provided insight into how it may be extended to provide practical results. To this end, there is a considerable

amount of further work that requires investigation.

The results obtained for the mixing or diffusion centre of a river indicated that variability of decay can shift it in either direction. Therefore, for an optimum and definite diffusion centre, optimisation techniques should be applied to control the diffusion centre.

In a meandering channel the complexity of the flow field and the strong dependence of the transverse-dispersion coefficient upon the flow curvature, means there is the practical alternative to use a generalized co-ordinate system to reflect the naturality of rivers in the computations of the diffusion centre. In this case the computations may not only be analytical but numerical computations are inevitable for practical purposes.

The memory character of longitudinal dispersion processes as well as the importance of centrifugal effects as regards transverse dispersion in rivers are available in literature. Therefore, the incorporation of curvature effects for further studies in this work is in order.

Rivers do not necessarily constitute constant hydraulic geometry (width, depth and velocity), thus, turbulent mixing analyses and investigations of potential environmental impacts of contaminants downstream be conducted with varying-geometry river characteristics.

Branchings of fluid flow are extremely common in rivers and involve various complex geometrical configurations and flow conditions. Branchings greatly affect the fluid dynamics and are common sites of contaminant trapping. A natural continuation of this work is the modelling of the proximity of the discharge site to the branching and upon how the rate of discharge is adjusted to enhance optimum discharging.

The various investigations of the research involved small discharges that do not change the flow. Therefore, further work for best discharging in rivers should incorporate large discharges with volumetric discharge rates comparable to that of the rivers.

The accumulative message of this dissertation is that an easy, effective and robust way of reducing the environmental impact of unavoidable wastewater discharges in rivers is to determine the loss mechanisms of contaminants which modify the diffusion centre. It is

hoped that the developments made herein to steady discharges will find effective use in direct computations of best discharging sites and in the building of discharge outlets that make more environmentally aware waste discharges.